Experimental Investigation of Plume Dilution in Three-Dimensional Porous Media

Dissertation

der Mathematisch-Naturwissenschaftlichen Fakultät

der Eberhard Karls Universität Tübingen

zur Erlangung des Grades eines

Doktors der Naturwissenschaften

(Dr. rer. nat.)

vorgelegt von

M.Sc. Yu Ye

aus Zhejiang, China

Tübingen

2016

Tag der mündlichen Qualifikation:	27.04.2016
Dekan:	Prof. Dr. Wolfgang Rosenstiel
1. Berichterstatter:	Prof. Dr. Massimo Rolle
2. Berichterstatter:	Prof. Dr. Peter Grathwohl

Abstract

Transverse dispersion is of critical importance for plume dilution and transport in groundwater and represents a key mechanism controlling degradation of contaminant plumes. This work presents an experimental investigation supported by model-based interpretation of plume dilution in fully three-dimensional saturated porous media. High-resolution experiments were performed to study lateral mixing and dilution of steady-state plumes in homogeneous and heterogeneous experimental setups. The investigation aimed at the detailed study of key mechanisms controlling solute transport in saturated porous media and was structured according to a progressively increasing level of complexity. First, dimensionality and compound-specific effects on plume dilution were studied in homogeneous porous media. We performed multi-tracer (i.e., fluorescein and oxygen) experiments in a fully three-dimensional setup and compared the results with analogous experiments conducted in a quasi two-dimensional system. The concept of flux-related dilution index was used to quantify plume dilution and it was experimentally calculated considering the flow rates and the concentrations measured at the inlet and outlet ports. A semi-analytical solution was proposed to predict plume dilution in three-dimensional setup. Subsequently, the effects of flow focusing in high-permeability inclusions were investigated. The results show a dependence of transverse mixing on dimensionality and on the parameterization of transverse dispersion coefficients. Furthermore, the experimental results confirm that although dilution is stronger in three-dimensional porous media, dilution enhancement by flow-focusing in high-permeability inclusions is less effective in 3-D than in 2-D systems. The spatial arrangements of the high-permeability inclusions also significantly influence the dilution enhancement in three-dimensional heterogeneous porous media. Finally, transport and plume dilution in three-dimensional heterogeneous anisotropic porous media was investigated. Flow-through experiments performed in macroscopically anisotropic porous media provided the first experimental proof of the occurrence of helical flow. Such complex flow conditions, entailing streamlines twisting, were shown to significantly enhance plume dilution and mixing-controlled reactive transport.

Kurzfassung

Die Quervermischung ist von entscheidender Bedeutung für die Verdünnung und den Transport einer Schadstofffahne im Grundwasser. Sie stellt einen wichtigen Mechanismus dar, der den Abbau von Schadstofffahnen bestimmt. In dieser Arbeit wird eine experimentelle Studie präsentiert, die durch eine modellbasierte Interpretation der Verdünnung einer Schadstofffahne in vollständig 3-dimensionalen gesättigten porösen Medien unterstützt wird. Hochauflösende Experimente wurden durchgeführt, um die seitliche Durchmischung und Verdünnung stationärer Fahnen in homogenen und heterogenen Versuchsaufbauten zu untersuchen. Die Studie zielte auf die detaillierte Betrachtung der wichtigsten den Stofftransport in gesättigten porösen Medien kontrollierenden Mechanismen ab und wurde entsprechend eines zunehmenden Grads an Komplexität gegliedert. Zunächst wurden der Einfluss der Dimensionalität und substanzspezifischer Effekte auf die Verdünnung einer Schadstofffahne in homogenen porösen Medien untersucht. Es wurden Multi-Tracer-Experimente (d.h. mit Uranin und Sauerstoff) in einem vollständig 3-dimensionalen Versuchsaufbau durchgeführt und die Ergebnisse mit analogen Experimenten verglichen, die in einem quasi 2-dimensionalen System umgesetzt wurden. Das Konzept des abfluss-gewichteten Verdünnungsindex wurde verwendet, um die Verdünnung der Schadstofffahne zu quantifizieren. Der Verdünnungsindex wurde experimentell durch Berücksichtigung der an den Ein- und Auslassports ermittelten Flussraten und Konzentrationen berechnet. Eine semi-analytische Lösung wurde aufgestellt, um die Durchmischung einer Schadstofffahne in 3-dimensionalen Versuchsaufbauten vorherzusagen. Anschließend wurden die Auswirkungen der Fokussierung der Strömung in hochdurchlässigen Zonen betrachtet. Die Ergebnisse zeigen eine Abhängigkeit der Quervermischung von der Dimensionalität und der Parametrisierung der transversalen Dispersionskoeffizienten. Darüber hinaus bestätigen die Versuchsergebnisse, dass – obwohl die Verdünnung in 3-dimensionalen porösen Medien stärker ist – die Verbesserung der Verdünnung aufgrund der Fokussierung der Strömung in 3-dimensionalen gegenüber 2-dimensionalen Systemen weniger effektiv ist. Zudem beeinflusst die räumliche Anordnung der hochdurchlässigen Zonen signifikant die Verbesserung der Verdünnung in 3-dimensionalen heterogenen porösen Medien. Abschließend wurden der Transport und die Verdünnung von Schadstofffahnen in 3-dimensionalen heterogenen anisotropen porösen Medien untersucht. In makroskopisch anisotropen porösen Medien wurden Durchfluss-experimente durchgeführt, die den ersten experimentellen Beweis für das Auftreten einer „verzwirbelten“ Strömung erbrachten. Es wurde gezeigt, dass solch komplexe

Strömungsbedingungen, die eine Verzwirbelung der Strömungslinien zur Folge haben, die Verdünnung der Fahne und den mischungskontrollierten reaktiven Transport deutlich verbessern.

Acknowledgement

This work would not have been finished without the guidance and help of many people. First and foremost I would like to thank Prof. Dr. Massimo Rolle for giving me the chance to do this Ph.D work. During my doctoral study, he could always be reached even when he was not in Tübingen. He inspired me with new ideas; discussed with me whenever I had questions; encouraged me when I was frustrated by unsuccessful works. His patience and attitude towards scientific research also influenced me in my entire Ph.D. Besides, I would like to thank Prof. Dr. Peter Grathwohl, who offered me an excellent lab for doing my experiments and supported me constantly. I also want to thank Prof. Dr-.Ing. Olaf A. Cirpka for his help with the modeling, the constructive comments and the fruitful discussions. Special thanks to Dr. Gabriele Chiogna, who motivated me, helped me and supported me in these years. I could always understand more and improve more every time after his visit in Tübingen. The week I spent in Trento is also unforgettable. We worked together day and night, which ended up in our second joint paper. Of course, the original Italian food he cooked was the most fantastic part of that trip. Besides, I owe a great deal to Christina Haberer, who helped me a lot in conducting flow-through experiments in the beginning of my Ph.D. When we were sharing the same office, her diligence also encouraged me to work harder. I also want to thank the people working in the hydrogeochemistry lab, i.e., Dr. Thomas Wendel, Renate Seelig, Bernice Nisch and Sara Cafisso, and Wolfgang Körner who made my excellent tank. I would like to express my appreciation to Dr. Carsten Leven, who offered me space in his soil mechanic lab during my pregnancy. I also want to thank Dr. Wolfgang Bott, Willi Kappler, Elisabetha Kraft, Peter Merkel, Monika Jekelius and Christine Bär for sorting and filling the documents in German language. I would like to thank my friends and colleagues for everything: Munir, Biao, Zhongwen, Gaëlle, Donimik, Chuanhe, Stéphane, Kennedy, Zhengrong, Shaojian, Tingting, Jana, Sven… Thanks to all my friends in Europe and in China. Last but not the least, I would like to thank to my husband Junxiao, who accompanied me and shared with me all the happiness and sorrow in the last six years in Germany. My daughter Qingtian brings not only happiness but also a lot of hope to my life. Many thanks to my mom and my parents-in-law for their understanding and unconditional support.

This study was funded by German Research Foundation (DFG), which is gratefully acknowledged here.

Contents

Abstract **3**

Kurzfassung **4**

Acknowledgement **6**

1. Introduction **10**

1.1 Motivation 10

1.2 Objectives and Structure of the Thesis 12

References 14

2. Experimental Investigation of Compound-Specific Dilution of Solute Plumes in Saturated Porous Media: 2-D vs. 3-D Flow-Through Systems **17**

Abstract 17

2.1 Introduction 18

2.2 Material and Methods 19

2.2.1 Bench-Scale Experiments 20

2.2.2 Evaluation of Transverse Dispersion Coefficients 22

2.2.3 Evaluation of Plume Dilution 25

2.3 Results and Discussion 28

2.3.1 Concentration Measurements 28

2.3.2 Transverse Dispersion Coefficients 31

2.3.3 Plume Dilution 35

2.4 Summary and Conclusions 38

Acknowledgments 39

Appendix A. Semi-analytical solutions for the flux-related dilution index of steady-state plumes in homogeneous porous media 40

References 42

3. Enhancement of Plume Dilution in Two- and Three-Dimensional Porous Media by Flow Focusing in High-Permeability Inclusions **47**

Abstract 47

3.1 Introduction 48

3.2 Theory 50

3.2.1 Governing Flow and Transport Equations 50

3.2.2 Quantification of Transverse Mixing 52

3.3 Experimental Setup 59

3.4 Model Description and Validation 62

3.5 Results and Discussion 64

3.5.1 Effects of Flow Focusing in 3-D Heterogeneous Setups 64
3.5.2 Effects of Dimensionality on Dilution and Dilution Enhancement 70
3.5.3 Compound-Specific Effects 73
3.6 Conclusions 75
Acknowledgments 77
Appendix B. Summary of the average normalized fluorescein concentrations measured in the flow-through experiments. 78
References 82
4. Experimental Evidence of Helical Flow in Porous Media 89
Abstract 89
References 98
5. Experimental Investigation of Transverse Mixing under Helical Flow Conditions in Saturated Porous Media 100
Abstract 100
5.1 Introduction 101
5.2 Experimental Operation and Model Description 102
5.3 Quantification of Dilution and Spreading 105
5.4 Theory about Reactive Transport 106
5.5 Results and Discussion 107
5.5.1 Conservative Transport 107
5.5.2 Reactive Transport 111
5.6 Conclusions 113
Acknowledgments 114
Appendix C. Analytical expression of the critical dilution index for the plumes in the three-dimensional homogeneous systems 115
References 116
6. Conclusions and Outlook 118
6.1 Conclusions 118
6.2 Outlook 120
References 122

1. Introduction

1.1 Motivation

Groundwater serves as one of the main sources of fresh water in our planet. It is used as drinking water, and also for irrigation and industrial purposes. Therefore, the quality of groundwater is of crucial importance for human health and the functioning of ecological systems. However, groundwater quality is seriously threatened by industrial activities, pesticides and herbicides use in agriculture, leaking underground storages, oil and gas explorations, traffic and landfill sites. Pollutants released in groundwater include hydrocarbons, phenolic compounds, chlorinated solvents, polychlorinated byphenils, heavy metals and some radio-active chemicals. Such anthropogenic compounds form persistent contaminant plumes in aquifer systems. A detailed understanding of contaminant transport is fundamental for the management of groundwater resources.

The investigation of mixing processes is of pivotal importance for natural attenuation as well as in situ engineered remediation of subsurface contamination (Kitanidis and McCarty, 2012). For instance, in the cases of natural attenuation, mixing between reactants is proved to be the limiting step in most circumstances by both numerical studies (e.g., Cirpka et al., 1999; Maier and Grathwohl, 2006; Tartakovsky et al., 2009) and laboratory experiments (e.g., Bauer et al., 2009; Rolle et al., 2010). Important biodegradation reactions occur at the fringe of contaminant plumes, where multiple substrates such as electron donors and acceptors are simultaneous present through mixing processes (e.g., Amos et al., 2011; Anneser et al., 2008; Tuxen et al., 2006; Thornton et al., 2001; Davis et al., 1999). At the field scale, the importance of mixing for transport and biodegradation of contaminant plumes was shown by numerical simulations (e.g., Cirpka et al., 2012; Liedl et al., 2005; Prommer et al., 2009; Zarlenga and Fiori, 2013). Therefore, the investigation of mixing processes is instrumental for the evaluation of the overall contaminant biodegradation and the determination of the length of contaminant plumes. In many sites contaminated by NAPL spills and leaking landfills, contaminants are continuously emitted from the sources over typical time scales of decades. The released plumes reach steady-state conditions determined by the dynamic equilibrium between the contaminant mass released at the source and its destruction by degradation processes (e.g., Mace et al., 1997; Wiedemeier et al., 1999). Under these conditions, lateral mass exchange is dominant compared to the longitudinal mixing and it represents a key process estimating the steady-state plume length (e.g., Cirpka et al., 2012; Liedl et al., 2011;

Zarlenga and Fiori, 2014). Transverse mixing is also critical for transient transport processes such as the coalescence of plume lamellae within heterogeneous domains (e.g., Le Borgne et al., 2013) and the transition from longitudinal plume spreading to dilution (Kitanidis, 1994).

The heterogeneity of porous media can significantly enhance transverse mixing. In heterogeneous porous media, flow-focusing in high-permeability zones reduces the distance between streamlines, thus increasing lateral concentration gradients. In two-dimensional systems, the increase of transverse dispersive mass exchange between neighboring streamlines caused by flow focusing effects prevails over the decrease of the transport time in the high-permeability regions, resulting in the overall enhancement of transverse mixing (e.g., Werth et al., 2006; Willingham et al., 2008; Cirpka et al., 2011; Chiogna et al., 2011a). When dealing with the quantification of mixing in porous media, it is important to recognize that phenomena such as squeezing and stretching of solute plumes are purely advective mass displacements and should be distinguished from true mixing processes. Entropy-based metrics such as the dilution index (Kitanidis, 1994) and the flux-related dilution index (Rolle et al., 2009) were proved to be useful measures to quantify mixing processes in heterogeneous formations. Particularly, the concept of flux-related dilution index was extensively used and further developed in this study to assess transverse mixing and mixing enhancement in different fully 3-D experimental setups.

Besides heterogeneity, anisotropy is another important feature of geologic formations. The macroscopic anisotropy of porous media has been observed in sedimentary gravel deposits (e.g., Stauffer and Rauber, 1988; Nichols, 2009). Anisotropic structures have been simulated numerically using anisotropy in different layers and result in complex flow fields (e.g., Hemker et al., 2004). Analytical solutions were also derived for the flow computation in anisotropic porous media showing the possible development of whirling streamlines (e.g., Hemker and Bakker, 2006; Bakker and Hemker, 2004). However, the existence of helical flow in porous media has been debated in the literature (Sposito, 2001). Recently, Chiogna et al. (2015) and Cirpka et al. (2015) performed numerical experiments in 3-D heterogeneous anisotropic porous media. The outcomes of those studies show the occurrence of helical flow, which facilitates streamline twisting and intertwining in three-dimensional porous media, leading to a substantial deformation of the solute plumes and considerable mixing enhancement. Yet, clear experimental proof of helical flow in porous media has not been reported in the literature.

1.2 Objectives and Structure of the Thesis

Most of the studies regarding transverse mixing during solute transport in porous media were conducted in (quasi) two-dimensional flow-through systems using experimental or numerical approaches. In particular, the few three-dimensional laboratory experiments reported in the literature mainly focused on the development of non-invasive concentration measurement techniques and on the studies of longitudinal dispersion (e.g., Danquigny et al., 2004; Klise et al., 2008; Oswald and Kinzelbach, 2004). A detailed experimental investigation of three-dimensional transverse mixing is essential to understand the mechanisms controlling plume dilution in porous media.

The objectives of this study are:

- to experimentally determine mixing properties in porous media using a 3-D experimental setup allowing high-resolution measurements of solute concentrations and flow rates;
- to investigate the influence of dimensionality on dilution and transverse dispersion by direct comparison between quasi two-dimensional and three-dimensional experiments;
- to quantify compound-specific effects in three-dimensional homogeneous porous media and the influence of dimensionality on multi-tracer lateral displacement;
- to analyze the effects of flow-focusing in high permeability zones on dilution and dilution enhancement of steady-state plumes;
- to extend the proposed two-dimensional analytical frameworks of flux-related dilution index (Chiogna et al., 2011b) and mixing-enhancement factor (Werth et al., 2006) to three-dimensional systems;
- to experimentally demonstrate the existence of helical flow in heterogeneous anisotropic porous media;
- to investigate the impact of helical flow on conservative and reactive solute transport.

In this dissertation, the topics are organized according to the following structure:

- Chapter 2 presents a detailed experimental study on the effect of dimensionality on solute transport and plume dilution. Multi-tracer experiments were conducted in a three-dimensional saturated homogeneous porous media at different flow velocities. The results were compared with the outcomes of analogous experiments performed in a quasi two-dimensional system. Transverse dispersion coefficients and flux-related

dilution indices were determined from the high-resolution measurement of solutes' concentrations at the outlet of both flow-through systems. A semi-analytical expression was proposed to predict plume dilution during groundwater transport in homogeneous three-dimensional porous media.

- Chapter 3 investigates the effects of flow-focusing in high-permeability inclusions on transverse mixing and on mixing enhancement in three-dimensional versus quasi two-dimensional heterogeneous porous media. Multi-tracer experiments were performed in heterogeneous porous media with different arrangement of high-permeability inclusions. The experimental results were supported by numerical simulations as well as theoretical analysis.
- Chapter 4 aims at experimentally demonstrate the existence of helical flow in porous media. Flow-through experiments were performed in a macroscopic heterogeneous anisotropic porous medium. The latter was constructed by alternating angled stripes of coarse and fine grain sizes in different layers. Such porous medium is a simplified representation of herringbone cross-stratification. When water was allowed to flow through such heterogeneous anisotropic medium it clearly showed a helical behavior characterized by twisting streamlines resulting in important effects on solute transport and plume dilution.
- Chapter 5 further investigates the importance of helical flow on solute transport. Experiments were carried out in porous media with different grain sizes and, thus, hydraulic conductivity contrast. Mixing enhancement in the different setups was quantified by means of the flux-related dilution index. The investigation was also extended to reactive transport and the length of steady-state reactive plumes was determined. The concept of critical dilution index introduced in a previous study (Chiogna et al., 2011a) was applied and further developed for transport in 3-D heterogeneous anisotropic porous media.

References

Amos, R. T., B. A. Berkins, G. N. Delin, I. M. Cozzarelli, D. W. Blowes, and J. D. Kirshtein (2011), Methane oxidation in a crude oil contaminated aquifer: delineation of aerobic reactions at the plume fringes, J. Contam. Hydrol., 125, 13-25, doi: 10.1016/j.jconhyd.2011.04.003.

Anneser, B., F. Einsiedl, R. U. Meckenstock, L. Richters, F. Wisotzky, and C. Griebler (2008), High-resolution monitoring of biogeochemical gradients in a tar oil-contaminated aquifer, Appl. Geochem., 23(6), 1715-1730, doi: 10.1016/j.apgeochem.2008.02.003.

Bakker M., and K. Hemker (2004), Analytical solutions for groundwater whirls in box-shaped, layered anisotropic aquifers, Adv. Water Resour., 27(11), 1075-1086, doi: 10.1016/j.advwatres.2004.08.009.

Bauer, R. D., M. Rolle, P. Kürzinger, P. Grathwohl, R. U. Meckenstock, and C. Griebler (2009), Two-dimensional flow-through microcosms–Versatile test systems to study biodegradation processes in porous aquifers, J. Hydrol., 369(3-4), 284-295, doi: 10.1016/j.jhydrol.2009.02.037.

Chiogna, G., O. A. Cirpka, P. Grathwohl, and M. Rolle (2011a), Transverse mixing of conservative and reactive tracers in porous media: Quantification through the concepts of flux-related and critical dilution indices, Water Resour. Res., 47(2), W02505, doi: 10.1029/2010wr009608.

Chiogna, G., O. A. Cirpka, P. Grathwohl, and M. Rolle (2011b), Relevance of local compound-specific transverse dispersion for conservative and reactive mixing in heterogeneous porous media, Water Resour. Res., 47(7), W07540, doi: 10.1029/2010wr010270.

Chiogna, G., O. A. Cirpka, M. Rolle, and A. Bellin (2015), Helical flow in three-dimensional non-stationary anisotropic heterogeneous porous media, Water Resour. Res., 51(1), 261-280, doi: 10.1002/2014WR015330.

Cirpka, O. A., G. Chiogna, M. Rolle, and A. Bellin (2015), Transverse mixing in three-dimensional non-stationary anisotropic heterogeneous porous media, Water Resour. Res., 51(1), 241-260, doi: 10.1002/2014WR015331.

Cirpka, O. A., F. P. J. de Barros, G. Chiogna, M. Rolle, and W. Nowak (2011), Stochastic flux-related analysis of transverse mixing in two-dimensional heterogeneous porous media, Water Resour. Res., 47(6), W06515, doi: 10.1029/2010wr010279.

Cirpka, O. A., E. O. Frind, and R. Helmig (1999), Numerical simulation of biodegradation controlled by transverse mixing, J. Contam. Hydrol., 40(2), 159-182, doi: 10.1016/S0169-7722(99)00044-3.

Cirpka, O. A., M. Rolle, G. Chiogna, F. P. de Barros, and W. Nowak (2012), Stochastic evaluation of mixing-controlled steady-state plume lengths in two-dimensional heterogeneous domains, J. Contam. Hydrol., 138-139, 22-39, doi: 10.1016/j.jconhyd.2012.05.007.

Danquigny, C., P. Ackerer, and J. P. Carlier (2004), Laboratory tracer tests on three-dimensional reconstructed heterogeneous porous media, J. Hydrol., 294(1-3), 196-212, doi: 10.1016/j.jhydrol.2004.02.008.

Davis, G. B., C. Barber, T. R. Power, J. Thierrin, B. M. Patterson, J. L. Rayner, and Q. Wu (1999), The variability and intrinsic remediation of a BTEX plume in anaerobic sulphate-rich groundwater, J. Contam. Hydrol., 36, 265–290, doi: 10.1016/S0169-7722(98)00148-X.

Heinz, J. and Aigner, T. (2003), Three-dimensional GPR analysis of various Quaternary gravel-bed braided river deposits (southwestern Germany), in Ground Penetrating Radar in Sediments, Special Publications, 211, edited by C. Bristow and H. Jol, pp. 99-110, Geological Society, London.

Hemker K., and M. Bakker (2006), Anallytical solutions for whirling groundwater flow in two-dimensional heterogeneous anisotropic aquifers, Water Resour. Res., 42(12), W12419, doi: 10.1029/2006wr004901.

Hemker K., E. van den Berg, and M. Bakker (2004), Ground water whirls, Ground Water, 42 (2), 234-242, doi: 10.1111/j.1745-6584.2004.tb02670.x.

Kitanidis, P. K. (1994), The concept of dilution index, Water Resour. Res., 30(7), 2011-2026, doi: 10.1029/94w00762.

Kitanidis, P. K., and P. L. McCarty (2012), Dilivery and mixing in the subsurface, Springer, New York, doi: 10.1007/978-1-4614-2239-6.

Klise, K.A., V.C. Tidwell, and S.A. McKenna (2008), Comparison of laboratory-scale solute transport visualization experiments with numerical simulation using cross-bedded sandstone, Adv. Water Resour., 31(12): 1731-1741, doi: 10.1016/j.advwatres.2008.08.013.

Le Borgne, T., M. Dentz, and E. Villermaux (2013), Stretching, coalescence, and mixing in porous media, Phys. Rev. Let., 110(20), 204501, doi: 10.1103/PhysRevLett.110.204501.

Liedl, R., A. J. Valocchi, P. Dietrich, and P. Grathwohl (2005), Finiteness of steady state plumes, Water Resour. Res., 41(12), W12501, doi: 10.1029/2005wr004000.

Liedl, R., P. K. Yadav, and P. Dietrich (2011), Length of 3-D mixing-controlled plumes for a fully penetrating contaminant source with finite width, Water Resour. Res., 47(8), W08602, doi: 10.1029/2010wr009710.

Mace, R. E., R. S. Fisher, D. Welch, and S. Parra (1997), Extent, mass, and duration of hydrocarbon plumes from leaking petroleum storage tank sites in texas, Geologic Circular 97-1, Bureau of Economic Geology, University of Texas at Austin.

Maier, U., and P. Grathwohl (2006), Numerical experiments and field results on the size of steady state plumes, J. Contam. Hydrol., 85(1-2), 33-52, doi: 10.1016/j.jconhyd.2005.12.012.

Nichols, G. (2009), Sedimentology and Stratigraphy, Wiley-Blackwell, Chichester.

Oswald, S. E., and W. Kinzelbach (2004), Three-dimensional physical benchmark experiments to test variable-density flow models, J. Hydrol., 290(1-2), 22-42, doi: 10.1016/j.jhydrol.2003.11.037.

Prommer, H., B. Anneser, M. Rolle, F. Einsiedl, and C. Griebler (2009), Biogeochemical and isotopic gradients in a BTEX/PAH contaminant plume: Model-based interpretation of a high-resolution field data set, Environ. Sci. Technol., 43, 8206–8212, doi: 10.1021/es901142a.

Renard P., and D. Allard (2013), Connectivity metrics for subsurface flow and transport, Adv. Water Resour., 51, 168-196, doi: 10.1016/j.advwatres.2011.12.001.

Rolle M., G. Chiogna, R. Bauer, C. Griebler, and P. Grathwohl (2010), Isotopic fractionation by transverse dispersion: flow-through microcosms and reactive transport modeling study, Environ. Sci. Technol., 44, 6167-6173.

Rolle, M., C. Eberhardt, G. Chiogna, O. A. Cirpka, and P. Grathwohl (2009), Enhancement of dilution and transverse reactive mixing in porous media: experiments and model-based interpretation, J. Contam. Hydrol., 110(3-4), 130-142, doi: 10.1016/j.jconhyd.2009.10.003.

Stauffer, F., and M. Rauber (1998), Stochastic macrodisperison models for gravel aquifers. J. Hydraul. Res., 36, 885-896.

Sposito, G. (2001), Topological groundwater hydrodynamics, Adv. Water Resour., 24, 793-801, doi: 10.1016/S0309-1708(00)00077-4.

Tartakovsky, A. M., G. D. Tartakovsky, and T. D. Scheibe (2009), Effects of incomplete mixing on multicomponent reactive transport, Adv. Water Resour., 32(11), 1674-1679, doi: 10.1016/j.advwatres.2009.08.012.

Thornton, S. F., S. Quigley, M. J. Spence, S. A. Banwart, S. Bottrell, and D. N. Lerner (2001), Process controlling the distribution and natural attenuation of dissolved phenolic compounds in a deep sandstone aquifer, J. Contam. Hydrol., 53, 233-267, doi: 10.1016/S0169-7722(01)00168-1.

Tuxen, N., H. -J. Albrechtsen, and P. L. Bjerg (2006), Identification of a reactive degradation zone at a landfill leachate plume fringe using high resolution sampling and incubation techniques, J. Contam. Hydrol., 85, 179-194.

Werth, C. J., O. A. Cirpka, and P. Grathwohl (2006), Enhanced mixing and reaction through flow focusing in heterogeneous porous media, Water Resour. Res., 42(12), W12414, doi: 10.1029/2005wr004511.

Wiedemeier, T. H., H. S. Rifai, C. J. Newell, and J. T. Wilson (1999), Natural attenuation and fuels and chlorinated solvents in the subsurface, John Wiley & Sons, Inc., Hoboken, NJ, USA.

Willingham, T. W., C. J. Werth, and A. J. Valocchi (2008), Evaluation of the effects of porous media structure on mixing-controlled reactions using pore-scale modeling and micromodel experiments, Environ. Sci. Technol., 42(9), 3185-3193, doi: 10.1021/Es7022835.

Zarlenga, A., and A. Fiori (2013), Steady plumes in heterogeneous porous formations: A stochastic Lagrangian approach, Water Resour. Res., 49(2), 864-873, doi: 10.1002/Wrcr.20106.

Zarlenga, A., and A. Fiori (2014), Stochastic analytical modeling of the biodegradation of steady plumes, J. Contam. Hydrol., 157, 106-116, doi: 10.1016/j.jconhyd.2013.11.003.

2. Experimental Investigation of Compound-Specific Dilution of Solute Plumes in Saturated Porous Media: 2-D vs. 3-D Flow-Through Systems

Yu Ye, Gabriele Chiogna, Olaf Cirpka, Peter Grathwohl and Massimo Rolle

Journal of Contaminant Hydrology (2015), vol. 172, pp. 33-47, doi: 10.1016/j.jconhyd.2014.11.002.

Abstract

Dilution of solute plumes in groundwater strongly depends on transverse mixing. Thus, the correct parameterization of transverse dispersion is of critical importance for the quantitative description of solute transport. In this study we perform flow-through laboratory experiments to investigate the influence of transport dimensionality on transverse mixing. We present a high-resolution experimental setup to study solute dilution and transverse dispersion in three-dimensional porous media. We conduct multi-tracer experiments in the new 3-D setup and compare the results with the outcomes of analogous tracer experiments performed in a quasi 2-D system. We work under steady-state flow and transport conditions and consider a range of velocities relevant for groundwater flow (0.5–8 m/day). Transverse dispersion coefficients are determined from high-resolution concentration profiles at the outlet of the flow-through chambers (7 × 7 ports in the 3-D setup and 7 ports in the quasi 2-D system), considering conservative tracers with significantly different aqueous diffusion coefficients, namely fluorescein and dissolved oxygen. To quantify dilution in the 2-D and 3-D systems, we experimentally determine the flux-related dilution index using the flow rates and the concentrations measured at the inlet and outlet ports, and we propose semi-analytical expressions to predict its evolution with travel distance in uniform groundwater flow. The experimental results in the quasi 2-D and 3-D flow-through systems are consistent and show a compound-specific behavior of the transverse dispersion coefficient and its non-linear dependence on the seepage velocity in both setups. The degree of dilution and the compound-specific effects of transverse dispersion are considerably more pronounced in 3-D than in quasi 2-D transport systems.

Keywords: dilution; transverse dispersion; mixing; flux-related dilution index; laboratory experiments

2.1 Introduction

The characterization of transverse mixing is critical for the understanding and quantitative assessment of solute transport and reactions in groundwater. Especially for continuously emitted contaminant plumes, transverse mixing represents the principal process of mass exchange between the polluted plume and the clean ambient water (e.g., Cirpka et al., 1999). This mechanism is necessary for biodegradation processes occurring at the plume fringes that require the simultaneous availability of multiple substrates such as dissolved electron donors and acceptors. Steep concentration gradients and favorable conditions for microbial activity at the fringes of groundwater plumes have been identified in a number of high-resolution field investigations of contaminated aquifers (e.g., Amos et al., 2011; Anneser et al., 2008; Davis et al., 1999; Thornton et al., 2001; Tuxen et al., 2006). Furthermore, modeling studies have shown the importance of transverse mixing for transport and natural attenuation of organic contaminant plumes at the field scale (e.g., Cirpka et al., 2012; Herrera et al., 2009, 2010; Liedl et al., 2005; Maier and Grathwohl, 2006; Prommer et al., 2009; Zarlenga and Fiori, 2013). Although at the field-scale effective dispersion parameters are often needed for the interpretation and modeling of contaminant plumes, their definition requires a correct parameterization of the processes occurring at the smaller Darcy and pore-scales (e.g., Chiogna et al., 2011a; Rolle et al., 2013b). Indeed, biogeochemical reactions take place at the microscopic (pore) scale and local diffusive/dispersive processes are important and often limit the overall contaminant degradation (e.g., Bauer et al., 2009; Rolle et al., 2010; Steefel et al., 2005). Therefore, the detailed investigation of transverse mixing at the pore and Darcy scales is instrumental for the understanding and the accurate parameterization of the interactions between the fundamental physical processes of advection and diffusion, which are necessary to obtain up-scaled dispersion coefficients relevant in field applications.

At the pore scale, transverse mixing has been studied in microfluidic experiments (e.g., de Anna et al., 2014;Willingham et al., 2008; Zhang et al., 2010) and numerical simulations (e.g., Acharya et al., 2007; Bijeljic and Blunt, 2007; Hochstetler et al., 2013; Knutson et al., 2007; Porter et al., 2010; Rolle and Kitanidis, 2014). At the Darcy scale, flow-through laboratory experiments have been conducted to study lateral displacement of conservative and reactive solutes in homogeneous and heterogeneous porous media (e.g., Chiogna et al., 2010; Delgado, 2006; Olsson and Grathwohl, 2007; Rolle et al., 2013a; Seagren et al., 1999). Most of these pore-scale studies and laboratory experiments were performed in two-dimensional computational domains or in quasi two-dimensional experimental setups (e.g., Castro-Alcala

et al., 2012; McNeil et al., 2006). Pore-scale investigations showed the importance of the fundamental interactions between advection and diffusion at the pore scale resulting in incomplete dilution in the pore channels (e.g., Klenk and Grathwohl, 2002; Rolle et al., 2012) and demonstrated the controlling role of transverse mixing for a number of abiotic and microbially-mediated reactions (e.g., Hochstetler et al., 2013; Knutson et al., 2007; Zhang et al., 2010).

Three-dimensional simulations of pore-scale transport are computationally very expensive and have not been performed very often (e.g.,Molins et al., 2012; Scheibe et al., 2013). To the best of our knowledge, these studies have not addressed the question of transverse mixing. Likewise, most existing 3-D laboratory-scale experiments have focused on the development of non-invasive concentration measurement techniques and on the study of longitudinal dispersion (e.g., Danquigny et al., 2004; Gheith and Schwartz, 1998; Klise et al., 2008; Oswald and Kinzelbach, 2004; Oswald et al., 1997; Stohr et al., 2003).

In this work, we investigate transverse mixing and plume dilution in a three-dimensional laboratory setup. We performed conservative multi-tracer experiments using fluorescein and dissolved oxygen, which differ significantly in their aqueous diffusion coefficients, and considered a range of seepage velocities (0.5–8 m/day) representative of groundwater flow. The 3-D setup was designed to collect high-resolution measurements of concentration and flow rates in a dense network of sampling points at the outlet of the flow-through system (7 × 7 ports). This allows the accurate experimental determination of the solute mass flux and the dilution of steady-state plumes. The outcomes of the 3-D experiments were compared with the results of analogous multi-tracer experiments performed in a more conventional quasi 2-Dsetup at the same scale. The main objective of this study is to experimentally evaluate the effect of transport dimensionality on transverse dispersion and on steady-state plume dilution in homogeneous saturated porous media and to show the increased importance of compound-specific effects, arising from distinct incomplete mixing of different solutes in the pore channels, for three-dimensional solute transport. Furthermore, we propose semi-analytical solutions to quantify plume dilution at different cross-sections and we test their predictive capability with the experimental results in the 2-D and 3-D systems.

2.2 Material and Methods

In this section we describe the new three-dimensional and the quasi two-dimensional setups used to measure solute concentrations and flow rates in the steady-state multi-tracer

experiments performed in this study. In addition, we provide the description of the analytical models applied to estimate the transverse dispersion coefficients and the flux-related dilution index for the different experimental runs.

2.2.1 Bench-Scale Experiments

Multi-tracer experiments of solute transport in porous media were performed in quasi 2-D and 3-D flow-through systems in a temperature-controlled room at 22 ℃. The selected tracers were fluorescein and oxygen, which have significantly different aqueous diffusion coefficients: 4.8 $\times 10^{-10}$ m^2s^{-1} and 1.97 $\times 10^{-9}$ m^2s^{-1}, respectively, at T = 22 ℃ (e.g., Atkins, 1990; Worch, 1993). Fig. 2.1 shows a schematic overview of the quasi 2-D and 3-D experimental setups. A photograph of the new 3-D experimental apparatus is shown in Fig. 2.2.

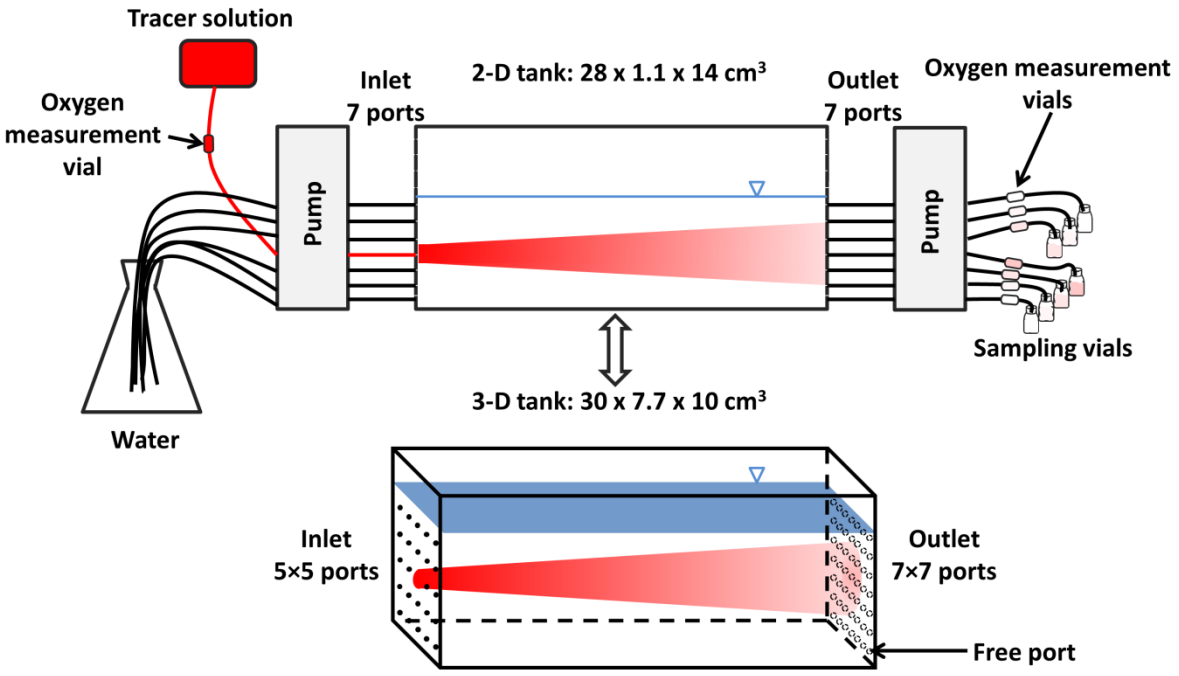

Fig. 2.1. Schematic overview of the quasi 2-D and the 3-D experimental setups.

Both flow-through chambers are made of acrylic-glass. The quasi two-dimensional setup has inner dimensions of 28 cm × 1.1 cm × 14 cm while the three-dimensional system has inner dimensions of 30 cm × 7.7 cm × 10 cm. The 2-D setup is equipped with 11 equally-spaced ports (1.27 cm) at the inlet and at the outlet. The 3-D setup has an array of 5 × 5 injection ports at the inlet and 7 × 7 extraction ports at the outlet. The ports at the inlet are equally-spaced with a distance of 1.54 cm, while at the outlet the distance between the ports is 1.1 cm. All ports are plugged by rubber septa; syringe needles (ID 0.9mm) are inserted into the septa

for liquid injection and extraction. Peristaltic pumps (IPC and IPC-N, Ismatec, Glattbrugg, Switzerland) were used to obtain constant flux boundary conditions. For the 2-D setup 14 ports (7 at the inlet and 7 at the outlet, counting from the bottom) were active and connected to an IPC-N pump. This allows a direct comparison of the outlet measurements with the 3-D system that also has at the outlet arrays of 7 ports in the vertical direction. In both systems a similar height of the water table was established. The 25 inlet ports of the 3-D setup were connected to an IPC-N-12 (P1 in Fig. 2.2) and an IPC-N-18 (P2 in Fig. 2.2) pump. At the outlet, 48 ports were connected to two 24-channel IPC-N pumps (P3 and P4 in Fig. 2.2) and one port (right corner in the bottom row) was left free to maintain a stable water table. Fluran pump tubings (ID 0.64 mm, Ismatec, Glattbrugg, Switzerland) and stainless steel capillaries were used for the connections between the injection and extraction needles and the pumps. Both flow-through systems were homogeneously filled with glass beads (Sigmund Lindner, Germany) with a grain size of 0.4–0.6 mm (saturated hydraulic conductivity K=2.1 ×10^{-3} m/s, Haberer et al., 2014). A wet-packing procedure was applied to avoid air entrapment within the water-saturated medium (e.g., Haberer et al., 2012). The porosity of the homogeneous media was 0.4 in both setups. The multi-tracer experiments were performed in a range of flow velocities between 0.5 m/day and 8 m/day in both flow-through systems.

An oxygen-depleted sodium fluorescein solution was used as tracer solution, thus allowing the simultaneous detection of the two tracers (i.e., fluorescein and oxygen) in the saturated porous medium. The oxygen concentration of the solution at the inlet was kept below1.0 mg/l, while the inlet concentration of fluorescein was in the range of 10–20 mg/l. The solution was stored in a gastight Tedlar bag (Alltech, Germany). After establishing steady-state flow conditions, the tracer solution was injected through the central inlet port (red in Fig. 2.1), while tap water with no fluorescein and oxygen concentration of 8.5 mg/L was injected from the surrounding inlet ports. Steady-state plumes were obtained after the injection of at least two pore volumes.

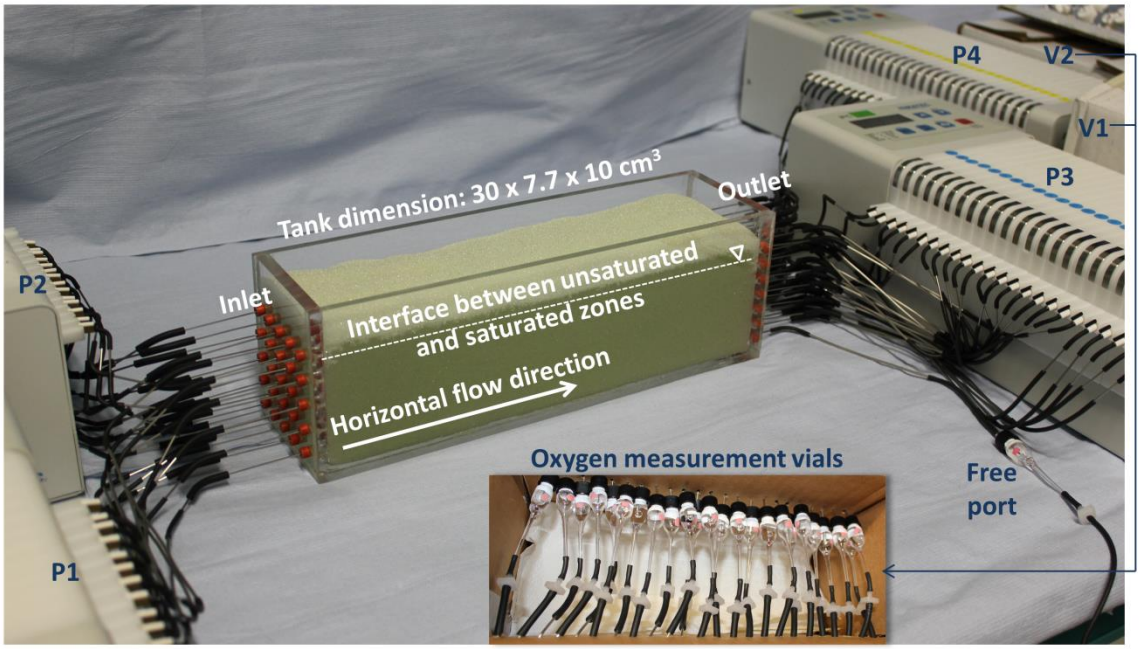

Fig. 2.2. Photograph of the 3-D experimental setup, with high-resolution injection (25 ports) and extraction (49 ports) of the tracers and of the ambient solution. P1–P4 are the multi-channel pumps at the inlet and at the outlet, and V1–V2 denote the flow-through vials for oxygen measurement shown in detail in the inset.

Oxygen concentrations were measured in the vials right after the outlet pumps (Fig. 2.2) and at the central inlet port, to check the effectiveness of oxygen stripping from the inlet solution, using the non-invasive optode technique (PreSens, Germany) described by Haberer et al. (2011). The technique is based on the dynamic luminescence quenching of a luminophore by molecular oxygen. Samples were also collected at the outlet ports and fluorescein concentrations were measured using a UV-spectrometer (Perkin Elmer LS-3B) with an extinction wavelength of 492 nm and an absorbance wavelength of 513 nm. The flow rate at the outlet ports was determined by weighing the samples collected at each port.

2.2.2 Evaluation of Transverse Dispersion Coefficients

Analytical solutions of the advection–dispersion equation are useful to estimate transport parameters in laboratory experiments in porous media (e.g., Robbins, 1989). We estimated the effective transverse dispersion coefficients for the quasi 2-D and 3-D experimental setups by fitting the analytical solutions of the advection–dispersion equation for uniform flow to the experimental data. Under steady-state transport conditions, the contribution of longitudinal dispersion becomes negligible compared to the one of transverse dispersion (e.g., Cirpka et al., 2011) and the governing equations can be written as:

2-D: $$v\frac{\partial c}{\partial x} - D_t \frac{\partial^2 c}{\partial^2 z} = 0 \tag{2.1}$$

3-D: $$v\frac{\partial c}{\partial x} - D_t \frac{\partial^2 c}{\partial^2 y} - D_t \frac{\partial^2 c}{\partial^2 z} = 0 \tag{2.2}$$

where c [ML^{-3}] is the concentration, x [L], y [L] and z [L] are the spatial coordinates in longitudinal, lateral and vertical directions, respectively, v [LT^{-1}] is the average flow velocity and D_t [L^2T^{-1}] denotes the transverse dispersion coefficient. Since the porous medium is assumed homogeneous and isotropic, lateral and vertical dispersion coefficients are assumed to be identical.

In the two-dimensional case, we consider a line source as boundary condition:

2-D: $$c(x=0,z) = \begin{cases} c_0 & \forall |z| < \dfrac{Z}{2} \\ c_{bg} & \forall |z| \geq \dfrac{Z}{2} \end{cases} \tag{2.3}$$

where c_0 [ML^{-3}] is the concentration of the injected tracer solution, c_{bg} [ML^{-3}] is the background concentration in the ambient solution and Z [L] is the source thickness. The analytical solution of the two-dimensional problem, adapted after Domenico and Palciauskas (1982) and satisfying the conditions pointed out by Srinivasan et al. (2007), reads as:

2-D: $$c_{norm}(x,z) = \frac{c - c_{bg}}{c_0 - c_{bg}} = \frac{1}{2}\left\{ \mathrm{erf}\left[\frac{z + Z/2}{2(D_t\, x/v)^{1/2}} \right] - \mathrm{erf}\left[\frac{z - Z/2}{2(D_t\, x/v)^{1/2}} \right] \right\} \tag{2.4}$$

which is formulated here for an infinitely high domain. The solution is valid if $Z+2(2D_tx/v)^{1/2}$ remains significantly smaller than the height of the domain; otherwise image sources are needed to account for no-flux conditions at the bottom and top boundaries of the domain.

In the 3-D case we consider a rectangular source of width Y and thickness Z as boundary condition:

3-D: $$c(x=0,y,z) = \begin{cases} c_0 & \forall |y| < \dfrac{Y}{2} \cap \forall |z| < \dfrac{Z}{2} \\ c_{bg} & \forall |y| \geq \dfrac{Y}{2} \cup \forall |z| \geq \dfrac{Z}{2} \end{cases} \tag{2.5}$$

The analytical solution of the three-dimensional, steady-state transport problem reads as:

$$c_{norm}(x,y,z) = \frac{c - c_{bg}}{c_0 - c_{bg}}$$

3-D:
$$= \frac{1}{4}\left\{\mathrm{erf}\left[\frac{y + Y/2}{2(D_t\, x/v)^{1/2}}\right] - \mathrm{erf}\left[\frac{y - Y/2}{2(D_t\, x/v)^{1/2}}\right]\right\} \qquad (2.6)$$
$$\left\{\mathrm{erf}\left[\frac{z + Z/2}{2(D_t\, x/v)^{1/2}}\right] - \mathrm{erf}\left[\frac{z - Z/2}{2(D_t\, x/v)^{1/2}}\right]\right\}$$

Like Eq. (2.4), the expression of Eq. (2.6) does not account for no-flux boundaries in a domain of finite width and height. Eqs. (2.4) and (2.6) were used to interpret the experimental results in the quasi 2-D and in the 3-D flow-through systems, respectively. These analytical solutions are simplified models of the experimental flow-through systems. However, for the permeable and uniformly packed porous media considered in our study, they allow a satisfactory interpretation of the experimental results. This was also verified in previous studies (e.g., Rolle et al., 2009) where the outcomes of simplified analytical solutions were shown to be in good agreement with those of more complex and detailed numerical models. In the quasi 2-D system the observed source thickness was 1.27 cm, and the concentration was uniform within the thin width of the flow-through chamber (1.1 cm). Thus, the 2-D analytical solution with a line source thickness Z equal to of 1.27 cm was used to evaluate the vertical concentration profiles measured at the outlet. In the 3-D setup Eq. (2.6) with a square source ($Y = Z = 1.54$ cm) was used to fit the concentration measurements at the 49 outlet ports.

The trust-region-reflective method for the minimization of non-linear least squares problems implemented in the MATLAB function `lsqnonlin` (e.g., Coleman and Li, 1996) was adopted to fit the experimental results with the analytical solutions (Eqs. (2.4) and (2.6)), using D_t as fitting parameter. The hydrodynamic transverse dispersion coefficient was estimated for each seepage velocity tested in the experiments and for each tracer in both the quasi two-dimensional and three-dimensional laboratory setups. These values of D_t were also used to obtain a parameterization of transverse dispersion. We consider a non-linear, compound-specific parameterization that was inspired by an earlier statistical model (Bear and Bachmat, 1967) and validated in previous studies in quasi two-dimensional experimental setups (e.g., Chiogna et al., 2010; Rolle et al., 2012) and in two-dimensional pore-scale domains (e.g., Hochstetler et al., 2013; Rolle et al., 2012):

$$D_t = D_p + D_{aq}\left(\frac{Pe^2}{Pe + 2 + 4\delta^2}\right)^{\beta} \tag{2.7}$$

where D_p [L^2/T] is the velocity-independent pore diffusion coefficient given by the ratio of the aqueous diffusion coefficient and the tortuosity of the porous medium and approximated as $D_p=nD_{aq}$, with n [-] representing the porosity of the medium. $Pe=vd/D_{aq}$ [-] is the grain Péclet number, d [L] is the average grain size, δ [-] is the ratio between the length of a pore channel and its hydraulic radius and β [-] is an empirical exponent that captures the degree of incomplete mixing within the pore channels (e.g., Chiogna and Bellin, 2013; Tartakovsky et al., 2009). Compared to the traditional linear parameterization (e.g., Scheidegger, 1961), Eq. 2.7 describes more accurately the interactions between the fundamental processes of advection and diffusion at the pore scale. In fact, in this compound-specific parameterization, D_t retains an explicit dependence of the mechanical dispersion term on the aqueous diffusion coefficient of the transported tracers at all velocities and a (possibly) non-linear relationship with the average seepage velocity, quantified by the exponent β in the mechanical dispersion term.

The same fitting procedure described above for the estimation of D_t in each experimental run was adopted to determine the values of the empirical exponent β and the geometrical parameter δ of the transverse dispersion parameterization (Eq. 2.7) from the outcomes of all multi-tracer experiments in both the quasi 2-D and the 3-D flow-through systems.

2.2.3 Evaluation of Plume Dilution

Dilution of conservative tracers in porous media can be quantified using different metrics such as the scalar dissipation rate (e.g., Bellin et al., 2011; Bolster et al., 2010; De Simoni et al., 2005) and the dilution index (e.g., Kitanidis, 1994). The dilution index is defined as the exponential of the Shannon entropy. It was introduced to quantify true mixing in porous media, as opposed to plume spreading, which is associated with the deformation and stretching of a solute plume due to the variability of the velocity field. For steady-state transport problems, a modified version of the dilution index, the flux-related dilution index, was proposed by Rolle et al. (2009). This metric expresses dilution as the "act of distributing a given solute mass flux over a larger water flux" and was applied to quantify dilution and reactive mixing in porous media at different scales (e.g., Chiogna et al., 2011b; Chiogna et al., 2012; Rolle and Kitanidis, 2014). In a three-dimensional domain, the flux-related dilution index is defined as:

$$E_Q(x) = \exp\left[-\int_{-\infty}^{+\infty}\int_{-\infty}^{+\infty} p_Q(x,y,z) \ln p_Q(x,y,z) q_x(x,y,z) dydz \right] \tag{2.8}$$

where $p_Q(x,y,z)$ is defined as:

$$p_Q(x,y,z) = \frac{c(x,y,z)}{F(x)} = \frac{c(x,y,z)}{\int_{-\infty}^{+\infty}\int_{-\infty}^{+\infty} c(x,y,z) q_x(x,y,z) dydz} \tag{2.9}$$

and $q_x(x,y,z)$ is the specific discharge [LT^{-1}].

For the analysis of the results of the flow-through experiments performed in this study, we express the flux-related dilution index in discrete form:

2-D: $$E_Q(x) = \exp\left(-\sum_{k=1}^{N_v} p_{Qk} \ln p_{Qk} q_k \Delta z W \right) \tag{2.10}$$

3-D: $$E_Q(x) = \exp\left(-\sum_{k=1}^{N_v}\sum_{j=1}^{N_h} p_{Qk,j} \ln p_{Qk,j} q_{k,j} \Delta z \Delta y \right) \tag{2.11}$$

with

2-D: $$p_{Qk} = \frac{c_k}{\sum_{k=1}^{N_v} c_k q_k} \tag{2.12}$$

and

3-D: $$p_{Qk,j} = \frac{c_{k,j}}{\sum_{k=1}^{N_v}\sum_{j=1}^{N_h} c_{k,j} q_{k,j}} \tag{2.13}$$

where c_k and $c_{k,j}$ [ML^{-3}] are the measured concentrations at each sampling port. The ports are located on a vertical array of N_v elements for the 2-D case and on a $N_v \times N_h$, array with N_v rows and N_h columns, in the 3-D setup. q_k and $q_{k,j}$ [L^3T^{-1}] are the flow rates at each port. Fig. 2.3 shows an example of how the solute mass flux is determined at the outlet of the quasi 2-D (upper plots) and the 3-D (lower plots) flow-through setups. The mass flux is calculated from the product of the flow rates and the concentrations measured at each port. Both in the quasi 2-D system, where 7 ports were sampled, and in the 3-D setup, where samples were taken from 49 outlet ports, the measured flow rates show minimal fluctuations. Considering the uniform flow rates, the uniform filling and only negligible effects of vertically asymmetric

geometry, we conjecture that uniform flow within the porous media can be assumed for the analysis of the data. The measured concentrations show a regular and symmetric behavior, characteristic of transport in homogeneous isotropic packed beds.

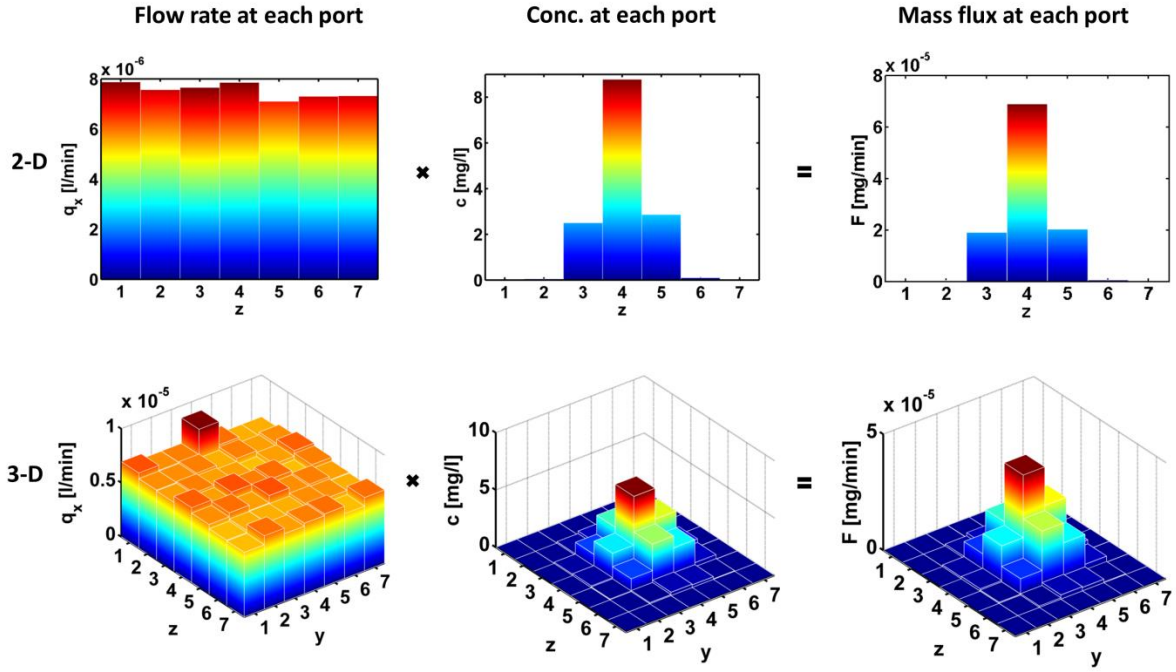

Fig. 2.3. Experimental determination of flow rates, fluorescein concentrations and mass fluxes in the quasi 2-D and 3-D flow-through systems. The numbers on the abscissae represent the outlet ports in the experimental setups.

For the 2-D and 3-D transport problems considered in this study it is possible to derive semi-analytical solutions describing the spatial evolution of the flux-related dilution index of the solute plumes. Following the approach proposed by Chiogna et al. (2011b) we assume a nested radical form for the value of the flux-related dilution index and obtain the following relations to the inverse dynamic Péclet numbers, ε_z and ε_y, in the transverse vertical and transverse horizontal directions, respectively:

2-D:
$$E_Q(\varepsilon_z) = ZWq_x\left(1-\sqrt{\frac{4\pi\varepsilon_z}{4\pi\varepsilon_z+1+f(\varepsilon_z)}}+\sqrt{4\pi\exp(1)\varepsilon_z}\right) \qquad (2.14)$$

$$E_Q(\varepsilon_y,\varepsilon_z) = YZq_x\left(1-\sqrt{\frac{4\pi\varepsilon_y}{4\pi\varepsilon_y+1+f(\varepsilon_y)}}+\sqrt{4\pi\exp(1)\varepsilon_y}\right)$$

3-D:
$$\left(1-\sqrt{\frac{4\pi\varepsilon_z}{4\pi\varepsilon_z+1+f(\varepsilon_z)}}+\sqrt{4\pi\exp(1)\varepsilon_z}\right) \qquad (2.15)$$

where, $f(\varepsilon_y)$ and $f(\varepsilon_z)$ are functions of the inverse dynamic Péclet numbers in the transverse directions, $\varepsilon_y = nxD_t/(q_xY^2)$ and $\varepsilon_z = nxD_t/(q_xZ^2)$, and W [L] is the width of the quasi 2-D setup. The derivation of these expressions is outlined in Appendix A.1.

As will be illustrated in Section 2.3.3, the predictive capability of Eqs. (2.14) and (2.15) was tested with the values of plume dilution measured for the steady-state plumes of fluorescein and oxygen established in the quasi 2-D and in the 3-D laboratory setups.

2.3 Results and Discussion

2.3.1 Concentration Measurements

Concentration profiles where measured twice at the outlet of the quasi two-dimensional and three-dimensional flow-through systems for each experimental run and each tracer solution with a time interval corresponding to half pore volume of the flow-through systems. We obtained a mean absolute difference between the two normalized concentration profiles of 5.7 $\times 10^{-3}$. In order to investigate the reproducibility of the experimental results, the experiment at 6.5 m/day was repeated after repacking the porous medium. The results were in very good agreement (mean absolute difference between the two normalized concentration profiles of 9.9 $\times 10^{-3}$), thus showing the reliability of the experimental setup. In the following we will refer to the mean value of the two measured concentrations from the two successive samplings in each flow-through experiment. In each setup, we conducted nine experiments covering flow velocities ranging from 0.5 m/day to 8 m/day. Fig. 2.4 shows the concentration distribution at the outlet of the 3-D flow-through system for the experiment with a seepage velocity of 5 m/day. The measurements are shown as normalized concentrations of fluorescein (plots on the left) and oxygen (plots on the right). Fig. 2.4a and d show 2-D maps of normalized concentration at the outlet. The white crosses indicate the location of the sampling ports, whereas the white contour lines represent the bicubic interpolation of the measured tracer concentrations at the outlet ports. The color plot in the background shows the concentration distributions computed using the analytical solution (Eq. (2.6)) fitted to the

experimental data of fluorescein and oxygen. The comparison between the measured concentrations and the outcome of the 3-D analytical model with best-fit D_t are also shown as transverse horizontal (Fig. 2.4b and e) and vertical profiles (Fig. 2.4c and f). The approximately Gaussian profiles of the analytical solution are in good agreement with the measured tracer concentrations. The experimental concentration distribution shows a slight shift towards the right, but otherwise there is no significant difference between the horizontal and vertical profiles so that fitting a single transverse dispersion coefficient appears justified.

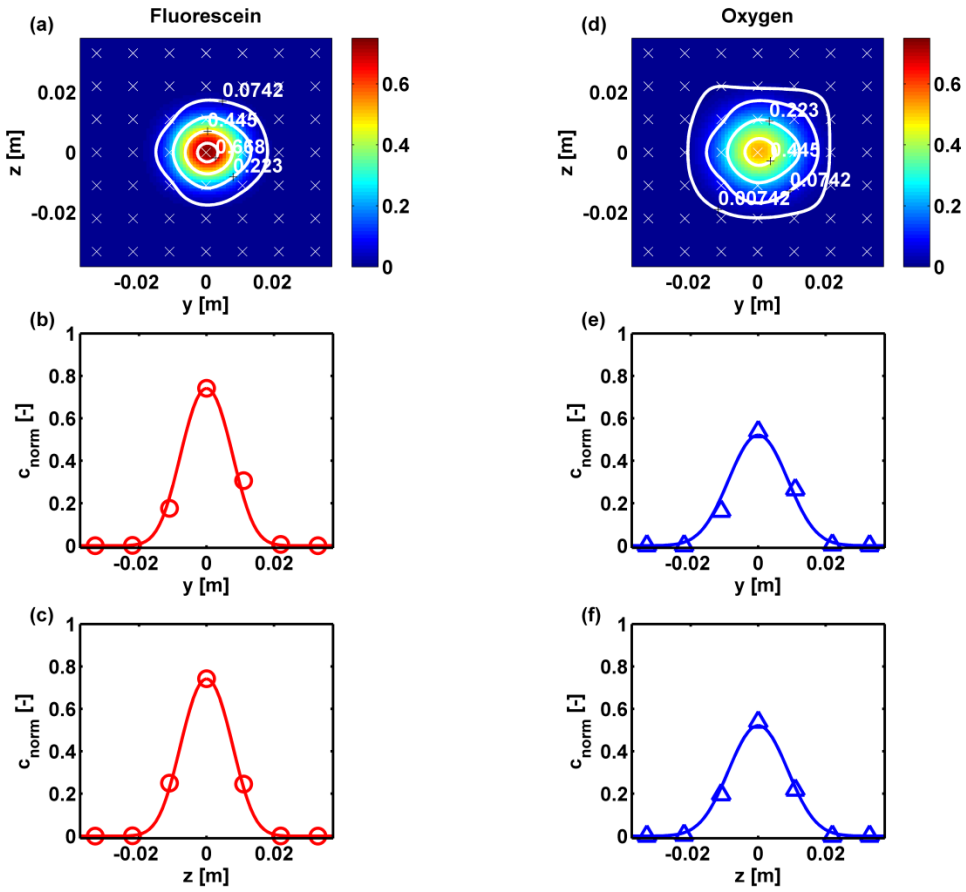

Fig. 2.4. Concentration distributions at the outlet of the 3-D flow-through system for fluorescein (a) and oxygen (d) in a flow-through experiment at 5 m/day. Measured (symbols) and simulated (lines) transverse profiles in the horizontal (b and e) and vertical (c and f) directions.

The measured peak concentrations of the two tracers differ significantly. The fluorescein plume has a remarkably higher peak concentration and is less spread in the transverse direction compared with the one of oxygen, indicating different transverse dispersion coefficients of the two tracers. Such differences for the two tracers simultaneously transported in the same porous medium arise from the different diffusivities of the two solutes and cannot be explained if one would assume the validity of a classical linear parameterization of

transverse dispersion (e.g., Scheidegger, 1961), with the additive contribution of a velocity-independent pore-diffusion term and a diffusion-independent mechanical dispersion term. In fact, at the velocity of 5 m/day at which the flow-through experiment was performed the transport regime is strongly advection-dominated and the contribution of pore diffusion to the hydrodynamic dispersion coefficient is < 17% for oxygen and < 8% for fluorescein, so that the predicted concentration distributions according to the linear parameterization would be practically identical for the two compounds. Thus, the observed differences between the two solutes confirm that also the mechanical dispersion term depends on the aqueous diffusion coefficient of the compound, as expressed in Eq. (2.7). Such compound-specific behavior has already been observed in quasi 2-D multi-tracer experiments (e.g., Chiogna et al., 2010). Pore-scale simulations (e.g., Rolle et al., 2012) allowed explaining the compound-specific behavior by the different extent of incomplete mixing and the development of compound-specific concentration gradients in the pore channels.

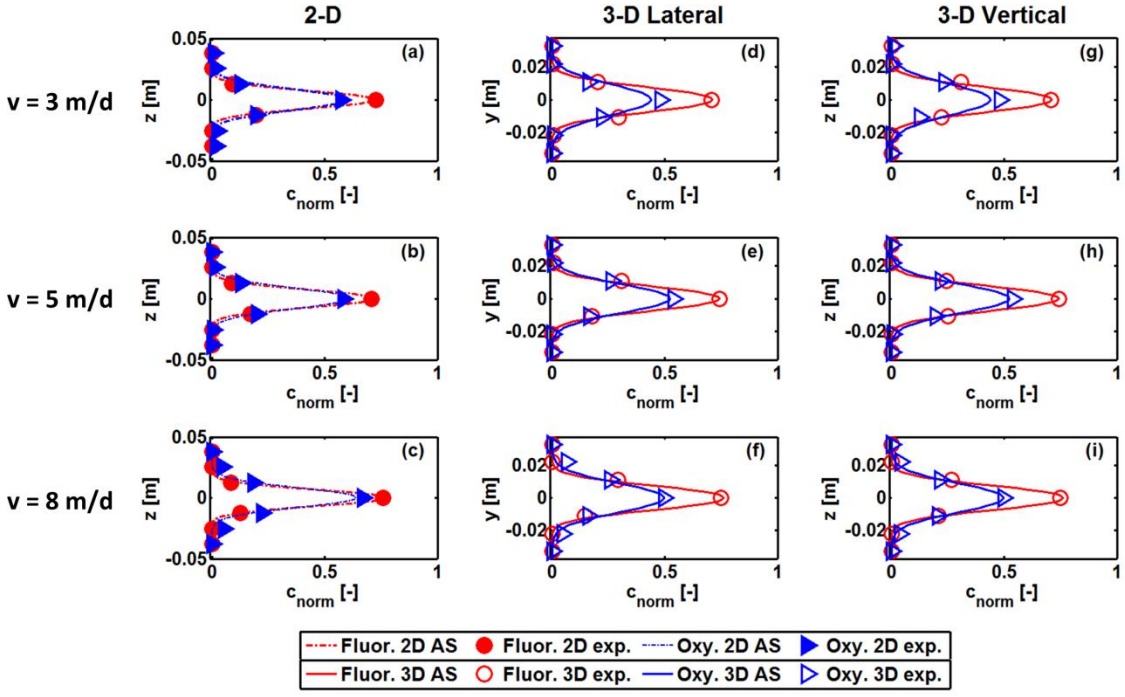

Fig. 2.5. Concentration profiles of fluorescein and oxygen at the outlet of the quasi 2-D setup (a-c) and of the 3-D system in the transverse horizontal (d–f) and vertical (g–i) directions. The experiments were performed at seepage velocities of 3 m/day, 5 m/day and 8 m/day.

Fig. 2.5 shows a comparison between the concentration profiles of fluorescein and oxygen in the quasi 2-D and 3-D setups for three distinct advection-dominated conditions, at flow velocities of 3, 5, and 8 m/day. Distinct quasi-Gaussian profiles are obtained for the two tracers at the outlet of the quasi 2-D (plots a–c) and 3-D experimental setups (plots d–i).

However, the differences in peak concentration among the compounds are significantly more pronounced in the 3-D (37%–50%) than in the 2-D (13%–28%) setup for all velocities. This is consistent with the peak concentration scaling with with $D_t^{-1/2}$ in 2-D, and with D_t^{-1} in 3-D, if the source is sufficiently small. Thus, the 3-D setup is better suited to appreciate the dependence of transverse mixing on compound-specific diffusivity than the quasi 2-D setup.

2.3.2 Transverse Dispersion Coefficients

Table 2.1 lists all fitted transverse dispersion coefficients D_t for fluorescein and oxygen in both setups at all flow velocities. The mean relative difference in the transverse dispersion coefficients estimated using the two concentration profiles measured for each experimental run is equal to 3%, while the mean relative uncertainty on the estimated D_t values varies between 10% and 15%, for fluorescein and oxygen, respectively. In the following we will refer to the mean value of the transverse dispersion coefficient. We used these values to estimate the parameters δ and β of the compound-specific parameterization according to Eq. (2.7).

Table 2.1. Summary of the flow-through experiments and values of transverse dispersion coefficients and flux-related dilution index at the inlet and at the outlet.

v [m/day]	$D_{t,fluor}$ [m^2/s]	$D_{t,oxy}$ [m^2/s]	$E_{Q,in}$ [m^3/s]	$E_{Q,fluor}$ [m^3/s]	$E_{Q,oxy}$ [m^3/s]
2-D Setup					
0.485	5.74×10^{-10}		3.23×10^{-10}	8.37×10^{-10}	
0.729	7.15×10^{-10}		4.85×10^{-10}	1.20×10^{-9}	
0.951	9.23×10^{-10}		6.47×10^{-10}	1.53×10^{-9}	
1.43	1.22×10^{-9}	3.06×10^{-9}	9.70×10^{-10}	2.18×10^{-9}	2.57×10^{-9}
2.95	2.09×10^{-9}	3.51×10^{-9}	1.93×10^{-9}	4.10×10^{-9}	6.04×10^{-9}
4.01	2.49×10^{-9}	4.76×10^{-9}	2.58×10^{-9}	5.39×10^{-9}	8.42×10^{-9}
4.97	3.57×10^{-9}	5.70×10^{-9}	3.25×10^{-9}	6.82×10^{-9}	8.46×10^{-9}
6.39	3.93×10^{-9}	6.62×10^{-9}	4.18×10^{-9}	8.26×10^{-9}	1.24×10^{-8}
7.84	4.53×10^{-9}	7.76×10^{-9}	5.17×10^{-9}	1.00×10^{-8}	1.66×10^{-8}
3-D Setup					
0.49	6.21×10^{-10}		5.37×10^{-10}	3.08×10^{-9}	
0.769	8.55×10^{-10}		8.55×10^{-10}	4.12×10^{-9}	
1.02	9.36×10^{-10}		1.14×10^{-9}	4.85×10^{-9}	
1.46	1.25×10^{-9}	3.77×10^{-9}	1.63×10^{-9}	6.75×10^{-9}	1.64×10^{-8}
2.89	1.65×10^{-9}	3.60×10^{-9}	3.12×10^{-9}	1.23×10^{-8}	1.36×10^{-8}
3.99	2.43×10^{-9}	5.30×10^{-9}	4.33×10^{-9}	1.64×10^{-8}	2.08×10^{-8}
4.81	2.51×10^{-9}	4.67×10^{-9}	5.43×10^{-9}	1.93×10^{-8}	2.13×10^{-8}
6.42	3.78×10^{-9}	6.82×10^{-9}	7.13×10^{-9}	2.45×10^{-8}	4.76×10^{-8}
8.03	3.94×10^{-9}		9.08×10^{-9}	3.08×10^{-8}	
8.25		8.39×10^{-9}	9.13×10^{-9}		5.07×10^{-8}

The values for δ and β, fitted independently for the two tracers and the two setups, are listed in Table 2.2 together with their 95% confidence intervals. The two parameters have been

computed according to the non-linear least squared method described in Rolle et al. (2012), in which the estimated error depends on the measurement error of D_t and on the sensitivity to the parameters. The fitted coefficients are comparable among the quasi 2-D and 3-D experiments and between the two tracers. The δ values obtained from the fluorescein concentrations are slightly larger than those from oxygen, whereas the β-values are slightly smaller for fluorescein. Like in previous quasi 2-D experiments (e.g., Chiogna et al., 2010; Rolle et al., 2012), the exponent β is close to 0.5, indicating a dependence of transverse dispersion on the square root of the grain Péclet number (Pe) at high flow velocities.

Table 2.2. Fitted parameters β and δ of the compound-specific transverse dispersion parameterization according to Eq. 7. Mean: best-fit solution, CI: confidence interval.

Solute	Tank dimension	β		δ	
		Mean	**95% CI**	**Mean**	**95% CI**
Fluorescein	2-D	0.53	0.51 – 0.56	3.6	3.2 – 4.0
	3-D	0.47	0.43 – 0.52	3.3	2.5 – 4.0
Oxygen	2-D	0.56	0.48 – 0.64	2.7	2.1 – 3.2
	3-D	0.55	0.30 – 0.80	2.6	1.0 – 4.3

Fig. 2.6 shows the transverse dispersion coefficients obtained in the quasi 2-D and 3-D experiments as a function of the seepage velocity. The continuous lines represent compound-specific parameterization of D_t according to Eq. (2.7) with β and δ parameters determined by the simultaneous fit of the 2-D and 3-D data (β = 0.50 and δ = 3.4 for fluorescein; β = 0.55 and δ = 2.6 for oxygen). The results for fluorescein are presented in Fig. 2.6a while the ones for oxygen are shown in Fig. 2.6b. The nonlinear relationship consistently explains the dependence of D_t on velocity and the remarkable differences among compounds. The agreement between the experimental data in the 3-D (full symbols) and quasi 2-D (empty symbols) setups and Eq. (2.7) is satisfactory for both fluorescein and oxygen. For oxygen, the data from the experiments at low flow velocities were not considered in the analysis (and not shown in Table 2.1 and in Fig. 2.6b) since, under such low flow conditions, the oxygen concentrations at the outlet are too homogeneously distributed along the transverse profiles to provide a reliable estimation of the transverse dispersion coefficient. The good agreement between the values of D_t determined in the quasi 2-D and 3-D setups for both fluorescein and oxygen shows that although the dimensionality of the system clearly influences the measured concentrations at the outlet (Fig. 2.5), it does not affect the estimation of the parameter controlling transverse mixing. In fact, consistent values of transverse dispersion coefficients were obtained from the experimental results in the quasi two-dimensional and in the three-dimensional porous media.

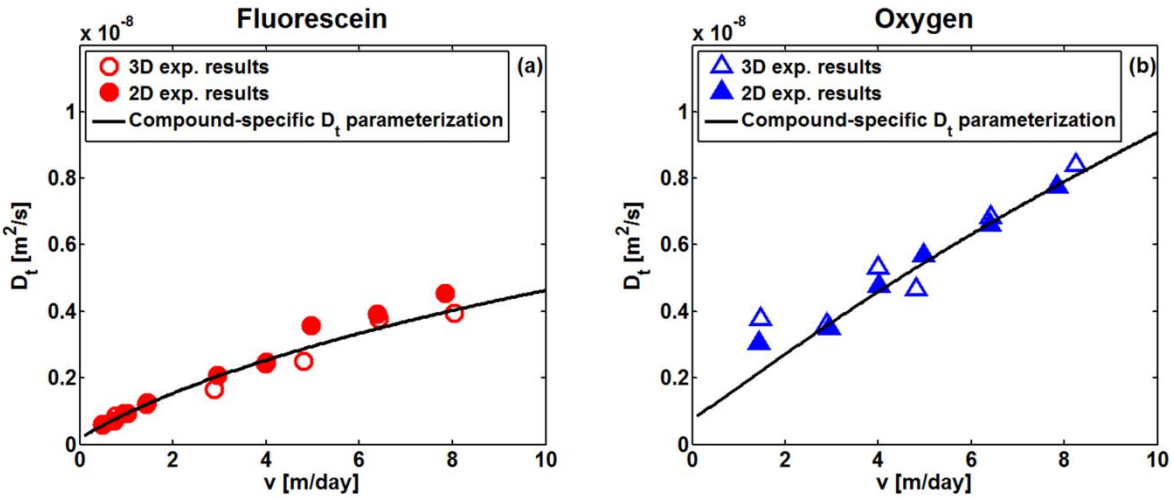

Fig. 2.6. Relationship between the transverse dispersion coefficient and the seepage velocity: experimental data (symbols) and compound-specific parameterization (lines) for fluorescein (a) and for oxygen (b).

Although it does not affect the estimation of the transverse dispersion coefficient, the dimensionality of the system plays an important role in the interpretation of the experimental results. To illustrate this point in Fig. 2.7a we report the vertical profiles of a 3-D flow-through experiment at 4.81 m/day, using fluorescein as a tracer. The results show that interpreting such measurements with a purely 2-D approach (Eq. (2.4)) leads to more than 50% overestimation of the D_t value determined with a correct 3-D interpretation using Eq. (2.6). Such overestimation reduces to 10% in case the tracer is injected from a wider source (i.e., 3 central horizontal ports in the 3-D setup) as shown in Fig. 2.7b. As shown for example by the modeling study of Liedl et al. (2011), such dimensionality effects have important implications in predicting mixing-controlled reactive transport.

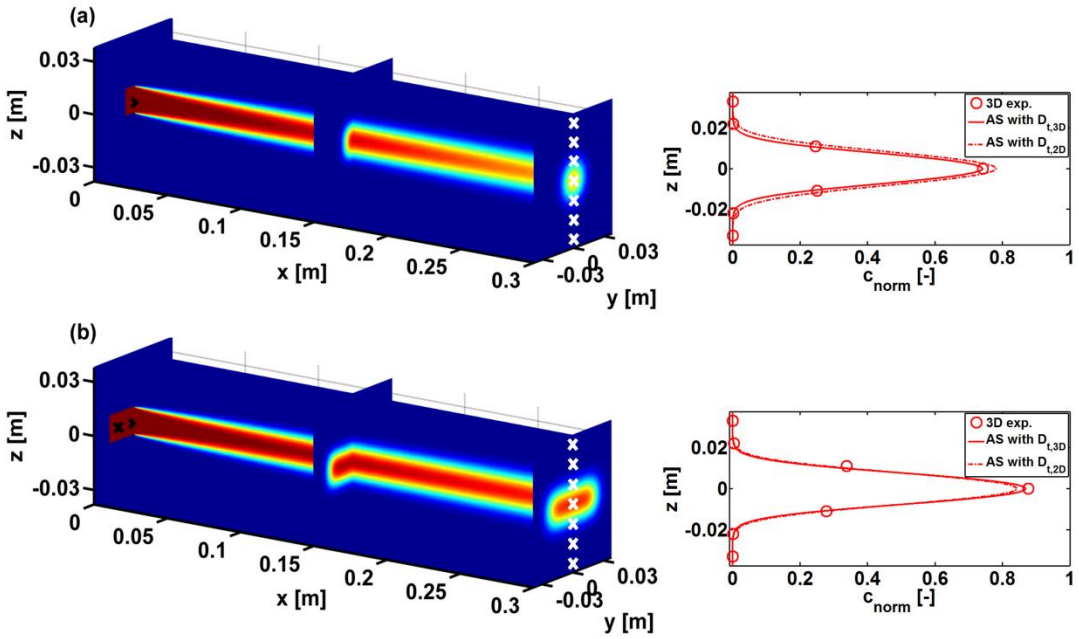

Fig. 2.7. Steady-state fluorescein plumes and vertical concentration profiles at the center of the 3-D flow-through system for the cases: (a) tracer injection from a single central inlet port and (b) tracer injection from three inlet ports in the central row.

To conclude the discussion on transverse dispersion coefficients, we compare in Fig. 2.8 the experimental results of this study with literature data (e.g., Blackwell, 1962; Chiogna et al., 2010; Grane and Gardner, 1961; Harleman and Rumer, 1964; Olsson and Grathwohl, 2007; Schwille, 1988; Seagren et al., 1999). The results are plotted as inverse dynamic Péclet number (D_t/vd) as a function of the grain Péclet number (Pe). In the same figure, we present the result of Eq. (2.7) considering the average values of β and δ (0.5 and 5.37, respectively) from these and previous multi-tracer experiments performed in porous media with different grain sizes (e.g., Chiogna et al., 2010; Rolle et al., 2012). The non-linear model captures the trend of the experimental data in the range of Péclet numbers between 10^{-1} and 10^{4}. For higher Pe numbers, the effects of inertia on flow cannot be neglected anymore, and the assumption of creeping flow in porous media becomes invalid (e.g., Bear, 1972). Fig. 2.8 also shows the classical linear parameterization of the transverse dispersion coefficient assuming a diffusion-independent mechanical dispersion term:

$$\frac{D_t}{vd} = \frac{n}{Pe} + C \tag{2.16}$$

in which C is a dimensionless constant term, set to 3/16 (e.g., Saffman, 1959). The linear parameterization predicts a constant value for the inverse dynamic Péclet number when Pe is

larger than 10 and does not allow reproducing the behavior observed in the flow-through experiments.

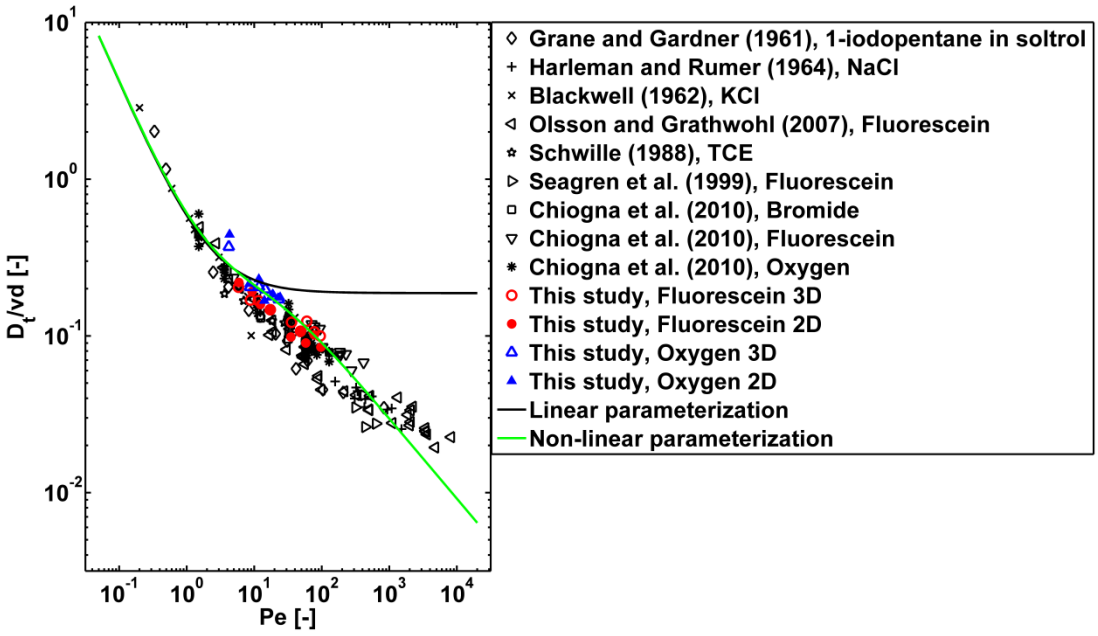

Fig. 2.8. Comparison between literature data on transverse dispersion in porous media (black symbols) and the results of this study in the quasi 2-D (full color symbols) and 3-D (empty color symbols) setups. The lines indicate the classical linear (black) and the non-linear compound-specific D_t parameterizations (green).

2.3.3 Plume Dilution

Mass-flux measurements were performed at the inlet and at the outlet of the quasi two-dimensional and three-dimensional flow-through systems by measuring flow rates and concentrations at the highly spatially-resolved sampling ports. The mean absolute difference in the mass fluxes measured at a time interval corresponding to half pore volume was 8.7×10^{-6} mg/min. With such measurements, it was possible to experimentally evaluate the flux-related dilution index of the steady-state plumes at the inlet and at the outlet of the flow-through setup using Eqs. (2.10) and (2.11). Thus, for each experiment at a given flow velocity values of the flux-related dilution index in the quasi 2-D and 3-D setups were available for the fluorescein and for the oxygen plumes. As an illustrative example, Fig. 2.9 shows the results for the flow-through experiments carried out at a seepage velocity of 8 m/day. At the inlet, the flux-related dilution indices of fluorescein and oxygen are identical since the tracers are injected through the same inlet port. At the outlet, the fluorescein plumes are considerably less diluted than the oxygen plumes since the compounds underwent compound-specific

transverse mixing in the porous media. The values of flux-related dilution index measured in the quasi 2-D system indicate that the oxygen mass flux is distributed over a volumetric discharge larger than the one carrying fluorescein. The different dilution between the fluorescein and oxygen plumes is even more remarkable in the 3-D setup. The proposed analytical solutions for the 2-D and 3-D transport problems (Eqs. (2.14) and (2.15)) allow the computation of the flux-related dilution index inside the porous media. The results (continuous and dash–dot lines in Fig. 2.9) show that the flux-related dilution index monotonically increases for both tracers and the rate of increase is higher for oxygen, since the dilution of this solute in the porous media is more effective than the one of fluorescein due to its higher transverse dispersion coefficient. The agreement between experimental data and the analytical solutions is very good for the fluorescein plumes in both the quasi 2-D and 3-D systems, whereas the semi-analytical solutions for oxygen slightly underestimate the dilution of the steady-state plumes compared with the measured values. We believe that the latter discrepancy is an experimental artifact that is related to the higher accuracy of fluorescein concentrations, which can be measured over seven orders of magnitude, in comparison with those of oxygen, which can be determined over a considerably smaller range (i.e., three orders of magnitude). Notice that the semi-analytical solutions for E_Q (Eqs. (2.14) and (2.15)) were applied directly without any additional fitting using the values of the transverse dispersion evaluated from the concentration profiles measured at the outlet of the flow-through systems.

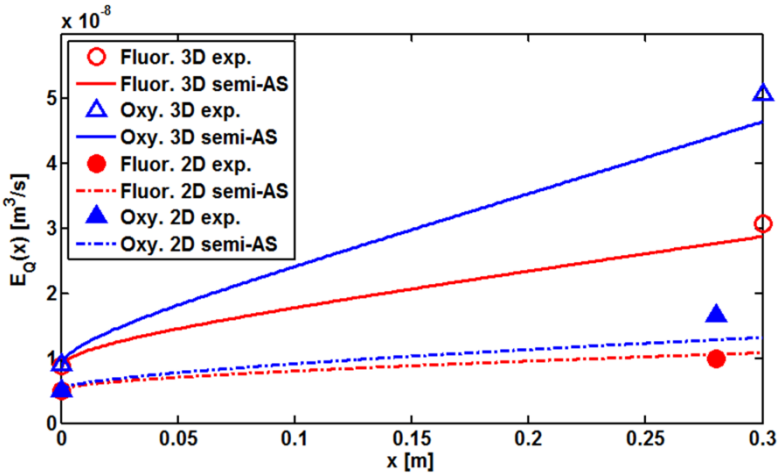

Fig. 2.9. Flux-related dilution index along the longitudinal direction in the quasi 2-D and 3-D flow-through systems.

The analysis of plume dilution was carried out for every experimental run. Table 2.1 lists the values of the flux-related dilution index for fluorescein and oxygen in all experiments. These results are also plotted in Fig. 2.10 as a function of the seepage velocity. The results show an

increasing dilution of the steady-state plumes with increasing flow velocity. While the dimensionality of the problem does not affect the value of the determined transverse dispersion coefficient that is the same in the quasi 2-D and 3-D setups for any given flow velocity (Fig. 2.6), dilution is considerably more effective in the three-dimensional domain than in the quasi 2-D system. This finding provides an experimental validation of the theory developed by Kitanidis (1994), for which dilution of a solute plume is a process depending on the dimensionality of the problem. The predictions of the proposed semi-analytical solutions are in very good agreement with the experimental data of fluorescein in both the quasi 2-D and the 3-D systems (Fig. 2.10a). The oxygen data show more scattering, in particular in the 3D setup; however, the semi-analytical predictions still capture the distinct dilution trends in both quasi 2-D and 3-D setups (Fig. 2.10b).

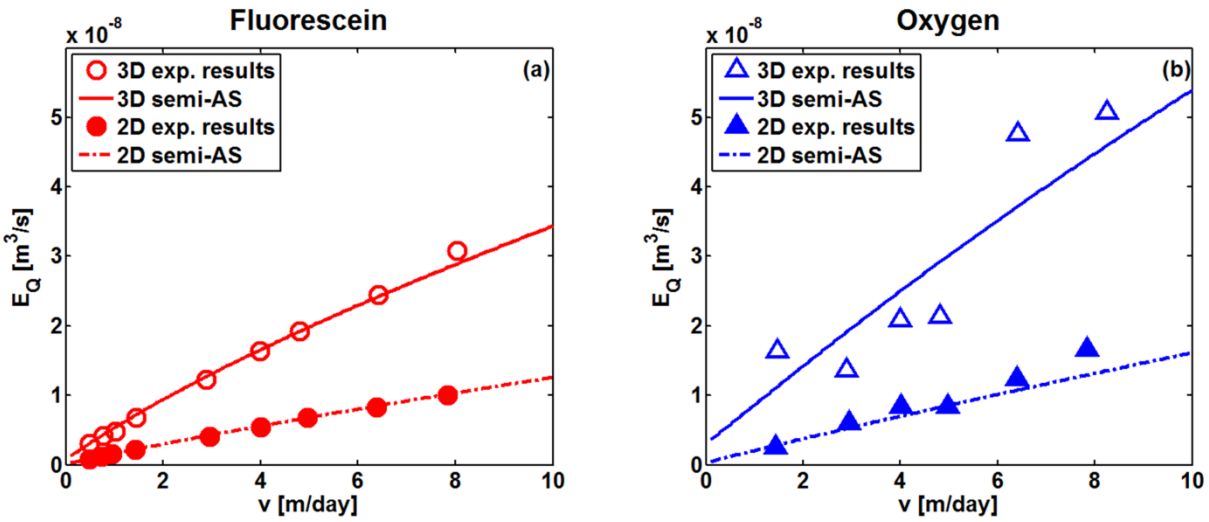

Fig. 2.10. Relationship between the flux-related dilution index and the seepage velocity in the quasi 2-D and 3-D setups: experimental data and interpretation with the semi-analytical solution for fluorescein (a) and for oxygen (b).

As observed from the analysis of the concentration profiles at the outlet (Figs. 2.4 and 2.5), also the measured and simulated values of the flux-related dilution index show a clear compound-specific behavior across the whole range of seepage velocities. Such compound-specific differences are more pronounced in the three-dimensional case and have significant implications for mixing-controlled reactive transport processes. For instance, this will influence transport of organic contaminants in groundwater, in particular when the release occurs from a small or point source, since important biodegradation reactions occur in a thin 3-D fringe zone surrounding a three-dimensional contaminant plume.

2.4 Summary and Conclusions

In this study we experimentally investigated transverse mixing in homogeneous, isotropic porous media using quasi two-dimensional and three-dimensional flow-through systems. To this end, we designed a fully 3-D laboratory setup in which we measured the outlet concentration of dissolved compounds and the volumetric flow rate at high spatial resolution (i.e., in 49 outlet ports). The direct comparison between the results of the quasi 2-D and the 3-D systems is illustrative of the influence of transport dimensionality on plume dilution. In fact, the results show a strong enhancement of plume dilution in the fully three-dimensional system in comparison with the quasi 2-D setup where transverse dispersion acts only in one direction. We quantified the degree of plume dilution using the flux-related dilution index, E_Q. This quantitative metric of mixing was up to three times larger for the fully 3-D plumes compared with those in the quasi 2-D system. We also presented closed-form approximations of E_Q for steady-state plumes in uniform flow, which were in agreement with the observed data.

Although the transport dimensionality had a strong influence on the concentrations measured at the outlet of the flow-through systems and on the dilution of steady-state plumes, it did not affect the value of the parameter controlling lateral mixing: the transverse dispersion coefficient. In fact, for a specific compound and at any given seepage velocity, a good agreement was found between the values of D_t determined in the quasi 2-D and 3-D systems, confirming that the quasi 2-D and 3-D experiments were fully consistent. The parameterization of D_t is critical to properly describe solute transport under different flow-through conditions. In both the quasi 2-D and 3-D setups a non-linear compound-specific D_t parameterization, acknowledging the dependence of the mechanical dispersion term on the diffusive properties of the transported solute (e.g., Chiogna et al., 2010; Rolle et al., 2012), was necessary to interpret the experimental observations. The multi-tracer experiments performed in this study showed that the compound-specific description of transverse dispersion is particularly needed in predicting fully three-dimensional plumes. This has also implications for mixing-controlled reactive transport. For instance, in a theoretical study, Liedl et al. (2011) showed a significant difference of steady-state reactive plume lengths in uniform flow when a fully three-dimensional solution was adopted in contrast to a 2-D representation (e.g., Liedl et al., 2005).

Upscaling to effective transverse mixing in more complex flow fields remains an open question. In a recent study restricted to two-dimensional systems, Rolle et al. (2013a) showed

that the effects of compound-specific diffusive processes, occurring at the scale of a pore channel, propagate at larger macroscopic scales and have a significant impact both on transient and steady-state transport of conservative and reactive species. For 2-D porous media, Werth et al. (2006) showed that transverse mixing is enhanced in zones of high velocity, which was experimentally confirmed by Bauer et al. (2009). Chiogna et al. (2011a) and Cirpka et al. (2011) could show by numerical and theoretical studies that the compound-specific effects of transverse dispersion do not vanish in heterogeneous two-dimensional systems, despite mixing enhancement by flow focusing. Truly three-dimensional flow fields in heterogeneous anisotropic media, however, may lead to complex flow topologies involving for example intertwining streamlines (e.g., Bakker and Hemker, 2004). This may facilitate mixing mechanisms that are impossible in homogeneous or two-dimensional heterogeneous domains (e.g., Chiogna et al., 2014). Thus, more research is needed to analyze the importance of compound-specific local-scale transverse dispersion on macroscopic transverse mixing in real geological formations. We are convinced that well designed 3-D bench-scale experiments can contribute to answer these questions.

Acknowledgments

This study was supported by the Deutsche Forschungsgemeinschaft (DFG), grants RO 4169/3-1 and CI-26/11-1. M.R. also acknowledges the support of the Marie Curie International Outgoing Fellowship (DILREACT project, grant 273049) within the 7th European Community Framework Programme.

Appendix A. Semi-analytical solutions for the flux-related dilution index of steady-state plumes in homogeneous porous media

Table A1. Analytical solutions for the flux-related dilution index at the asymptotic limits.

Limit	Interpretation	Line source (quasi 2-D[a]) theoretical E_Q	Square source (3-D) theoretical E_Q
$\varepsilon_z \to 0, \varepsilon_y \to 0$	Dilution at the source	ZWq_x	YZq_x
$\varepsilon_z \to \infty, \varepsilon_y \to \infty$	Dilution at infinite distance from the source	$W\sqrt{4\pi\, exp(1)\, nxD_t q_x}$	$4\pi\, exp(1)\, nxD_t$

[a] Uniform concentration is assumed along the width W of the quasi 2-D domain

We consider the dilution of steady-state plumes for the cases of continuous release from (i) a line source in a quasi 2-D homogeneous domain and (ii) a square source in a 3-D homogeneous porous medium. In both cases the semi-analytical expressions for the flux-related dilution index under steady-state flow and transport conditions have to satisfy the two asymptotic limits reported in Table A1.

Considering the constraints given in Table A1, Chiogna et al. (2011a) derived the following semi-analytical expression for the estimation of the flux-related dilution index in a quasi 2-D domain:

$$E_Q(\varepsilon_z) = ZWq_x\left(1 - \sqrt{\frac{4\pi\varepsilon_z}{4\pi\varepsilon_z + 1}} + \sqrt{4\pi \exp(1)\varepsilon_z}\right) \qquad \text{(A1)}$$

where Z is the source thickness, W is the width of the quasi 2-D domain, q_x is the longitudinal component of the specific discharge and ε_z represents the inverse dynamic Péclet numbers. The first radical term in Eq. (A1) is a function allowing the transition between the two limiting cases expressed in Table A1.

The direct extension of Eq. A1 to the 3-D case leads to an underestimation of the dilution index, when compared with the numerical integration of Eq. 8. Therefore, in this work we consider a slightly modified version of the first square root term, introducing a correction factor $f(\varepsilon_z) = \sqrt{a\varepsilon_z}$, which allows improving the match with the direct numerical integration of Eq. 8 both for the 2-D and the 3-D cases (see Fig. A1). The semi-analytical expressions for the flux-related dilution index in the quasi 2-D and 3-D cases read as:

2-D:
$$E_Q(\varepsilon_z) = ZWq_x\left(1-\sqrt{\frac{4\pi\varepsilon_z}{4\pi\varepsilon_z+1+f(\varepsilon_z)}}+\sqrt{4\pi\exp(1)\varepsilon_z}\right) \quad \text{(A2)}$$

3-D:
$$E_Q(\varepsilon_y,\varepsilon_z) = YZq_x\left(1-\sqrt{\frac{4\pi\varepsilon_y}{4\pi\varepsilon_y+1+f(\varepsilon_y)}}+\sqrt{4\pi\exp(1)\varepsilon_y}\right)$$
$$\left(1-\sqrt{\frac{4\pi\varepsilon_z}{4\pi\varepsilon_z+1+f(\varepsilon_z)}}+\sqrt{4\pi\exp(1)\varepsilon_z}\right) \quad \text{(A3)}$$

in which the best-fit procedure over a wide range of inverse dynamic Péclet numbers yields a value of the parameter a=5, thus resulting in the correction terms: $f(\varepsilon_y)=\sqrt{5\varepsilon_y}$ and $f(\varepsilon_z)=\sqrt{5\varepsilon_z}$.

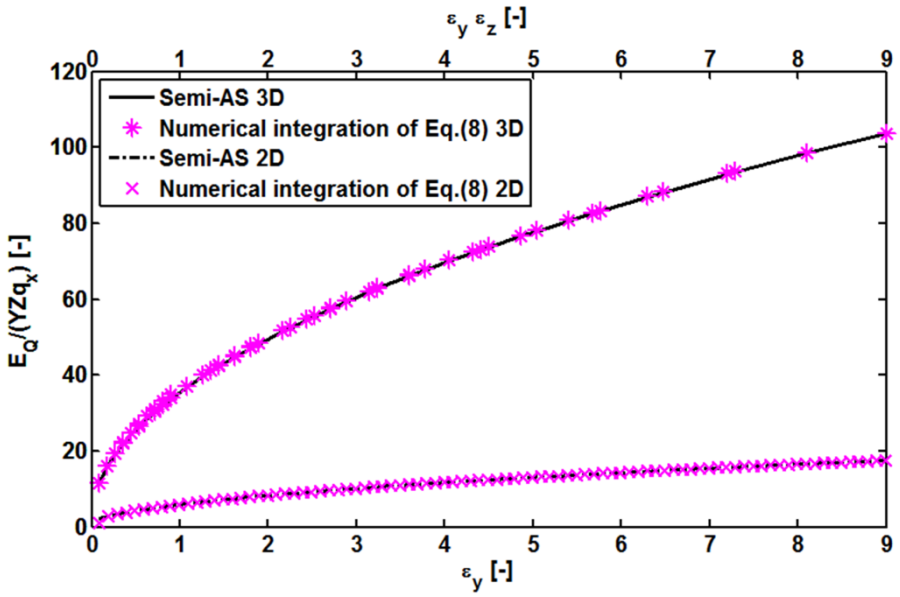

Fig. A1. Comparison of the flux-related dilution index computed by numerical integration of Eq. (2.8) and with the semi-analytical solutions Eqs. (A2) and (A3).

References

Acharya, R.C., Valocchi, A.J., Werth, C.J., Willingham, T.W., 2007. Pore-scale simulation of dispersion and reaction along a transverse mixing zone in two-dimensional porous media.Water Resour. Res. 43 (10).

Amos, R.T., Berkins, B.A., Delin, G.N., Cozzarelli, I.M., Blowes, D.W., Kirshtein, J.D., 2011. Methane oxidation in a crude oil contaminated aquifer: delineation of aerobic reactions at the plume fringes. J. Contam. Hydrol. 125, 13–25.

Anneser, B., Einsiedl, F.,Meckenstock, R.U., Richters, L., Wisotzky, F., Griebler, C., 2008. High-resolution monitoring of biogeochemical gradients in a tar oil-contaminated aquifer. Appl. Geochem. 23 (6), 1715–1730.

Atkins, P.W., 1990. Physical Chemistry. Oxford University Press, Oxford, UK.

Bakker, M., Hemker, K., 2004. Analytic solutions for groundwater whirls in box-shaped, layered anisotropic aquifers. Adv. Water Resour. 27 (11), 1075–1086.

Bauer, R.D., Rolle, M., Bauer, S., Eberhardt, C., Grathwohl, P., Kolditz, O., Meckenstock, R.U., Griebler, C., 2009. Enhanced biodegradation by hydraulic heterogeneities in petroleum hydrocarbon plumes. J. Contam. Hydrol. 105 (1–2), 56–68.

Bear, J., 1972. Dynamics of Fluids in Porous Media. Dover Publications, New York.

Bear, J., Bachmat, Y., 1967. A generalized theory on hydrodynamic dispersion in porousmedia. IASH Symposiumon Artificial Recharge and Management of Aquifers, Haifa, Israel IASH, P.N. 72, pp. 7–16

Bellin, A., Severino, G., Fiori, A., 2011. On the local concentration probability density function of solutes reacting upon mixing. Water Resour. Res. 47 (1), W01514.

Bijeljic, B., Blunt, M.J., 2007. Pore-scale modeling of transverse dispersion in porous media. Water Resour. Res. 43 (12).

Blackwell, R.J., 1962. Laboratory studies of microscopic dispersion phenomena. Soc. Petrol. Eng. J. 225, 1–8.

Bolster, D., Benson, D.A., Le Borgne, T., Dentz, M., 2010. Anomalous mixing and reaction induced by super diffusive nonlocal transport. Phys. Rev. E. 82 (2), 021119.

Castro-Alcala, E., Fernandez-Garcia, D., Carrera, J., Bolster, D., 2012. Visualization of mixing processes in a heterogeneous sand box aquifer. Environ. Sci. Technol. 46 (6), 3228–3235.

Chiogna, G., Bellin, A., 2013. Analytical solution for reactive solute transport considering incomplete mixing within a reference elementary volume. Water Resour. Res. 49 (5), 2589–2600.

Chiogna, G., Eberhardt, C., Grathwohl, P., Cirpka, O.A., Rolle, M., 2010. Evidence of compound-dependent hydrodynamic and mechanical transverse dispersion by multitracer laboratory experiments. Environ. Sci. Technol. 44 (2), 688–693.

Chiogna, G., Cirpka, O.A., Grathwohl, P., Rolle, M., 2011a. Transverse mixing of conservative and reactive tracers in porous media: quantification through the concepts of flux-related and critical dilution indices. Water Resour. Res. 47.

Chiogna, G., Cirpka, O.A., Grathwohl, P., Rolle, M., 2011b. Relevance of local compound-specific transverse dispersion for conservative and reactive mixing in heterogeneous porous media. Water Resour. Res. 47 (7).

Chiogna, G., Hochstetler, D.L., Bellin, A., Kitanidis, P.K., Rolle, M., 2012. Mixing, entropy and reactive solute transport. Geophys. Res. Lett. 39.

Chiogna, G., Rolle, M., Bellin, A., Cirpka, O.A., 2014. Helicity and flow topology in three-dimensional anisotropic porous media. Adv. Water Resour. 73, 134–143.

Cirpka, O.A., Frind, E.O., Helmig, R., 1999. Numerical simulation of biodegradation controlled by transverse mixing. J. Contam. Hydrol. 40 (2), 159–182.

Cirpka, O.A., de Barros, F.P.J., Chiogna, G., Rolle, M., Nowak, W., 2011. Stochastic flux-related analysis of transverse mixing in two-dimensional heterogeneous porous media. Water Resour. Res. 47.

Cirpka, O.A., Rolle, M., Chiogna, G., de Barros, F.P., Nowak, W., 2012. Stochastic evaluation of mixing-controlled steady-state plume lengths in two-dimensional heterogeneous domains. J. Contam. Hydrol. 138–139, 22–39.

Coleman, T.F., Li, Y., 1996. An interior, trust region approach for nonlinear minimization subject to bounds. SIAM J. Optim. 6, 418–445.

Danquigny, C., Ackerer, P., Carlier, J.P., 2004. Laboratory tracer tests on three-dimensional reconstructed heterogeneous porous media. J. Hydrol. 294 (1–3), 196–212.

Davis, G.B., Barber, C., Power, T.R., Thierrin, J., Patterson, B.M., Rayner, J.L.,Wu, Q., 1999. The variability and intrinsic remediation of a BETX plume in anaerobic sulphate-rich groundwater. J. Contam. Hydrol. 36, 265–290.

de Anna, P., Jimenez-Martinez, J., Tabuteau, H., Turuban, R., Le Borgne, T., Derrien, M., Meheust, Y., 2014. Mixing and reaction kinetics in porous media: an experimental pore scale quantification. Environ. Sci. Technol. 48 (1), 508–516.

De Simoni,M., Carrera, J., Sánchez-Vila, X., Guadagnini, A., 2005. A procedure for the solution of multicomponent reactive transport problems. Water Resour. Res. 41 (11),W11410.

Delgado, J.M.P.Q., 2006. A critical review of dispersion in packed beds. Heat Mass Transf. 42 (4), 279–310.

Domenico, P.A., Palciauskas, V.V., 1982. Alternative boundaries in solid waste management. Ground Water 20 (3), 303–311.

Gheith, H.M., Schwartz, F.W., 1998. Electrical and visual monitoring of small scale three-dimensional experiments. J. Contam. Hydrol. 34 (3), 191–205.

Grane, F.E., Gardner, G.H.F., 1961. Measurements of transverse dispersion in granular media. J. Chem. Eng. Data 6, 283–287.

Haberer, C.M., Rolle, M., Liu, S., Cirpka, O.A., Grathwohl, P., 2011. A high-resolution non-invasive approach to quantify oxygen transport across the capillary fringe and within the underlying groundwater. J. Contam. Hydrol. 122 (1–4), 26–39.

Haberer, C.M., Rolle, M., Cirpka, O.A., Grathwohl, P., 2012. Oxygen transfer in a fluctuating capillary fringe. Vadose Zone J. http://dx.doi.org/10.2136/ vzj2011.0056.

Haberer, C.M., Rolle, M., Cirpka, O.A., Grathwohl, P., 2014. Impact of heterogeneity on oxygen transfer in a fluctuating capillary fringe. Ground Water http://dx.doi.org/10.1111/gwat.12149.

Harleman, D.R.F., Rumer, R.R., 1964. Longitudinal and lateral dispersion in an isotropic porous medium. J. Fluid Mech. 16 (03), 385–394.

Herrera, P.A., Massabó, M., Beckie, R.D., 2009. A meshless method to simulate solute transport in heterogeneous porous media. Adv. Water Resour. 32 (3), 413–429.

Herrera, P.A., Valocchi, A.J., Beckie, R.D., 2010. A multidimensional streamline-based method to simulate reactive solute transport in heterogeneous porous media. Adv.Water Resour. 33 (7), 711–727.

Hochstetler, D.L., Rolle, M., Chiogna, G., Haberer, C.M., Grathwohl, P., Kitanidis,

P.K., 2013. Effects of compound-specific transverse mixing on steady-state reactive plumes: Insights from pore-scale simulations and Darcy-scale experiments. Adv. Water Resour. 54, 1–10.

Kitanidis, P.K., 1994. The concept of the dilution index. Water Resour. Res. 30 (7), 2011–2026.

Klenk, I.D., Grathwohl, P., 2002. Transverse vertical dispersion in groundwater and the capillary fringe. J. Contam. Hydrol. 58 (1–2), 111–128.

Klise, K.A., Tidwell, V.C., McKenna, S.A., 2008. Comparison of laboratory-scale solute transport visualization experiments with numerical simulation using cross-bedded sandstone. Adv.Water Resour. 31 (12), 1731–1741.

Knutson, C., Valocchi, A.,Werth, C., 2007. Comparison of continuum and pore-scale models of nutrient biodegradation under transverse mixing conditions. Adv. Water Resour. 30 (6–7), 1421–1431.

Liedl, R., Valocchi, A.J., Dietrich, P., Grathwohl, P., 2005. Finiteness of steady state plumes. Water Resour. Res. 41 (12).

Liedl, R., Yadav, P.K., Dietrich, P., 2011. Length of 3-Dmixing-controlled plumes for a fully penetrating contaminant sourcewith finitewidth. Water Resour. Res. 47.

Maier, U., Grathwohl, P., 2006. Numerical experiments and field results on the size of steady state plumes. J. Contam. Hydrol. 85, 33–52.

McNeil, J.D., Oldenborger, G.A., Schincariol, R.A., 2006. Quantitative imaging of contaminant distributions in heterogeneous porous media laboratory experiments. J. Contam. Hydrol. 84 (1–2), 36–54.

Molins, S., Trebotich, D., Steefel, C.I., Shen, C.P., 2012. An investigation of the effect of pore scale flow on average geochemical reaction rates using direct numerical simulation. Water Resour. Res. 48.

Olsson, Å., Grathwohl, P., 2007. Transverse dispersion of non-reactive tracers in porous media: a new nonlinear relationship to predict dispersion coefficients. J. Contam. Hydrol. 92 (3–4), 149–161.

Oswald, S.E., Kinzelbach, W., 2004. Three-dimensional physical benchmark experiments to test variable-density flow models. J. Hydrol. 290 (1–2), 22–42.

Oswald, S., Kinzelbach, W., Greiner, A., Brix, G., 1997. Observation of flow and transport processes in artificial porous media via magnetic resonance imaging in three dimensions. Geoderma 80 (3–4), 417–429.

Porter, M.L., Valdés-Parada, F.J., Wood, B.D., 2010. Comparison of theory and experiments for dispersion in homogeneous porous media. Adv. Water Resour. 33, 1043–1052.

Prommer, H., Anneser, B., Rolle, M., Einsiedl, F., Griebler, C., 2009. Biogeochemical and isotopic gradients in a BTEX/PAH contaminant plume: model-based interpretation of a high-resolution field data set. Environ. Sci. Technol. 43 (21), 8206–8212.

Robbins, G.A., 1989. Methods for determining transverse dispersion coefficients of porous media in laboratory column experiments. Water Resour. Res. 25 (6), 1249–1258.

Rolle, M., Kitanidis, P.K., 2014. Effects of compound-specific dilution on transient transport and solute breakthrough: a pore-scale analysis. Adv. Water Resour. 71, 186–199.

Rolle, M., Eberhardt, C., Chiogna, G., Cirpka, O.A., Grathwohl, P., 2009. Enhancement of dilution and transverse reactive mixing in porous media: experiments and model-based interpretation. J. Contam.Hydrol. 110 (3–4), 130–142.

Rolle, M., Chiogna, G., Bauer, R., Griebler, C., Grathwohl, P., 2010. Isotopic fractionation by transverse dispersion: flow-through microcosms and reactive transport modeling study. Environ. Sci. Technol. 44 (16), 6167–6173.

Rolle, M., Hochstetler, D., Chiogna, G., Kitanidis, P.K., Grathwohl, P., 2012. Experimental investigation and pore-scale modeling interpretation of compound-specific transverse dispersion in porous media. Transp. Porous Media 93 (3), 347–362.

Rolle, M., Chiogna, G., Hochstetler, D.L., Kitanidis, P.K., 2013a. On the importance of diffusion and compound-specific mixing for groundwater transport: an investigation from pore to field scale. J. Contam. Hydrol. 153, 51–68.

Rolle, M., Muniruzzaman, M., Haberer, C.M., Grathwohl, P., 2013b. Coulombic effects in advection-dominated transport of electrolytes in porous media: multicomponent ionic dispersion. Geochim. Cosmochim. Acta 120, 195–205.

Saffman, P.G., 1959. A theory of dispersion in a porous medium. J. Fluid Mech. 6 (03), 321–349.

Scheibe, T.D., Hou, Z., Palmer, B.J., Tartakovsky, A.M., 2013. Pore-scale simulation of intragranular diffusion: effects of incomplete mixing on macroscopic manifestations. Water Resour. Res. 49 (7), 4277–4294.

Scheidegger, A.E., 1961. General theory of dispersion in porous media. J. Geophys. Res. 66 (10), 3273–3278.

Schwille, F., 1988. Dense Chlorinated Solvents in Porous and Fractured Media — Model Experiments. Lewis Publishers, Boca Raton.

Seagren, E.A., Rittmann, B.E., Valocchi, A.J., 1999. An experimental investigation of NAPL pool dissolution enhancement by flushing. J. Contam. Hydrol. 37 (1–2), 111–137.

Srinivasan, V., Clement, T.P., Lee, K.K., 2007. Domenico solution—is it valid? Ground Water 45 (2), 136–146.

Steefel, C., Depaolo, D., Lichtner, P., 2005. Reactive transport modeling: an essential tool and a new research approach for the Earth sciences. Earth Planet. Sci. Lett. 240 (3–4), 539–558.

Stohr, M., Roth, K., Jahne, B., 2003.Measurement of 3D pore-scale flow in index-matched porous media. Exp. Fluids 35 (2), 159–166.

Tartakovsky, A.M., Tartakovsky, G.D., Scheibe, T.D., 2009. Effects of incomplete mixing on multicomponent reactive transport. Adv.Water Resour. 32 (11), 1674–1679.

Thornton, S.F., Quigley, S., Spence, M.J., Banwart, S.A., Bottrell, S., Lerner, D.N., 2001. Processes controlling the distribution and natural attenuation of dissolved phenolic compounds in a deep sandstone aquifer. J. Contam. Hydrol. 53, 233–267.

Tuxen, N., Albrechtsen, H.-J., Bjerg, P.L., 2006. Identification of a reactive degradation zone at a landfill leachate plume fringe using high resolution sampling and incubation techniques. J. Contam. Hydrol. 85, 179–194.

Werth, C.J., Cirpka, O.A., Grathwohl, P., 2006. Enhanced mixing and reaction through flow focusing in heterogeneous porous media. Water Resour. Res. 42 (12).

Willingham, T.W., Werth, C.J., Valocchi, A.J., 2008. Evaluation of the effects of porous media structure on mixing-controlled reactions using pore-scale modeling and micromodel experiments. Environ. Sci. Technol. 42 (9), 3185–3193.

Worch, E., 1993. A new equation for the calculation of diffusion coefficients for dissolved substances. Vom Wasser 81, 289–297.

Zarlenga, A., Fiori, A., 2013. Steady plumes in heterogeneous porous formations: a stochastic Lagrangian approach. Water Resour. Res. 49 (2), 864–873.

Zhang, C., Dehoff, K., Hess, N., Oostrom, M., Wietsma, T.W., Valocchi, A.J., Fouke, B.W., Werth, C., 2010. Pore-scale study of transverse mixing induced CaCO3 precipitation and permeability reduction in a model subsurface sedimentary system. Environ. Sci. Technol. 44, 7833–7838.

3. Enhancement of Plume Dilution in Two- and Three-Dimensional Porous Media by Flow Focusing in High-Permeability Inclusions

Yu Ye, Gabriele Chiogna, Olaf Cirpka, Peter Grathwohl and Massimo Rolle

Water Resources Research (2015), vol. 51, pp. 5582-5602, doi: 10.1002/2015WR016962.

Abstract

In porous media, lateral mass exchange exerts a significant influence on the dilution of solute plumes in quasi steady state. This process is one of the main mechanisms controlling transport of continuously emitted conservative tracers in groundwater and is fundamental for the understanding of many degradation processes. We investigate the effects of high-permeability inclusions on transverse mixing in three-dimensional versus two-dimensional systems by experimental, theoretical, and numerical analyses. Our results show that mixing enhancement strongly depends on the system dimensionality and on the parameterization used to model transverse dispersion. In particular, no enhancement of transverse mixing would occur in three-dimensional media if the local transverse dispersion coefficient was uniform and flow focusing in both transverse directions was identical, which is fundamentally different from the two-dimensional case. However, the velocity and grain size dependence of the transverse dispersion coefficient and the correlation between hydraulic conductivity and grain size lead to prevailing mixing enhancement within the inclusions, regardless of dimensionality. We perform steady state bench-scale experiments with multiple tracers in three-dimensional and quasi two-dimensional flow-through systems at two different velocities (1 and 5 m/d). We quantify transverse mixing by the flux-related dilution index and compare the experimental results with model simulations. The experiments confirm that, although dilution is larger in three-dimensional systems, the enhancement of transverse mixing due to flow focusing is less effective than in two-dimensional systems. The spatial arrangement of the high-permeability inclusions significantly affects the degree of mixing enhancement. We also observe more pronounced compound-specific effects in the dilution of solute plumes in three-dimensional porous media than in two-dimensional ones.

Keywords: dilution; mixing enhancement; dilution index; heterogeneity; laboratory experiments; porous media

3.1 Introduction

Groundwater flow in natural aquifers is characterized by low flow velocities [10^{-3} to 10 m/d, e.g., Fetter, 2000], leading to rather small transverse hydrodynamic dispersion coefficients [10^{-11} to 10^{-8} m^2/s, e.g., Bear, 1972] and thus rather inefficient transverse mixing [e.g., Davis et al., 1999; Prommer et al., 2006; van der Kamp et al., 1994]. This is a key factor for understanding the fate and transport of widespread contaminants in groundwater, including compounds released from NAPL spills or leaking landfills. In these cases, the contaminants are continuously emitted from the source over typical time scales of decades and the released plumes approach steady state conditions determined by the dynamic equilibrium between the contaminant mass released at the source and its destruction by degradation processes [e.g., Mace et al., 1997; Wiedemeier et al., 1999]. Under these conditions, the reaction of continuously emitted pollutants with dissolved reactants in the ambient groundwater is typically controlled by transverse dispersive mixing [e.g., Anneser et al., 2008; Cirpka et al., 1999; Ham et al., 2004; Knutson et al., 2007; Mayer et al., 2001; Prommer et al., 2009; Thornton et al., 2001], although shearing and longitudinal dispersion can play an important role at the front of the plume. Transverse mixing represents the key process in estimating the length of steady state contaminant plumes [e.g., Cirpka et al., 2012; Liedl et al., 2005, 2011; Maier and Grathwohl, 2006; Zarlenga and Fiori, 2013, 2014]. In transient transport, local lateral mass exchange controls the transition of longitudinal plume spreading to dilution [Kitanidis, 1994], the coalescence of plume lamellae within heterogeneous domains [e.g., Le Borgne et al., 2013], and is critical in interpreting solute breakthrough curves [e.g., Pedretti et al., 2013; Rolle and Kitanidis, 2014].

The heterogeneity of porous media can sustain concentration gradients by deforming the plume boundary, enhancing therefore diffusive fluxes [e.g., Cirpka et al., 2012; Rolle et al., 2009; Werth et al., 2006]. Flow focusing in high-permeability zones squeezes streamlines in narrow regions of the domain, thus increasing concentration gradients of the solutes in the direction transverse to the streamlines. In two-dimensional systems, the increase in concentration gradients caused by flow focusing prevails over the decrease of transport time in such regions, thus leading to a net enhancement of transverse mixing [e.g., Chiogna et al., 2011a; Cirpka et al., 2011; Werth et al., 2006; Willingham et al., 2008]. The role of this process is particularly relevant for degradation reactions occurring at the narrow fringe of contaminant plumes where reactants can physically mix [e.g., Anneser et al., 2008; Bauer et al., 2009; Bjerg et al., 2011; Cirpka et al., 2006; Lerner et al., 2000].

Due to the small spatial scale at which mixing occurs, resolving steep concentration gradients at the field scale remains challenging despite the rapid development of improved monitoring techniques [e.g., Annable et al., 2005; Anneser et al., 2008; Devlin et al., 2012]. Therefore, laboratory experiments [e.g., Castro-Alcala et al., 2012; de Anna et al., 2014; Haberer et al., 2015; Rolle et al., 2013a] and numerical simulations at multiple scales [e.g., de Dreuzy et al., 2012; Herrera and Valocchi, 2006; Hochstetler et al., 2013; Porta et al., 2013; Rolle et al., 2013b; Tartakovsky et al., 2009] are fundamental for the understanding of dilution in porous media. Most of these studies, however, focused on (quasi) two-dimensional systems, while detailed experimental and modeling investigations in three-dimensional domains are less common [e.g., Herrera et al., 2010; Rashidi et al., 1996; Silliman, 1996; Yoon and McKenna, 2012; Cirpka et al., 2015]. In particular, few experimental studies have been performed to investigate solute transport in fully three-dimensional porous media. Such studies have mostly focused on the development of noninvasive techniques to map solute concentrations and on the investigation of solute breakthrough [e.g., Chen et al., 2002; Danquigny et al., 2004; Marica et al., 2011; Oswald et al., 1997; Oswald and Kinzelbach, 2004], whereas systematic experimental studies on transverse mixing in fully three-dimensional systems are scarce.

Cirpka et al. [2015] proposed three mechanisms by which three-dimensional heterogeneity enhances transverse mixing: (a) flow focusing, which is the main transverse-mixing enhancing process in two-dimensional steady state transport, (b) depth-dependent plume meandering leading to an enlarged surface area of the plume, and (c) twisting streamlines caused by spatially variable anisotropy. The present contribution exclusively addresses the first mechanism, providing theoretical analyses, numerical results, and an experimental validation. In contrast to the other two processes, transverse mixing enhancement by flow focusing can occur both in 2-D and 3-D setups thus allowing for a clear comparison on the effects of such mechanism in two and three dimensions. Effects of transient flow on transverse mixing in heterogeneous media [e.g., Cirpka and Attinger, 2003; Dentz and Carrera, 2003], which are difficult to address by experiments, are not considered in the present study.

Laboratory bench-scale experiments greatly simplify natural aquifers and cannot capture the complex arrangements of heterogeneous anisotropic materials [e.g., Heinz and Aigner, 2003], the hydraulic connectivity of high-permeability inclusions [e.g., Renard and Allard, 2013; Pedretti et al., 2013], as well as the chemical and biogeochemical complexity of natural aquifer systems. However, flow-through laboratory experiments allow the detailed investigation of selected processes under well-defined and controlled conditions. They

advance process understanding and allow testing conceptual and numerical models against experimental data affected by significantly less uncertainty than field observations.

In this work, we aim at analyzing the effects of physical heterogeneity, with a very simplified geometrical and topological structure, on dilution and its enhancement under steady state transport conditions in three-dimensional setups. In particular, we investigate the enhancement of transverse mixing caused by flow focusing in high-permeability inclusions, comparing two-dimensional and three-dimensional laboratory flow-through systems. We performed conservative multi-tracer experiments at two velocities (1 and 5 m/d). Three heterogeneous setups were considered in the three-dimensional experiments. We performed also a multi-tracer experiment reproducing a cross section of one of the aforementioned setups in a quasi two-dimensional system. We measured solute mass fluxes with high-spatial resolution at the outlet of the flow-through chambers. We quantify dilution of the steady state plumes by the flux-related dilution index [Rolle et al., 2009] and derive an analytical solution of the mixing-enhancement factor for the 3-D case, extending the 2-D analysis performed by Werth et al. [2006]. A model-based interpretation of the experimental results allows quantifying the amount of mixing enhancement due to flow focusing in comparison to the homogeneous case.

The main objectives of this study are to (i) investigate steady state plume dilution by transverse mixing in fully 3-D flow-through systems with high-permeability inclusions; (ii) quantify the mixing enhancement by flow focusing in the inclusions in the 3-D setups and compare it with the effects observed in (quasi) 2-D systems; (iii) assess how the parameterization of transverse dispersion and compound-specific properties of different solutes affect the enhancement of dilution in high-permeability inclusions of three-dimensional porous media.

3.2 Theory

3.2.1 Governing Flow and Transport Equations

Flow in porous media can be described by combining the continuity equation and Darcy's law. The latter can be written as

$$\mathbf{q}(\mathbf{x}) = -\mathbf{K}(\mathbf{x}) \cdot \nabla \phi(\mathbf{x}) \qquad (3.1)$$

where **q** [LT^{-1}] is the specific discharge vector, **x** [L] denotes the vector of spatial coordinates, **K** [LT^{-1}] is the hydraulic conductivity tensor, which depends on water saturation, and ϕ [L] is the hydraulic-head field. In this study, we consider the case of an isotropic porous medium, so that **K** is a scalar field. While the main focus is on groundwater, where water saturation is unity, we include the unsaturated zone overlaying the capillary fringe of phreatic systems in the numerical analysis of our experiments.

We consider steady-state transport of a conservative compound, described by the steady-state version of the well-known advection-dispersion equation:

$$\mathbf{v}\cdot\nabla c-\nabla\cdot\left(\mathbf{D}\nabla c\right)=0 \tag{3.2}$$

where c [ML^{-3}] is the concentration, $\mathbf{v}=\mathbf{q}/\theta$ [LT^{-1}] is the seepage velocity, θ [-] is the volumetric water content equaling the effective porosity under water-saturated conditions, and **D** [L^2T^{-1}] is the dispersion tensor:

$$\mathbf{D}=\frac{\mathbf{v}\otimes\mathbf{v}}{\mathbf{v}\cdot\mathbf{v}}\left(D_\ell-D_t\right)+\mathbf{I}D_t \tag{3.3}$$

where $\mathbf{v}\otimes\mathbf{v}$ and $\mathbf{v}\ \mathbf{v}$ denote the tensor and scalar products of **v** with itself, respectively, and **I** is the identity matrix. D_ℓ [L^2T^{-1}] and D_t [L^2T^{-1}] are the longitudinal and transverse dispersion coefficients, respectively.

The experimental setup used in this work considers a continuous release of the solutes in the flow-through system under steady state conditions. In this case, dispersion occurs mainly in the directions perpendicular to the main flow, because from a sufficient distance to the source dispersive fluxes in the longitudinal direction can be neglected due to the small longitudinal concentration gradients compared to the ones in the transient direction [e.g., Wexler, 1992; Zarlenga and Fiori, 2013]. We further assume that the transverse dispersion coefficient D_t [L^2T^{-1}] is identical in both transverse directions.

Numerical and experimental studies have shown that incomplete mixing in pore channels arises during solute transport [e.g., *Chiogna and Bellin*, 2013; *Klenk and Grathwohl*, 2002; *Rolle et al.*, 2012; *Tartakovsky et al.*, 2009; *Willingham et al.*, 2008], especially under advection-dominated conditions. This results in a non-linear dependence of transverse dispersion on the seepage velocity. In this study, we use an empirical parameterization of transverse dispersion [e.g., *Chiogna et al.*, 2010; *Rolle et al.*, 2012; *Ye et al.*, 2015] based on an earlier statistical model [i.e., *Bear and Bachmat*, 1967]:

$$D_t = D_p + D_{aq}\left(\frac{Pe^2}{Pe + 2 + 4\delta^2}\right)^{\beta} \tag{3.4}$$

where $Pe=vd/D_{aq}$ [-] is the grain Péclet number, v [LT^{-1}] is the absolute value of the seepage-velocity vector, d [L] is the average grain size, δ [-] is the ratio between the length of a pore channel and its hydraulic radius, and β [-] is an empirical exponent that accounts for the degree of incomplete mixing within the pore channels. The mechanical-dispersion term of equation (3.4) entails a dependence on the aqueous diffusion coefficient of the transported solute. Previous studies [e.g., *Chiogna et al.*, 2010; *Rolle et al.*, 2012; *Ye et al.*, 2015] have shown a good agreement between equation (3.4) and experimental results in homogeneous porous media, providing also an average estimate of the two parameters (i.e., β=0.5 and δ=5.37) for a range of grain sizes between 0.2 mm and 1.5 mm.

3.2.2 Quantification of Transverse Mixing

Quantifying transverse mixing processes in heterogeneous porous media can be a challenging task since it is important to separate the purely advective effects of plume meandering, squeezing, and stretching from actual dilution, which ultimately is caused by diffusion [e.g., Cirpka et al., 2011; Rahman et al., 2005; Rolle et al., 2009]. In this section, we describe two metrics of transverse mixing in domains affected by high-permeability inclusions: the mixing-enhancement factor [Werth et al., 2006] and the flux-related dilution index [Rolle et al., 2009].

Figure 3.1 schematically shows the effect of a high-permeability inclusion on the flow field in an otherwise homogeneous 3-D confined water-saturated domain. Since the hydraulic conductivity of the inclusion, K_i [LT^{-1}], is larger than the hydraulic conductivity of the matrix, K_m [LT^{-1}], streamlines are focused in the inclusion, as shown by the black lines in Figure 3.1. In the inclusion, the flow velocity is higher than in the surrounding matrix, which has three effects: (1) the transverse dispersion coefficient D_t is higher in the inclusion than outside, (2) the time for a water parcel to pass the inclusion is smaller than the time needed to travel the same distance in the matrix, and (3) the vertical and horizontal distances between streamlines are smaller in the inclusion than outside so that a transverse dispersive mass exchange between two streamlines has to cover a smaller distance inside the inclusion than outside. An additional effect of the inclusion is that its larger grain size increases not only the hydraulic conductivity but also the transverse hydrodynamic dispersion coefficient; such increase of D_t is beyond the velocity-related effect listed above.

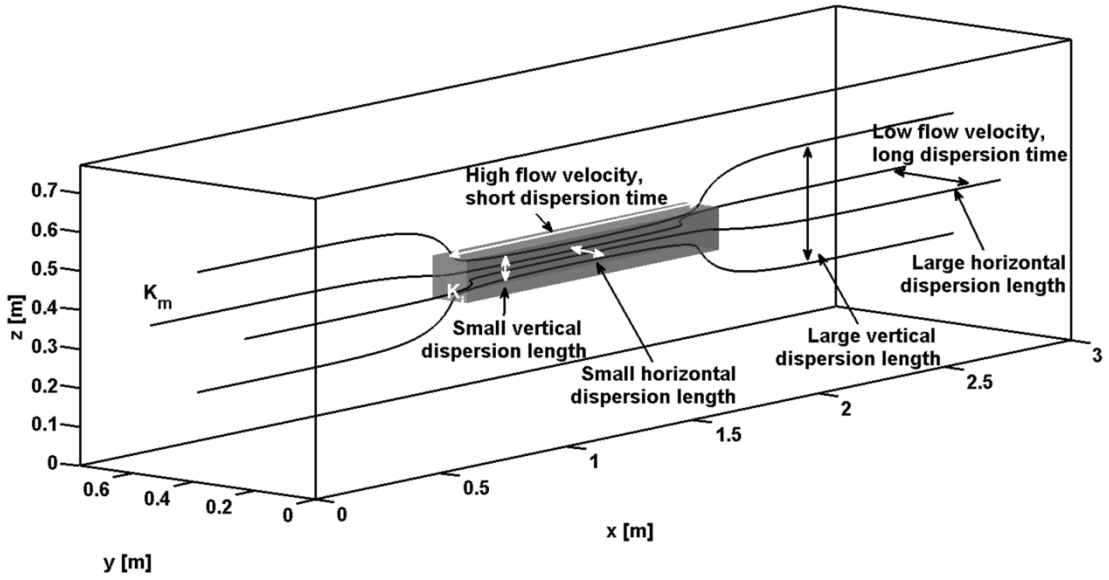

Fig. 3.1. Schematic overview of flow focusing effects in a high-permeability inclusion in a 3-D flow-through system. Gray volume: high-permeability inclusion; black lines: streamlines.

3.2.2.1 Mixing-Enhancement Factor

Werth et al. [2006] introduced the mixing-enhancement factor to quantify the enhancement of transverse mixing by a rectangular high-permeability inclusion of length L_i [L] and height h_i [L], inserted in a homogeneous two-dimensional matrix of length L_{tot} [L] and height h_{tot} [L].

Considering the characteristic dispersion length δ [L], which is commonly defined as $\delta = \sqrt{2Dt}$ (where t [T] is the time available for mixing and D [L^2T^{-1}] represents the hydrodynamic dispersion coefficient), *Werth et al.* [2006] assumed two limiting situations under steady-state flow conditions.

In the first case, the entire flow is focused in the high-permeability inclusion i. The degree of mixing in the vertical direction is expressed by the dimensionless ratio defined as

$$\frac{\delta_{tv,i}}{h_i} = \frac{1}{h_i}\sqrt{\frac{2D_{t,i}L_i}{v_i}} \tag{3.5}$$

where $\delta_{tv,i}$ [L] is the characteristic dispersion length in the vertical direction, $D_{t,i}$ [L^2T^{-1}] denotes the transverse dispersion coefficient in the inclusion, and the time t is substituted by the ratio between the length of the inclusion and the seepage velocity in the inclusion v_i [LT^{-1}].

In the second case, the inclusion is not present and the medium is homogeneous. Hence, the degree of mixing reads as

$$\frac{\delta_{tv,m}}{h_{tot}} = \frac{1}{h_{tot}}\sqrt{\frac{2D_{t,m}L_i}{v_m}} \tag{3.6}$$

where $\delta_{tv,m}$ [L] is the characteristic dispersion distance in the vertical direction within the homogeneous matrix, $D_{t,m}$ [L^2T^{-1}] denotes the transverse vertical dispersion coefficient in the homogeneous matrix and v_m [LT^{-1}] is the seepage velocity in the homogeneous matrix.

The mixing-enhancement factor for two-dimensional domains is then defined as the ratio of expressions in equations (3.5) and (3.6):

$$MF_{i,v} = \frac{h_{tot}}{h_i}\sqrt{\frac{D_{t,i}v_m}{D_{t,m}v_i}} \tag{3.7}$$

Assuming that the total discharge Q_{tot} [L^3T^{-1}] passes through the inclusion and considering the conservation of flow in the domain we can express v_i as

$$Q_{tot} = \theta_i v_i h_i = \theta_m v_m h_{tot} \Rightarrow v_i = \frac{v_m \theta_m h_{tot}}{\theta_i h_i} \tag{3.8}$$

where θ_i [-] and θ_m [-] are the effective porosities in the inclusion and in the homogeneous matrix, which are assumed identical for simplicity.

Under these idealized assumptions, the mixing-enhancement factor for a two-dimensional system reads as

$$MF_{i,v} = \sqrt{\frac{D_{t,i}h_{tot}}{D_{t,m}h_i}} \tag{3.9}$$

Note that two-dimensional transverse mixing is enhanced even for the unrealistic case that the transverse dispersion coefficients are identical within the inclusion and in the matrix, $D_{t,i} = D_{t,m}$. Werth et al. [2006] also considered the less idealized case in which not the entire discharge passes through the inclusion. In this case, transverse mixing outside the inclusion is reduced, but the average effect over the entire domain width was still an increase even for $D_{t,i} = D_{t,m}$.

We now consider the effect of a single high-permeability inclusion in a 3-D domain. Similarly to the 2-D case, we can define vertical ($MF_{i,v}$) and horizontal ($MF_{i,h}$) mixing-enhancement

factors for a three-dimensional domain, of length L_{tot} [L], height h_{tot} [L] and width w_{tot} [L], for an inclusion of length L_i [L], height h_i [L] and width w_i [L]:

$$MF_{i,v} = \frac{h_{tot}}{h_i}\sqrt{\frac{D_{t,i}v_m}{D_{t,m}v_i}} \tag{3.10}$$

$$MF_{i,h} = \frac{w_{tot}}{w_i}\sqrt{\frac{D_{t,i}v_m}{D_{t,m}v_i}} \tag{3.11}$$

In the three-dimensional case, the total discharge is defined as:

$$Q_{tot} = \theta_i v_i h_i w_i = \theta_m v_m h_{tot} w_{tot} \Rightarrow v_i = \frac{v_m \theta_m h_{tot} w_{tot}}{\theta_i h_i w_i} \tag{3.12}$$

such that equations (3.10) and (3.11), assuming a constant porosity, become:

$$MF_{i,v} = \sqrt{\frac{D_{t,i}h_{tot}w_i}{D_{t,m}h_i w_{tot}}} \tag{3.13}$$

$$MF_{i,h} = \sqrt{\frac{D_{t,i}w_{tot}h_i}{D_{t,m}w_i h_{tot}}} \tag{3.14}$$

These expressions show that mixing enhancement in three-dimensional domains is different than in two dimensions. For illustration, we may consider the enhancement of vertical mixing by a high-permeability inclusion. Equation (3.13) differs from equation (3.9) by the factor $\sqrt{w_i/w_{tot}}$, where w_i is the width of the inclusion and w_{tot} that of the domain. Note that $w_i \leq w_{tot}$, implying that the three-dimensional mixing-enhancement factor is smaller than the two-dimensional one. For the specific case of isotropic flow focusing, i.e. $w_i/w_{tot} = h_i/h_{tot}$, the geometric effects of mixing enhancement in equations (3.13) and (3.14) cancel, and the only remaining enhancement is caused by transverse dispersion within the inclusion being larger than outside, $D_{t,i} > D_{t,m}$.

We have tested the proposed relations for 3-D mixing enhancement by performing numerical transport simulations in a confined setup (length=3 m, width=0.77 m, height=0.77 m) with a high-permeability inclusion (Figure 3.1). The inclusion width was changed in different simulations, whereas its length and height were fixed and equal to 0.2 m and 0.066 m, respectively. The permeability ratio between the inclusion and the matrix was 13 and the

mean hydraulic gradient was set to 1.84×10^{-3}. Both the width and the height of the plume source were 0.0462 m. As shown in Figure 3.2a, an increase in the width of the inclusion enhances mixing in the vertical direction ($MF_{i,v}$) since it leads to a longer residence time of the plume in the inclusion (the velocity v_i is reduced). On the contrary, if we consider the horizontal mixing enhancement factor $MF_{i,h}$ (Figure 3.2a), we can observe a reduction in the mixing enhancement since, as w_i increases, the flow is distributed over a larger width. Considering the same model setup (i.e., variable inclusion width, constant length and height), we measure the square root of the second central moment of the plume at the outlet of the domain in both directions, $\sqrt{M_{2C,v}}$ [L] and $\sqrt{M_{2C,h}}$ [L], defined as

$$\sqrt{M_{2C,v}} = \sqrt{\frac{\int_0^{h_{tot}} \left(z - M_{1,v}\right)^2 c_v dz}{\int_0^{h_{tot}} c_v dz}} \tag{3.15}$$

$$\sqrt{M_{2C,h}} = \sqrt{\frac{\int_0^{w_{tot}} \left(y - M_{1,h}\right)^2 c_h dy}{\int_0^{w_{tot}} c_h dy}} \tag{3.16}$$

where $M_{1,v}$ [L] and $M_{1,h}$ [L] are the first spatial moment in vertical and horizontal directions, defined as

$$M_{1,v} = \frac{\int_0^{h_{tot}} z c_v dz}{\int_0^{h_{tot}} c_v dz} \tag{3.17}$$

$$M_{1,h} = \frac{\int_0^{w_{tot}} y c_h dy}{\int_0^{w_{tot}} c_h dy} \tag{3.18}$$

and c_v and c_h represent the average concentration of c_{norm} along horizontal and vertical directions, respectively:

$$c_v = \frac{\int_0^{w_{tot}} c_{norm} dy}{w_{tot}} \tag{3.19}$$

$$c_h = \frac{\int_0^{h_{tot}} c_{norm} dz}{h_{tot}} \tag{3.20}$$

In Figure 3.2b, we normalize $\sqrt{M_{2C,v}}$ and $\sqrt{M_{2C,h}}$ by the square root of the second central moment computed for the homogeneous porous medium (i.e., same setup but without the inclusion): $\sqrt{M_{2C,v}/M_{2CHom,v}}$ and $\sqrt{M_{2C,h}/M_{2CHom,h}}$. Comparing Figure 3.2a and 3.2b, it can be observed that the two metrics show a remarkable qualitative agreement.

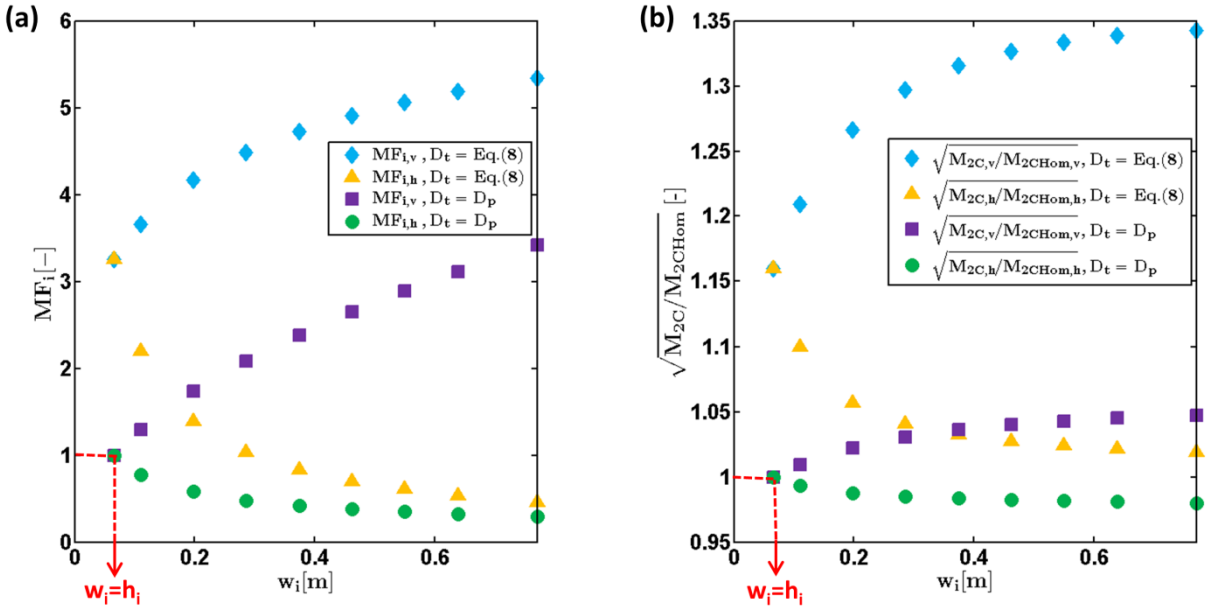

Fig. 3.2. Metrics of transverse mixing enhancement by a high-permeability inclusion in a 3-D model domain as function of the inclusion width. (a) Mixing-enhancement factor; (b) square root of the normalized second central moment. Blue diamonds: metrics of vertical transverse mixing enhancement with D_t according to equation (3.4); yellow triangles: metrics of horizontal transverse mixing enhancement with D_t according to equation (3.4); purple squares: metrics of vertical transverse mixing enhancement with pure pore diffusion D_p=1.92 × 10^{-10} m^2/s; green circles: metrics of horizontal transverse mixing enhancement with pure pore diffusion D_p=1.92 × 10^{-10} m^2/s. Red dashed line: symmetric case (w_i=h_i and w_{tot}=h_{tot}).

As shown in Figure 3.2, both vertical and horizontal mixing enhancement are significantly larger considering the velocity and grain-size dependent parameterization of D_t by euqation (3.4), in comparison to the mixing enhancement considering pure pore diffusion (D_t=D_p). In fact, the first model results in a spatially variable D_t that depends non-linearly on the spatially variable flow velocity and grain size in the heterogeneous domain; whereas the second model assumes a constant and velocity-independent D_t. This result is already indicative of the relevance of the physical model used to parameterize transverse dispersion for the correct computation of mixing enhancement in heterogeneous porous media.

The red dashed line in Figure 3.2 refers to the case of isotropic flow focusing (i.e., $w_i/w_{tot} = h_i/h_{tot}$) with constant local dispersion coefficient (e.g., D_t=D_p). As analytically derived above, the mixing enhancement in both the vertical and the horizontal directions reduces to the ratio of the transverse dispersion coefficient in the inclusion over that in the matrix when flow focusing is identical in the horizontal and vertical directions. Therefore, if the dispersion coefficient did not depend on the flow velocity, no mixing enhancement would occur, independently of the magnitude of the dispersion coefficient (i.e., this effect cannot be avoided by using an effective dispersion coefficient, which is constant in the entire domain).

Figure 3.2 also demonstrates that anisotropic flow focusing, that is $w_i/w_{tot} \neq h_i/h_{tot}$ leads to a strong directional dependence of transverse mixing. The scenarios reported in the figure show a considerably larger enhancement in the transverse vertical direction. For the case with constant local dispersion coefficient (e.g., D_t=D_p), even a reduction of transverse mixing is possible (e..g., horizontal transverse mixing in Figure 3.2). In this case, the reduction of mixing time in the inclusion has a stronger effect on transverse mixing than the reduction of the corresponding transverse mixing length. At the same time, mixing in the other transverse direction is more strongly enhanced.

As shown above, studies based on two-dimensional simulations likely overestimate mixing enhancement by flow focusing compared to fully 3-D descriptions. On the contrary, modeling studies assuming a constant dispersion coefficient in heterogeneous porous media result in the underestimation of mixing enhancement.

3.2.2.2 Flux-Related Dilution Index and Reactor Ratio

Rolle et al. [2009] introduced the flux-related dilution index to quantify dilution of solute plumes by transverse mixing at steady state. This metric is a modification of the volume-related dilution index [*Kitanidis*, 1994], which defines dilution as a measure of the disorder in the spatial distribution of solute concentration and is equivalent to the exponential of the Shannon entropy. While the dilution index describes how a solute slug is diluted in a volume, the flux-related dilution index represents a volumetric discharge and quantifies how a given solute mass flux is distributed over a larger water flux [e.g., *Chiogna et al.*, 2011a; *Chiogna et al.*, 2012; *Rolle et al.*, 2009]. The flux-related dilution index $E_Q(x)$ [L^3T^{-1}] in a bounded domain is defined as

$$E_Q(x) = \exp\left[-\int_\Omega p_Q(x,y,z) \ln p_Q(x,y,z) q_x(x,y,z) dA \right] \tag{3.21}$$

where Ω is the cross section perpendicular to the water flux, $q_x(x,y,z)$ [LT^{-1}] is the specific-discharge component in the longitudinal direction x and $p_Q(x,y,z)$ is the flux-weighted probability density function of the transverse particle location defined as

$$p_Q(x,y,z) = \frac{c(x,y,z)}{\int_\Omega c(x,y,z) q_x(x,y,z) dA} \tag{3.22}$$

The normalized form of flux-related dilution index, denoted as reactor ratio $M_Q(x)$ [-], is obtained by dividing equation (3.21) with the total flow rate Q_x [L^3T^{-1}]:

$$M_Q(x) = \frac{E_Q(x)}{Q_x} \tag{3.23}$$

The flux-related reactor ratio $M_Q(x)$ reaches its maximum value, $M_Q(x)=1$, when the solute flux is uniformly distributed over the total water flux.

3.3 Experimental Setup

Multi-tracer experiments were conducted in a three-dimensional and in a quasi two-dimensional flow-through chamber. The 3-D flow-through system (Figure 3.3a) has inner dimensions of 30 cm × 7.7 cm × 10 cm (length × width × height), while the quasi 2-D domain has inner dimensions of 28 cm × 1.1 cm × 14 cm. Both flow-through chambers are made of acrylic-glass. The 3-D setup is equipped with an array of 5 × 5 = 25 injection ports at the inlet and 7 × 7 = 49 extraction ports at the outlet. The ports at the inlet are equally spaced with a distance of 1.54 cm, while the distance at the outlet is 1.1 cm. The quasi 2-D flow-through chamber is equipped with seven injection ports at the inlet and seven extraction ports at the outlet, and the distance between each neighboring ports is 1.27 cm. All ports were connected to high-precision peristaltic pumps (IPC-N, Ismatec, Glattbrugg, Switzerland). A fully water-saturated zone was kept at the height of 7.7 cm for the 3-D setup and 9 cm for the 2-D setup. Both systems had a phreatic groundwater surface overlain by a shallow capillary fringe and an unsaturated zone even though active pumping was restricted to the water-saturated zone. Fluran pump tubings (ID 0.64 mm, Ismatec, Glattbrugg, Switzerland) and stainless steel capillaries were used as connection materials. More details about the experimental setups

have been provided by Ye et al. [2015]. The flow-through experiments were performed in a room with constant temperature (T=22 ℃) at the average flow velocities of 1 and 5 m/d.

High-permeability inclusions of coarse glass-bead packings with hydraulic conductivity $K=3.24\times10^{-2}$ m/s were inserted in a homogeneous matrix of hydraulic conductivity $K=2.5\times10^{-3}$ m/s. These values of hydraulic conductivity were computed based on the grain sizes and on the empirical correlation proposed by Hazen [1892], i.e., $K=(C\,d)^2$, where C=100 $m^{-0.5}s^{-0.5}$ and d [L] is the grain size. We constructed three heterogeneous setups for the 3-D flow-through system (Figure 3.3b) and one heterogeneous setup for the 2-D flow-through chamber. We used a grain size of 0.4–0.6 mm for the low-permeability matrix and a larger grain size of 1.6–2.0 mm for the high-permeability inclusions (Sigmund Lindner, Warmensteinach, Germany). In the experiments performed in the quasi 2-D porous medium, we inserted a single high-permeability inclusion. The size of the inclusion was 9 cm × 1.1 cm × 1.2 cm. The center of the lens was located 14 cm downstream of the inlet and 4.5 cm above the bottom of the 2-D flow-through chamber.

The front and side views of the three heterogeneous setups for the 3-D flow-through system and the dimensions and locations of the inclusions are shown in Figure 3.3b. One, two, and three inclusions were inserted in the homogeneous porous matrix to obtain three different flow configurations. The three cases are named Case 1, Case 2, and Case 3, respectively. The total volume of high-permeability material, as well as the ending position of the inclusions along the flow direction, was kept the same in the three heterogeneous setups. We always filled the material into the domains under water-saturated conditions to prevent air entrapment in the porous media [Haberer et al., 2012]. The measured total porosity was 0.4 for both the matrix and the high-permeability inclusions.

Two tracers, namely fluorescein and oxygen, were simultaneously transported in the flow-through system. The two tracers have significantly different aqueous diffusion coefficients, namely 4.8×10^{-10} m^2/s for fluorescein and 1.97×10^{-9} m^2/s for oxygen at T=22 °C [e.g., Atkins, 1990; Worch, 1993]. After reaching steady state flow conditions, an oxygen-depleted sodium fluorescein solution was injected through the central port at the inlet, whereas an ambient solution with no fluorescein and oxygen concentration of 8.5 mg/L was continuously injected from the surrounding inlet ports. The tracer solution was kept in a gastight Tedlar bag (Alltech, Germany) to keep the oxygen concentration smaller than 1.0 mg/L. The fluorescein concentration in the tracer solution was 15 mg/L. After injection of three pore volumes, the plumes of fluorescein and oxygen had reached steady state. Samples were collected at the

outlet ports twice for each experimental run, with a time interval of half a pore volume. The flow rate was experimentally determined by weighing the collected samples at each port, and the fluorescein concentration was measured using a UV-spectrometer (Perkin Elmer LS-3B). The oxygen concentration was measured using a noninvasive optode technique [see Haberer et al., 2011 for details] at each of the 49 flow-through vials at the outlet and at the central flow-through vial at the inlet of the setup [Ye et al., 2015]. The concentration and mass-flux values were in excellent agreement between the two subsequent measurements and the results in the following are presented as the average of the two measurements.

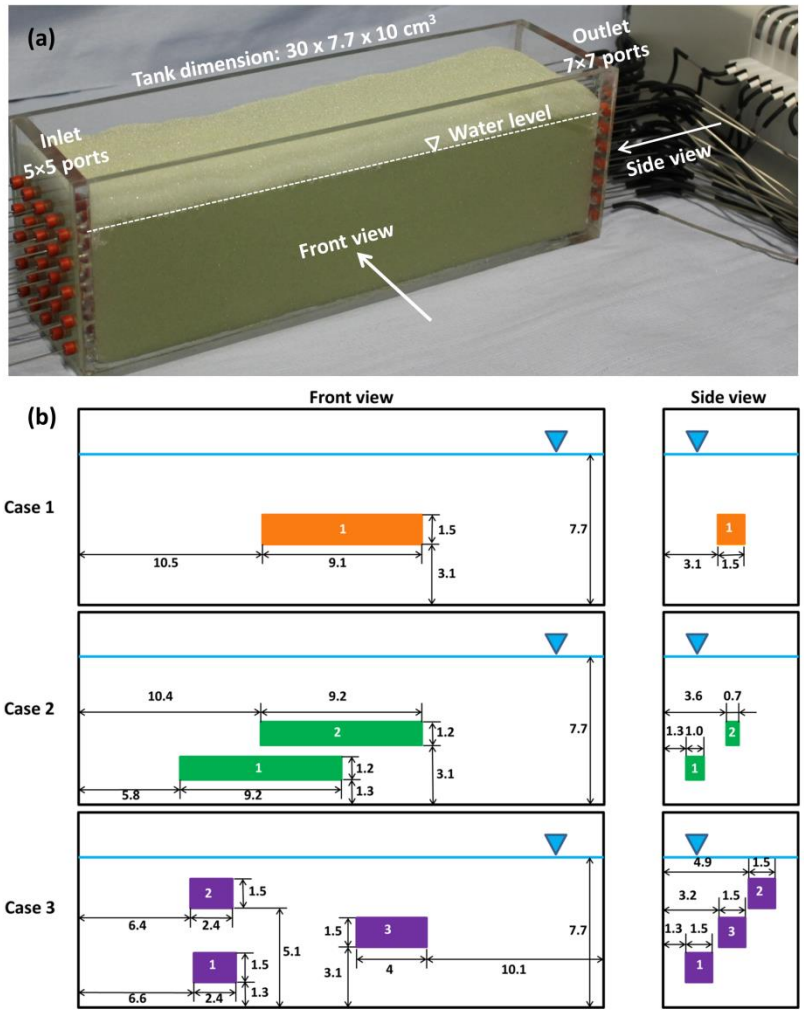

Fig. 3.3. (a) Photograph of the 3-D flow-through chamber; (b) front and side view of the 3-D heterogeneous setups: black rectangles represent the flow-through chamber, blue lines denote the water level, orange, green, and purple rectangles represent the high-permeability inclusions for Case 1, Case 2, and Case 3, respectively.

3.4 Model Description and Validation

In order to interpret the experimental results, we performed flow and transport simulations using the numerical code recently presented by *Cirpka et al.* [2015] with slight modifications discussed below. The domain was discretized into 150×35×41 cells for the 3-D setup, with Δx=0.2 cm and Δy=Δz=0.22 cm. For the 2-D setup, the domain was discretized into 140×5×41 cells, with Δx=0.2 cm, Δy=0.22 cm, and Δz=0.254 cm.

The governing flow equation was solved using a cell-centered Finite Volume method. The flow-through system was simulated as an unconfined medium, which is consistent with the experimental setup. Boundary conditions were set as constant flow at the inlet and at the outlet ports. No-flow boundary conditions were set to the bottom and the sides of the flow-through chamber. Since the flow-through systems were unconfined, unsaturated conditions were accounted for at the top of the domain, using the Mualem/van-Genuchten-parameterization [van Genuchten, 1980] and unsaturated parameters reflecting coarse sand [Carsel and Parrish, 1988]. This extension was necessary because a small fraction of the discharge passed through the overlaying unsaturated zone where the hydraulic conductivity was reduced but not zero [see also Haberer et al., 2014]. The particle-tracking scheme of Pollock [1988] was used to compute streamlines.

Steady state advective-dispersive transport was simulated in y-z cross sections at regular distances in x. In each cross section, we used Voronoi tessellation to construct polygons centered about the points where the streamlines intersected with the observation plane. Then, transport from one cross section to the next could be simulated by a Finite Volume method for transverse dispersion, in which time is replaced by the individual plane-to-plane travel time along each streamline. In contrast to Cirpka et al. [2015], we imposed zero mass-flux boundary conditions at the bottom, side, and top boundaries, and a constant mass-flux boundary condition at the inlet face. The advantage of this numerical scheme is the significant reduction of numerical dispersion in comparison to numerical solutions which rely on fixed Cartesian grids. The parameters used in the numerical code are listed in Table 3.1.

Table 3.1. Summary of flow and transport parameters used in the model parameter

Parameter	**Value**
Avarage fine grain diameter (mm)	0.5
Avarage coarse grain diameter (mm)	1.8
Porosity fine material	0.4
Porosity coarse material	0.4
Hydraulic conductivity fine material (m/s)	2.5×10^{-3}
Hydraulic conductivity coarse material (m/s)	3.24×10^{-2}
Van Genuchten parameter α[a] (m^{-1})	7.9
Van Genuchten parameter N[a] (-)	35.8
Aqueous diffusion coefficient fluorescein[b] (m^2/s)	0.48×10^{-9}
Aqueous diffusion coefficient oxygen[b] (m^2/s)	1.97×10^{-9}
Parameter δ of D_t (equation(3.4))[c]	5.37
Parameter β of D_t (equation(3.4))[c]	0.5

[a]From Haberer et al. [2011], consistent with McCray and Falta [1997].
[b]From Worch [1993] and Atkins [1990], at T=22 ℃.
[c]From Ye et al. [2015].

To show the low numerical dispersion affecting the numerical scheme, we computed the ratio between the flux-related dilution index in a three-dimensional confined domain similar to the one shown in Figure 3.1 (i.e., length=3 m, width=0.77 m, height=0.77 m). This domain has a horizontal upper boundary and is water saturated over the entire height, unlike the experimental device. The domain contains a high-permeability inclusion (length=0.2 m, width=0.066 m, height=0.066 m) located at a distance of 1.8 m from the inlet and in the corresponding homogenous case. The ratio between the conductivity value in the high-permeability inclusion and in the surrounding matrix is 13. This permeability contrast causes the focusing of the plume in the inclusion. We imposed the conditions $h_i=w_i$ and $h_{tot}=w_{tot}$ and considered the case in which D_t is parameterized according to equation (3.4) and the case in which D_t is constant ($D_t=D_p=1.92\times10^{-10}$ m^2/s). Figure 3.4 shows that in the first case transverse mixing is enhanced due to the difference in the dispersion coefficients, while in the second case the high-permeability inclusion does not cause an increase of the flux-related dilution index. As discussed in section 3.2.2.1, the latter behavior is expected for the case of pure pore diffusion. The fact that the numerical scheme reproduces this behavior indicates that the method is free of significant numerical transverse dispersion.

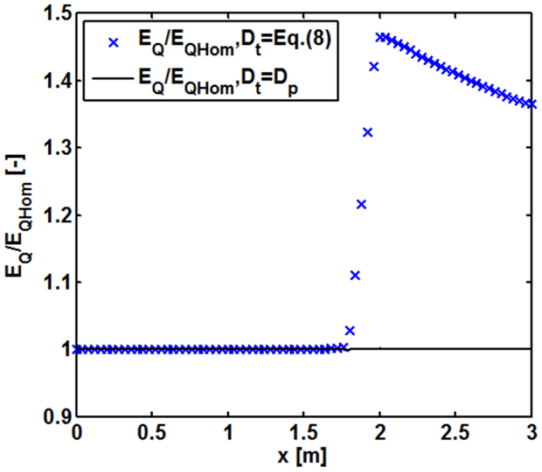

Fig. 3.4. Validation of the numerical scheme in a 3-D scenario with ratio of flux-related dilution index between heterogeneous and homogeneous cases along the travel distance. Blue crosses: simulations with D_t according to equation (3.4); black line: simulations with $D_t = D_p$ (pure pore diffusion).

3.5 Results and Discussion

The numerical model described in the previous section was used to interpret the experimental data and to quantitatively illustrate the effects of flow focusing on dilution and dilution enhancement observed in the flow-through experiments.

3.5.1 Effects of Flow Focusing in 3-D Heterogeneous Setups

Figure 3.5a shows the simulated influence of the high-permeability inclusions on the flow field for the three-dimensional setups. Streamlines were traced from the injection port to the end of the flow-through system. As can be observed, they converge towards the high-permeability inclusions. However, due to the nonuniformity of the flow field, some streamlines diverge from the initial bundle. In Case 1, all streamlines are focused at a distance of x=0.1 m and defocused at a distance of x=0.2 m. The focusing zone of the streamlines is exactly the location where the high- permeability inclusion lies (see Figure 3.3). The focusing of flow reduces the distance between streamlines, increases concentration gradients transverse to the flow direction, but reduces the mixing time within the inclusion. While the geometric effects should cancel for the given geometry (see the discussion on isotropic flow focusing above), the higher velocity within the inclusion causes an increased local transverse dispersion coefficient, the effect of which prevails in enhanced dilution, as reflected by the flux-related dilution index in Figures 3.5b and 3.5c. At the two flow velocities of 1 and 5 m/d, the red dashed line shows a jump in the flux-related dilution index (E_Q), with a higher slope,

after a travel distance of x=0.1 m; E_Q returns to the initial rate of increase after a travel distance of x=0.2 m (i.e., after the high-permeability inclusion).

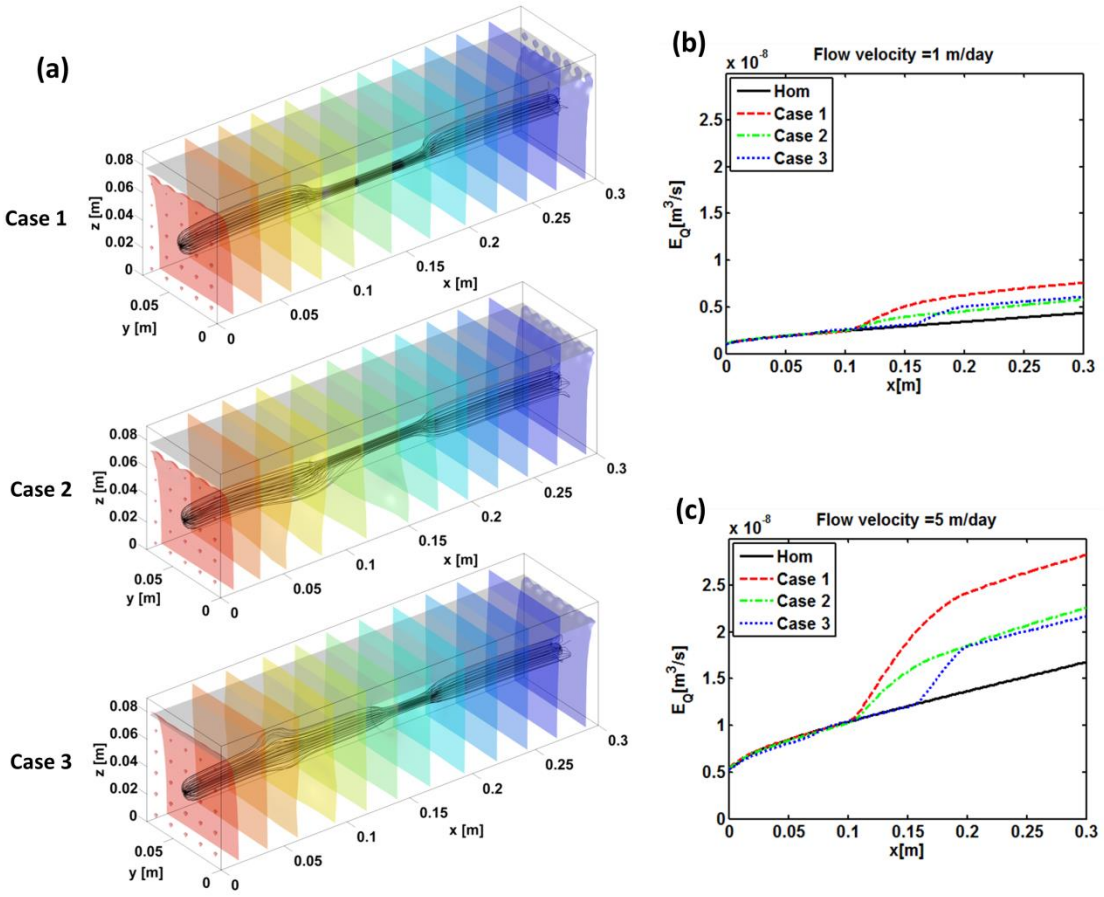

Fig. 3.5. (a) Streamlines (black lines) starting from the central inlet port, isopotential surfaces (colored surfaces), and water level (gray surface). (b) Flux-related dilution index in the flow-through chambers for the three heterogeneous cases and the homogeneous case for a mean flow velocity of 1 m/d. (c) Flux-related dilution index in the flow-through chambers for the three heterogeneous cases and the homogeneous one for a mean flow velocity of 5 m/d.

In Case 2, a few streamlines deviate from the flow path at a distance of x=0.06 m. This happens at the position where the first high-permeability inclusion is located (see Figure 3.3). For the given asymmetric setup, the plume fringe is not completely focused within the inclusion. Outside the inclusion, the streamlines meander in zones with lower-than-the-average flow velocity. As a consequence, while transverse mixing is enhanced within the inclusion, it is reduced in the fraction of the plume outside the high-conductivity material. The net effect is that the presence of the first inclusion does not enhance dilution (Figures 3.5b and 3.5c, green dash-dotted lines). When the plume reaches the second lens at the travel distance of x=0.1 m, all streamlines injected at the source are focused. Like in Case 1, dilution is

stronger in the inclusion due to the higher velocity causing the enhancement of transverse mass exchange. This is illustrated by the increasing slope of the flux-related dilution index starting at a travel distance of x=0.1 m (Figures 3.5b and 3.5c). The rate of dilution enhancement along the travel distance is smaller for Case 2 compared to Case 1. This is due to the stronger flow focusing effect in the larger cross-sectional area of the inclusion in Case 1 (2.25×10^{-4} m^2) than in Case 2 (0.84×10^{-4} m^2).

Case 3 shows a different development of the streamlines than the other two cases. At a distance of x=0.06 m, the streamlines deviate in both lateral and vertical directions due to the presence of two surrounding high-permeability inclusions (Figure 3.3). As shown by the blue dotted line in Figures 3.5b and 3.5c, the overall dilution in the first half of the domain is the same as for the homogeneous medium at the flow rate of 1 m/d whereas it is even smaller at the flow rate of 5 m/d. At the flow rate of 1 m/d, a balance occurs between dilution enhancement due to flow focusing inside the inclusions and the dilution decrease in the low velocity zones outside the lenses. At a higher flow rate, fewer streamlines carrying nonzero concentration are focused in the high-permeability inclusions. Hence, the decrease of dilution becomes slightly larger than the dilution enhancement. The third high-permeability inclusion appearing at a distance of x=0.15 m focuses the flow as in Case 1. However, since the inclusion is shorter compared to Case 1, lower dilution values are reached at the end of the domain.

For both flow velocities (1 and 5 m/d), the observed behavior is qualitatively the same, but the values of the flux-related dilution index are larger when the flow-through system is run at higher velocity. It should be noted, however, that the dimension of the flux-related dilution index is that of a discharge. In the cases with a mean velocity of 5 m/d, the discharge is 5 times larger than the one for the cases with 1 m/d. The values of the flux-related dilution index, however, are less than 5 times larger because the transverse dispersion coefficients increase less than linearly with the seepage velocity. That is, the reactor ratio, which scales the flux-related dilution index by the total discharge, is smaller in the case with higher mean flow velocity.

All heterogeneous setups enhance transverse mixing in comparison to the homogeneous setup. Case 1 shows the strongest dilution enhancement, whereas Case 2 has the lowest dilution enhancement at the flow velocity of 1 m/d and Case 3 has the lowest dilution enhancement at the flow velocity of 5 m/d. This difference in the behavior of the dilution enhancement can be

explained by considering that the inclusions have different geometries and that the transverse dispersion coefficient depends nonlinearly on the flow velocity.

Normalized fluorescein concentrations at the outlet ports are shown in Figures 3.6 and 3.7, for the flow velocities of 1 m/d and 5 m/d, respectively. Results of the 3-D homogeneous setup investigated by Ye et al. [2015] are also included in the plots for a direct comparison with the heterogeneous cases that are the focus of the present study. Color columns denote experimental measurements at the 7 × 7 outlet ports, whereas black outlines represent the results of forward simulations carried out without any parameter fitting using the 3-D numerical model presented in section 3.4. The match between experimental measurements and model results is good for all cases at both flow rates. We evaluated the model performance according to the χ^2 test, defined as

$$\chi^2 = \frac{1}{n_{ports}} \sum_{n=1}^{n_{ports}} \frac{(c_{meas} - c_{simu})^2}{\varepsilon^2} \tag{3.24}$$

where n_{ports} [-] is the number of ports (49 in our setup), c_{meas} [-] is the measured normalized concentration at each port, c_{simu} [-] is the simulated normalized concentration and ε [-] is the experimental error, which we estimate a posteriori such that $\chi^2 \approx 1$. For the eight cases shown in Figures 3.6 and 3.7, the mean experimental error is always smaller than 11% and thus comparable to the values obtained in experiments with homogeneous porous media [*Ye at al.*, 2015].

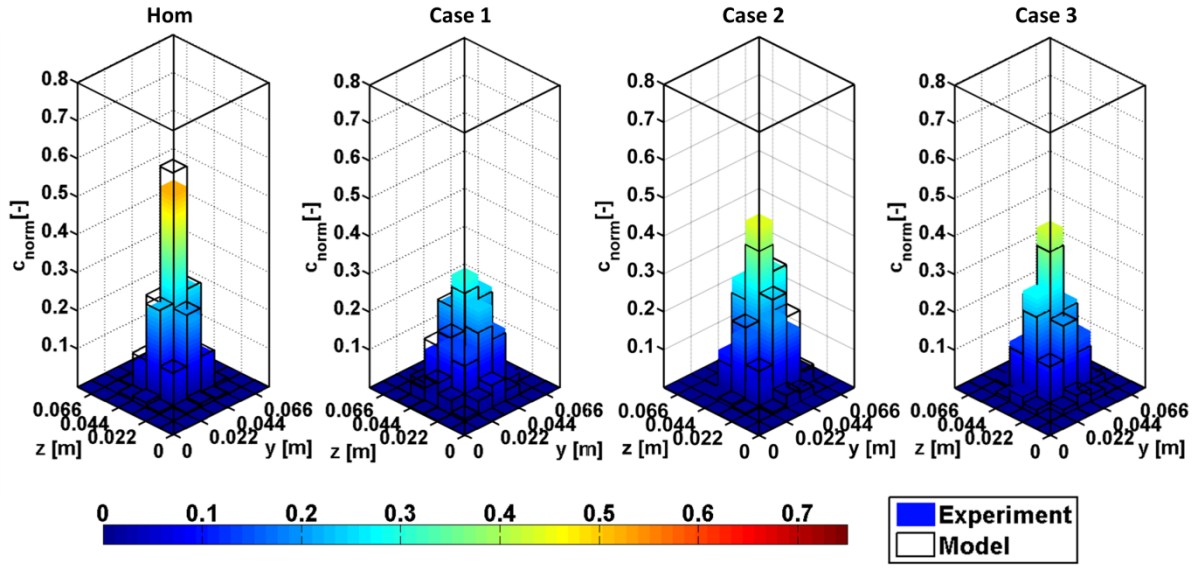

Fig. 3.6. Normalized fluorescein concentration distributions at the outlet for the 3-D homogeneous setup and the three 3-D heterogeneous setups: observed and simulated values at flow velocity of 1 m/d.

As shown in Figure 3.6, the peak concentrations differ significantly among the four cases. The peak concentrations in the heterogeneous cases are smaller in comparison to the homogeneous case, due to dilution enhancement in the high-permeability inclusions. Furthermore, Case 1 shows the lowest peak concentration value, whereas Cases 2 and 3 have similar values. This is consistent with the dilution predicted by the numerical simulations and quantified by the flux-related dilution index (Figure 3.5). While the total volume of the high-permeability inclusions is practically the same in the three heterogeneous setups, different spatial distributions of the high-permeability material in the matrix cause different enhancement of transverse mixing. Therefore, the volume ratio of the high-conductive to low-conductive materials and the conductivity contrast are not sufficient to predict plume dilution. In fact, the enhancement of transverse dispersion and dilution depends on how the plume fringe is focused in the high-permeability inclusions [e.g., Chiogna et al., 2011b; de Barros et al., 2012].

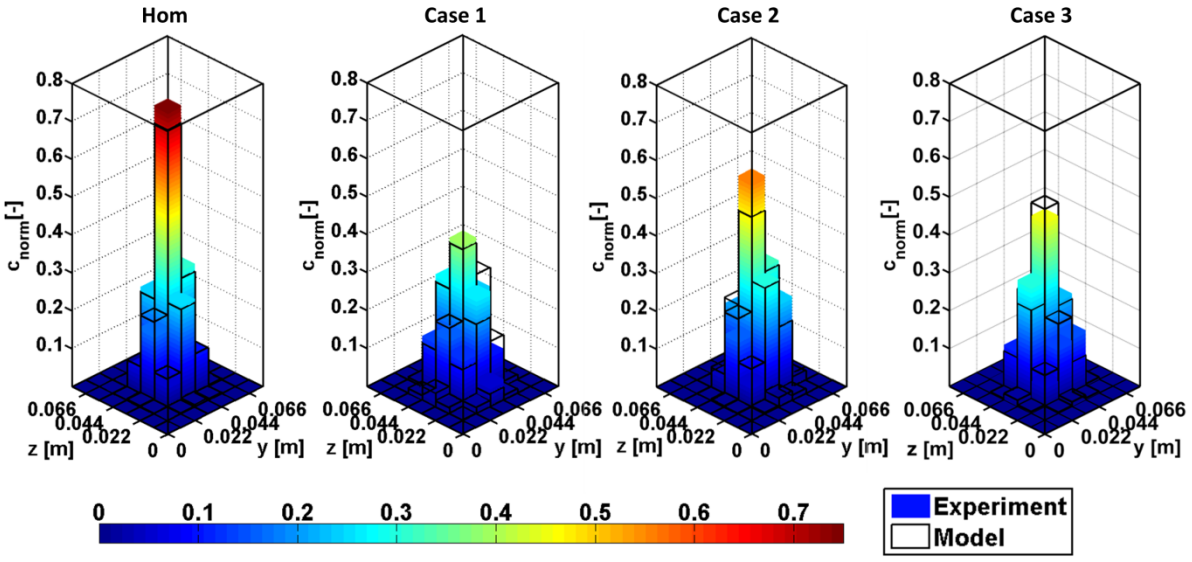

Fig. 3.7. Normalized fluorescein concentration distributions at the outlet for the 3-D homogeneous setup and the three 3-D heterogeneous setups: observed and simulated values at flow velocity of 5 m/d.

The results presented in Figure 3.7 for the high-velocity case are consistent with those presented in Figure 3.6. At higher flow velocity, the peak concentration is higher. This is due to the shorter residence time of the solute in the flow-through chamber in conjunction with a lower than linear dependence of transverse dispersion on the average flow velocity.

The flux-related dilution index and reactor ratio at the outlet of the domain have been computed for both experimental and model results at flow velocity of 1 and 5 m/d. They are listed in Table 3.2. The values of the flux-related dilution index, which have units of a discharge, are larger at 5 m/d than at 1 m/d. However, it should be noticed that at 5 m/d the

total volumetric fluxes are also 5 times larger than the ones at 1 m/d. Thus, besides quantifying the absolute dilution of the plume with E_Q it is also useful to consider the degree of dilution for a given flow rate. To this end, the reactor ratio is a useful metric since it is normalized by the total discharge in the flow-through system. The reactor ratio is consistently higher for the experiments at lower flow velocity. As discussed above, this behavior is expected since at lower velocity the residence time is 5 times larger than at 5 m/d, whereas the local transverse dispersion coefficient is less than 5 times smaller.

Table 3.2. Experimental and model results of flux-related dilution index and reactor ratio at the outlet of the 3-D setups at flow velocity of 1 and 5 m/d.

	1 m/d			**5 m/d**		
Setup	Experiment	Model	Norm. Error (%)	Experiment	Model	Norm. Error (%)
Flux-related dilution index [m^3/s]						
Hom	4.85×10^{-9}	5.13×10^{-9}	5	1.93×10^{-8}	2.10×10^{-8}	8
Case 1	7.83×10^{-9}	8.70×10^{-9}	10	3.16×10^{-8}	3.32×10^{-8}	5
Case 2	5.43×10^{-9}	6.78×10^{-9}	20	2.06×10^{-8}	2.73×10^{-8}	25
Case 3	6.20×10^{-9}	6.81×10^{-9}	9	2.46×10^{-8}	2.52×10^{-8}	3
Reactor ratio [-]						
Hom	0.18	0.18	5	0.15	0.16	8
Case 1	0.28	0.31	10	0.23	0.24	5
Case 2	0.20	0.24	20	0.15	0.20	25
Case 3	0.23	0.25	9	0.19	0.19	3

The normalized error between the experimental dilution index $E_{Q,meas}$ and the model results $E_{Q,sim}$ (i.e., abs($E_{Q,meas}$- $E_{Q,sim}$)/ $E_{Q,sim}$) is within 10% except for Case 2. The larger error for Case 2 (20% at 1 m/d and 25% at 5 m/d) may be explained by the fact that the transition between high-conductivity and low-conductivity materials in the real experiment is not as sharp as assumed by the model. In fact, the small glass beads may intrude into the pore space of the large ones at the sides of the inclusions. The width of this transition zone has a dimension of 1–2 grains in our experimental setup. This effect can be neglected if the dimension of the inclusion is large, as in Cases 1 and 3, while in Case 2 the influence of this transition zone is more relevant, thus potentially explaining the larger difference between model and experimental results.

Besides considering the values of the flux-related dilution index and of the reactor ratio in the different setups, it is illustrative to consider the enhancement of dilution determined by flow focusing in the heterogeneous setups. Table 3.3 lists the enhancement of dilution with respect to the homogeneous case as the ratio between the flux-related dilution index at the outlet of the flow-through chamber in the heterogeneous cases and in the homogeneous case. The

strongest dilution enhancement is observed for Case 1 (~65%), whereas Cases 2 and 3 yield smaller enhancements. Furthermore, for a given setup, the dilution enhancement is similar for both velocities.

Table 3.3. Ratio of flux-related dilution index at the outlet of flow-through chamber between the 3-D heterogeneous porous media and the 3-D homogeneous porous medium (E_{QHet}/ E_{QHom}) at flow velocity of 1 m/day and 5 m/day.

	1 m/d		**5 m/d**	
Heterogeneous setup	Experiment	Model	Experiment	Model
Case 1	1.61	1.70	1.64	1.58
Case 2	1.12	1.32	1.07	1.30
Case 3	1.28	1.33	1.28	1.20

3.5.2 Effects of Dimensionality on Dilution and Dilution Enhancement

Dilution in three-dimensional domains is in general larger than in two-dimensions [Kitanidis, 1994], due to the additional degree of freedom provided by the third spatial dimension. This was confirmed in the experiments carried out in this study and substantiated by the values of the flux-related dilution index measured at the outlet of the flow-through setups (Tables 3.2 and 3.4). Despite high-permeability inclusions may considerably enhance dilution in both 2-D and 3-D systems, the mixing enhancement is different depending on the dimensionality of the domain (section 3.2.2.1). Indeed, the effect of high-permeability inclusions enhance dilution in a considerably different way in 2-D than in 3-D flow-through systems. To confirm this statement by experimental evidence, we compare the dilution enhancement between 2-D and 3-D cases, in a very simple setup. A single inclusion was inserted in the quasi 2-D flow-through chamber and the results were compared with the analogous setup in the 3-D flow-through chamber (Case 1). In both setups, the inclusions are centered, have the same length and a height equal to the interspacing between inlet ports thus allowing a meaningful comparison of the effects of dimensionality. Fluorescein was used as tracer and the experiments were run at mean flow velocities of 1 and 5 m/d.

Figure 3.8 shows the flux-related dilution index at the outlet of the flow-through chamber for both 2-D and 3-D experiments, considering both homogeneous and heterogeneous setups at the mean flow velocities of 1 and 5 m/d. Notice that to provide a meaningful comparison between 2-D and 3-D systems, the flux-related dilution index is normalized by subtracting its values at the inlet, which is significantly different between 2-D and 3-D setups. The difference between experimental (black bars) and model (white bars) results is smaller than 17%

for all cases, showing the good performance of the model in predicting the experimental data. In both 2-D and 3-D setups, at a specific flow velocity, dilution is smaller in the homogeneous case than in the heterogeneous cases. Furthermore, the figure clearly illustrates that dilution is larger in the 3-D setup both in the homogeneous and in the heterogeneous porous media.

The absolute and normalized values of the flux-related dilution index as well as of the reactor ratio are listed in Table 3.4 for the 2-D and 3-D heterogeneous cases at flow velocity of 1 and 5 m/d. It is interesting to notice that, in contrast to the values of the flux-related dilution index, the reactor ratio shows larger values in the 2-D than in the 3-D system. This difference is due to the fact that the two metrics capture different features of plume dilution. Whereas the flux-related dilution index quantifies dilution that is larger in the 3-D cases, the reactor ratio expresses the degree of dilution and captures the fact that the solute mass flux is better distributed with respect to the total discharge in the 2-D than in the 3-D setups. The difference in the behavior of the flux-related dilution index and the reactor ratio is caused by the difference in the total discharge between 2-D and 3-D setups. Since the mean flow velocity is the same in both systems, the total discharge in the 3-D case is much larger than in the 2-D case. The reactor ratio is therefore indicative of the potential for further dilution in the system: the larger the value at the outlet, the better the plume is diluted and the smaller is the potential for further dilution. Combining the information from the two metrics used to quantify the effects of transverse mixing on plume dilution, it is possible to conclude that in the 3-D setup the plume is certainly more diluted and also has a larger potential for further dilution than in the 2-D system.

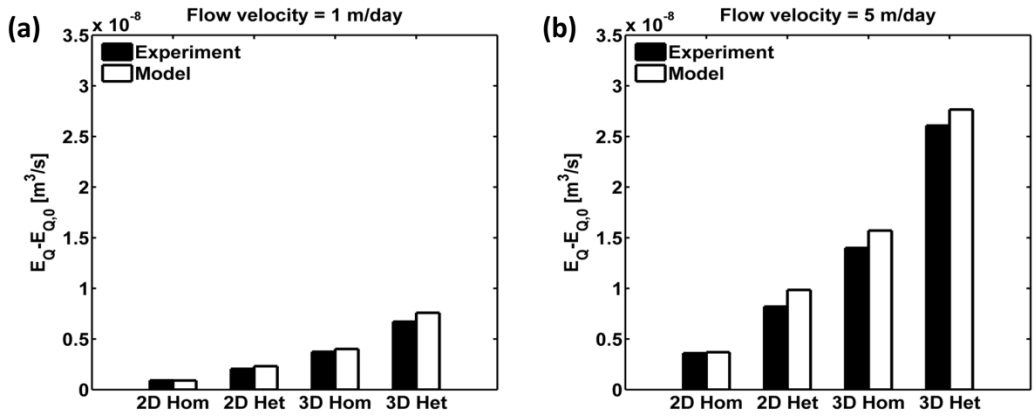

Fig. 3.8. Experimental and model results of normalized flux-related dilution indices at the outlet of the flow-through chamber for four setups: 2-D homogeneous, 2-D heterogeneous, 3-D homogeneous, and 3-D heterogeneous at flow velocity of (a) 1 m/d and (b) 5 m/d.

Table 3.4 Experimental and model results of flux-related dilution index, normalized flux-related dilution index, reactor ratio and normalized reactor ratio at the outlet of the 2-D and the 3-D heterogeneous setups at flow velocity of 1 and 5 m/d.

	3-D			2-D		
Flow velocity	Experiment	Model	Norm. Error (%)	Experiment	Model	Norm. Error (%)
Flux-related dilution index [m^3/s]						
1 m/d	7.83×10^{-9}	8.70×10^{-9}	10	2.69×10^{-9}	2.95×10^{-9}	9
5 m/d	3.16×10^{-8}	3.32×10^{-8}	5	1.14×10^{-8}	1.30×10^{-8}	13
Normalized Flux-related dilution index [m^3/s]						
1 m/d	6.71×10^{-9}	7.58×10^{-9}	12	2.05×10^{-9}	2.32×10^{-9}	11
5 m/d	2.61×10^{-8}	2.77×10^{-8}	6	8.21×10^{-9}	9.85×10^{-9}	17
Reactor ratio [-]						
1 m/d	0.28	0.31	10	0.61	0.67	9
5 m/d	0.23	0.24	5	0.51	0.58	13
Normalized reactor ratio [-]						
1 m/d	0.24	0.27	12	0.46	0.52	11
5 m/d	0.19	0.20	6	0.37	0.44	17

As done in the previous analysis for the different 3-D cases, dilution enhancement is computed as the ratio of the flux-related dilution index between heterogeneous and homogeneous setups at the outlet of the flow-through system. The results are presented in Table 3.5. Although dilution is larger for the 3-D flow-through systems than for the 2-D ones, dilution enhancement is stronger for the 2-D heterogeneous system (~1.8) than for the 3-D heterogeneous setup (~1.6). This indicates that results obtained in 2-D systems may overestimate the enhancement of transverse mixing by flow focusing in comparison to fully 3-D domains.

Table 3.5. Ratio of the flux-related dilution index at the outlet of flow-through chamber between heterogeneous porous media and homogeneous porous media for both 3-D and 2-D setups at flow velocity of 1 and 5 m/d.

	3-D		2-D	
Flow velocity	Experiment	Model	Experiment	Model
1 m/d	1.61	1.70	1.76	1.95
5 m/d	1.64	1.58	1.67	1.93

To compare vertical and horizontal mixing enhancement in the three-dimensional setup with the mixing enhancement in the two-dimensional setup, we compute the mixing-enhancement factor (Table 3.6) according to equations (3.9), (3.13), and (3.14), respectively.

Table 3.6. Analytical mixing-enhancement factor ($MF_{i,v}$ and $MF_{i,h}$ for 3-D and $MF_{i,v}$ for 2-D) at flow velocity of 1 and 5 m/d for 3-D and 2-D heterogeneous setups.

	3-D		**2-D**
Flow velocity	$MF_{i,v}$	$MF_{i,h}$	$MF_{i,v}$
1 m/d	3.2	3.2	6.9
5 m/d	2.8	2.8	6.2

The dilution enhancement quantified in Table 3.5 (~1.6 for 3-D case and ~1.8 for 2-D case) shows a qualitative agreement with the values based on the mixing-enhancement factor, reported in Table 3.6 (~3.0 for 3-D case and ~6.5 for 2-D case). Both results show a lower mixing enhancement due to flow focusing in three-dimensional than in two-dimensional systems. Notice that equations (3.8) and (3.12) assume complete flow focusing in the high-permeability inclusions. Using numerical simulations, we verified that at both mean flow velocities the fringe of the plume is only partially focused in the inclusion. As suggested by Werth et al. [2006], some corrections can be applied in order to consider such effects and this would lead to smaller values of *MF*. However, it is noticeable that the analytical equations for *MF*, although only valid under simplifying assumptions, are qualitatively supported by the outcomes of the flow-through experiments and allow capturing the distinct mixing enhancement in 2-D and 3-D systems. Despite the simplicity of the geometry of the system, Werth et al. [2006] have shown that the main outcomes of their two-dimensional analysis performed in a simplified setup, is useful to qualitatively interpret more realistic heterogeneous field-scale results. Similarly, the modeling and experimental results presented in this contribution, quantitatively describe mixing processes at the local scale and can help interpreting field-scale processes. In particular, they point to the relevance of considering fully three-dimensional structures in order to correctly describe mixing enhancement in porous media.

3.5.3 Compound-Specific Effects

In this part, we show the relevance of compound-specific effects upon transport of different solutes. Figure 3.9 shows the experimental and numerical results obtained at flow velocity of 5 m/d, using fluorescein (Figure 3.9a) and oxygen (Figure 3.9b) as tracer solutes. The normalized flux-related dilution index is reported for the 2-D and 3-D homogeneous and heterogeneous setups. Plume dilution at the outlet of the flow-through systems is larger for oxygen than for fluorescein in both 2-D and 3-D porous media. The match between the

predictive model and the experimental results is satisfactory, although oxygen measurements are affected by a larger uncertainty than the fluorescein ones, as discussed by Ye et al. [2015].

Computed and simulated values for the flux-related dilution index and the reactor ratio are summarized in Table 3.7. The difference between the normalized flux-related dilution index and reactor ratio can be explained with the same arguments used in the previous sections: dilution is larger in 3-D than in 2-D, whereas the mass flux is better distributed with respect to the total discharge in the 2-D systems than in the 3-D setups.

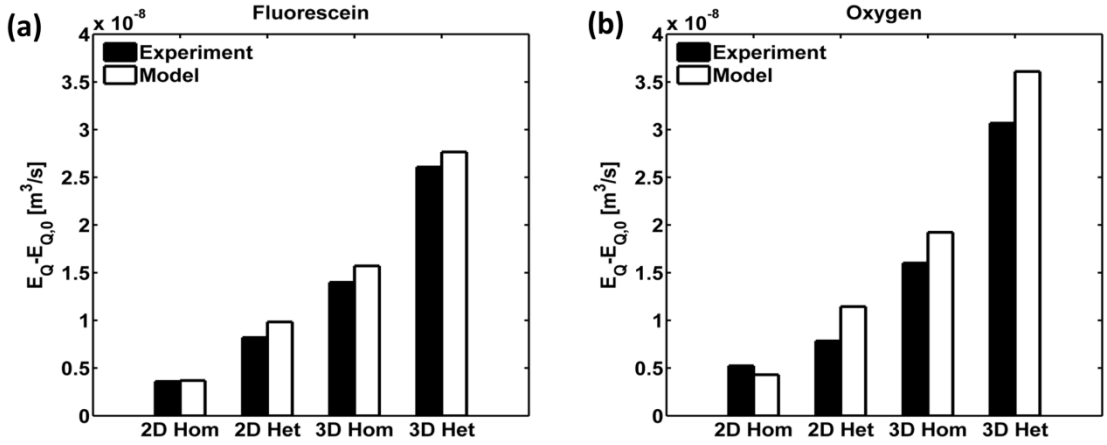

Fig. 3.9. Experimental and model results of normalized flux-related dilution indices for (a) fluorescein and (b) oxygen tracer solutes at the outlet of the flow-through chamber for four setups: 2-D homogeneous, 2-D heterogeneous, 3-D homogeneous, and 3-D heterogeneous at flow velocity of 5 m/d.

Table 3.7. Experimental and model results of flux-related dilution index, normalized flux-related dilution index, reactor ratio and normalized reactor ratio at the outlet of the 2-D and the 3-D heterogeneous setups for fluorescein and oxygen tracer plumes at mean flow velocity of 5 m/d.

	3-D			**2-D**		
Solute	Experiment	Model	Norm. Error (%)	Experiment	Model	Norm. Error (%)
Flux-related dilution index [m^3/s]						
Fluor.	3.16×10^{-8}	3.32×10^{-8}	5	1.14×10^{-8}	1.30×10^{-8}	13
Oxy.	3.62×10^{-8}	4.17×10^{-8}	13	1.10×10^{-8}	1.46×10^{-8}	25
Normalized Flux-related dilution index [m^3/s]						
Fluor.	2.61×10^{-8}	2.77×10^{-8}	6	8.21×10^{-9}	9.85×10^{-9}	17
Oxy.	3.07×10^{-8}	3.61×10^{-8}	15	7.84×10^{-9}	1.15×10^{-8}	32
Reactor ratio [-]						
Fluor.	0.23	0.24	5	0.51	0.58	13
Oxy.	0.26	0.30	13	0.49	0.66	25
Normalized reactor ratio [-]						
Fluor.	0.19	0.20	6	0.37	0.44	17
Oxy.	0.22	0.26	15	0.35	0.51	32

The experimental and modeling results shown in Figure 3.9 illustrate that compound-specific effects are not negligible even at very fast groundwater velocities (i.e., 5 m/d). In fact, also in such strongly advection-dominated regimes the transverse hydrodynamic dispersion coefficient and, in particular, the mechanical-dispersion term still depends on the diffusivity of the transported solutes, as also evidenced in previous theoretical and modeling works [e.g., Bijeljic and Blunt, 2007; Scheven, 2013]. This results in the larger dilution of oxygen plumes compared to the fluorescein plumes in the corresponding setups.

3.6 Conclusions

In this study, we theoretically analyzed, numerically simulated, and experimentally investigated dilution of steady state plumes in isotropic porous media with high-conductivity inclusions, with a simple geometry. We measured highly resolved concentration profiles and volumetric flow rates at the outlet of three different three-dimensional flow-through systems. The three different heterogeneous cases were obtained by inserting the same volume of high-permeability material into a homogeneous low-permeability matrix, but varying the geometry and the location of the inclusions. Dilution was quantified by the flux-related dilution index, which could be calculated for all travel distances in numerical simulations and at the outlet of the flow-through system in the experiments. The main outcomes of this study can be summarized as follows:

1. In high-permeability inclusions, both distances between streamlines and the time needed to travel a certain longitudinal distance are shortened. In 2-D systems, the effect of decreasing the transverse dispersion distance always prevails over the effect of decreasing the time available for mixing, thus resulting in an enhancement of transverse mixing and dilution in the inclusions even for the hypothetical case of pure, velocity-independent pore diffusion. In 3-D systems, the two effects cancel when flow focusing in the two transverse directions is identical. If flow focusing is anisotropic in the two transverse directions, the geometric effect is an increase in mixing in the direction in which the plume fringe is more strongly focused and a decrease in the direction corresponding to less focusing. In the simplified laboratory condition considered in this study, the mixing enhancement predicted for 2-D flow is the upper limit of that in 3-D media. The higher velocity in the high-conductivity inclusion, however, also leads to a higher value of the local transverse dispersion coefficient, which is further magnified by a larger grain size within the high-

conductivity material. This effect leads to an enhancement of 3-D transverse mixing if the plume fringe lies within the high-permeability inclusion, regardless of the geometry.

2. When the plume fringe is not focused within the high-permeability inclusion, the plume meanders in regions with lower flow velocity and dilution by transverse mixing diminishes. Therefore, the total dilution depends not only on the extent of the permeability contrast between the coarse material and the matrix and on the volumetric ratio of the two materials, but also on the exact spatial arrangement of the inclusions with respect to the location of the plume fringes. In all three heterogeneous setups studied in the experiment, dilution is enhanced in comparison to the homogeneous flow-through system, but to different extents. These results are in agreement with observations performed in similar two-dimensional experimental [e.g., Rolle et al., 2009] and modeling studies [e.g., Werth et al., 2006; Chiogna et al., 2011a].
3. Plume dilution by transverse mixing is more pronounced in the 3-D flow-through systems than in the 2-D system because transverse dispersion acts in two transverse directions in the 3-D case and only in one direction in the 2-D case. However, the dilution enhancement by flow focusing in high-permeability inclusions is larger in the quasi 2-D flow-through setup. Furthermore, we have shown that assuming a constant dispersion coefficient, which is a common assumption in stochastic subsurface hydrology, may lead to a significant underestimation of transverse-mixing enhancement in three-dimensional flow fields. Hence, it is crucial to determine the dimensionality of the problem and to correctly parameterize local dispersion to accurately interpret and model mixing processes in porous media.
4. The diffusivity of the transported solute affects the transverse hydrodynamic dispersion coefficient not just at low but also at high flow velocities, both in 2-D and 3-D systems. The relative importance of the local transverse dispersion coefficient for the enhancement of plume dilution is larger in 3-D than in 2-D systems [Ye et al., 2015], so that compound-specific effects on plume dilution are also more pronounced in 3-D than in 2-D flow-through systems. The heterogeneity of the medium does not decrease the compound-specific effects on transverse mixing, which is of particular relevance for reactive solute transport.

In natural aquifers and consolidated rocks, the complex shape, architecture, and connectivity of high-conductivity zones can lead to additional mixing-enhancement mechanisms [e.g., Stauffer, 2007; Chiogna et al., 2014, 2015; Cirpka et al., 2015] and complex pore-scale mixing dynamics [e.g., Bijeljic et al., 2013; Scheven et al., 2014], which have not been

investigated in this study. However, the difference between two-dimensional and three-dimensional mixing enhancement emerging from this analysis points to the need of considering fully three-dimensional geological structures in order to correctly describe mixing enhancement also at the field scale.

Despite the simple geometry of the heterogeneity used in the present study, we have been able to show that the dimensionality of the system and diffusion strongly influence transverse mixing and its enhancement. Such physical processes are fundamental mechanisms for mixing in porous media and therefore will contribute also to mixing of plumes at the larger field scale. Furthermore, we have shown that the outcomes derived from mixing studies focusing on two-dimensional simulations often performed with a simplified parameterization of the dispersion tensor, should be carefully extrapolated to the field scale. In more complex setups with multiple and randomly located inclusions the mixing enhancement will depend on the statistical properties of the field, on the geometric characteristic of the source, on the local dispersion coefficient, on the connectivity of the inclusions as well as on anisotropy of the formation.

Acknowledgments

This study was supported by the DFG (Deutsche Forschungsgemeinschaft, grants RO 4169/3-1 and CI-26/11-1).

Appendix B. Summary of the average normalized fluorescein concentrations measured in the flow-through experiments.

Table B1. Experimental measurements of normalized fluorescein concentration at the outlet for the 3-D homogeneous setup and the three 3-D heterogeneous setups at flow velocity of 1 m/d.

Sampling Location y [cm]	Sampling Location z [cm]	Hom	Case 1	Case 2	Case 3
0.55	0.55	6.74E-06	1.39E-05	1.48E-06	1.34E-05
1.65	0.55	1.14E-05	1.00E-09	1.40E-06	3.71E-06
2.75	0.55	1.53E-05	7.18E-05	3.59E-06	3.30E-05
3.85	0.55	1.00E-09	4.08E-04	9.31E-06	6.62E-05
4.95	0.55	2.53E-05	1.27E-04	1.06E-05	1.53E-05
6.05	0.55	6.35E-06	1.00E-09	3.33E-06	5.32E-06
7.15	0.55	1.37E-06	5.86E-06	1.00E-09	6.09E-06
0.55	1.65	7.07E-06	4.19E-06	2.24E-06	1.34E-05
1.65	1.65	1.29E-04	6.80E-04	2.42E-05	3.71E-06
2.75	1.65	1.81E-03	2.07E-02	7.74E-04	3.30E-05
3.85	1.65	4.92E-03	6.00E-02	5.98E-03	6.62E-05
4.95	1.65	2.18E-03	2.34E-02	7.32E-03	1.53E-05
6.05	1.65	1.20E-04	1.65E-03	3.79E-04	5.32E-06
7.15	1.65	6.67E-06	2.86E-06	5.20E-08	6.09E-06
0.55	2.75	1.36E-05	6.29E-06	4.68E-06	2.11E-05
1.65	2.75	4.19E-03	1.15E-02	8.37E-04	9.30E-03
2.75	2.75	7.33E-02	1.31E-01	5.12E-02	1.08E-01
3.85	2.75	2.06E-01	2.35E-01	2.09E-01	1.91E-01
4.95	2.75	9.15E-02	1.57E-01	1.59E-01	1.51E-01
6.05	2.75	5.13E-03	2.55E-02	9.07E-03	1.31E-02
7.15	2.75	2.73E-05	2.01E-04	2.16E-05	6.89E-05
0.55	3.85	5.69E-05	2.39E-05	1.90E-05	6.00E-05
1.65	3.85	1.36E-02	1.54E-02	6.65E-03	3.36E-02
2.75	3.85	2.26E-01	1.34E-01	1.61E-01	2.75E-01
3.85	3.85	5.27E-01	2.98E-01	4.42E-01	4.23E-01
4.95	3.85	2.48E-01	2.49E-01	2.99E-01	2.17E-01
6.05	3.85	1.81E-02	5.64E-02	2.12E-02	1.98E-02
7.15	3.85	1.45E-04	2.59E-04	2.59E-05	8.00E-05
0.55	4.95	2.06E-05	6.83E-06	2.57E-05	2.10E-05
1.65	4.95	3.96E-03	5.40E-03	6.46E-03	8.72E-03
2.75	4.95	6.48E-02	1.01E-01	1.00E-01	1.24E-01
3.85	4.95	1.78E-01	2.09E-01	2.73E-01	2.37E-01
4.95	4.95	7.63E-02	1.44E-01	1.45E-01	1.09E-01
6.05	4.95	6.27E-03	2.02E-02	8.31E-03	8.20E-03
7.15	4.95	4.95E-05	1.98E-05	1.50E-05	1.51E-05
0.55	6.05	3.92E-06	2.31E-06	5.05E-06	1.71E-06
1.65	6.05	6.01E-05	2.53E-04	2.91E-04	2.91E-04
2.75	6.05	1.39E-03	1.11E-02	3.37E-03	8.58E-03
3.85	6.05	4.06E-03	3.51E-02	1.51E-02	2.76E-02
4.95	6.05	2.21E-03	1.13E-02	6.13E-03	7.07E-03
6.05	6.05	7.22E-05	3.37E-04	1.32E-04	3.89E-04
7.15	6.05	6.67E-06	9.40E-07	4.81E-06	3.15E-06

0.55	7.15	3.40E-06	8.68E-07	1.30E-06	2.98E-06
1.65	7.15	3.24E-05	2.53E-07	6.30E-06	8.03E-06
2.75	7.15	6.03E-05	4.09E-06	1.40E-04	1.43E-05
3.85	7.15	9.83E-06	4.84E-05	2.86E-05	6.92E-05
4.95	7.15	9.10E-05	1.30E-06	2.36E-05	4.11E-05
6.05	7.15	9.93E-06	1.12E-06	1.74E-06	9.16E-06
7.15	7.15	2.81E-06	2.31E-06	7.54E-07	1.42E-06

Table B2. Experimental measurements of normalized fluorescein concentration at the outlet for the 3-D homogeneous setup and the three 3-D heterogeneous setups at flow velocity of 5 m/d.

Sampling Location y [cm]	Sampling Location z [cm]	Hom	Case 1	Case 2	Case 3
0.55	0.55	9.11E-07	1.82E-06	6.51E-06	2.00E-06
1.65	0.55	8.37E-07	1.39E-06	1.00E-09	2.39E-06
2.75	0.55	1.64E-06	1.57E-06	4.24E-06	2.96E-07
3.85	0.55	2.61E-06	2.75E-05	9.61E-06	1.05E-05
4.95	0.55	1.20E-07	2.89E-06	2.83E-06	2.34E-06
6.05	0.55	2.75E-06	9.87E-07	2.32E-06	2.60E-06
7.15	0.55	1.08E-06	8.36E-08	4.39E-06	1.91E-06
0.55	1.65	2.54E-06	1.44E-06	8.33E-07	7.51E-07
1.65	1.65	1.93E-06	5.49E-05	1.93E-05	1.39E-06
2.75	1.65	3.41E-04	1.77E-02	1.82E-04	8.42E-04
3.85	1.65	1.74E-03	5.56E-02	3.53E-03	3.11E-03
4.95	1.65	1.07E-03	1.21E-02	4.58E-03	3.32E-03
6.05	1.65	1.07E-05	5.25E-05	9.06E-05	4.85E-05
7.15	1.65	2.54E-06	1.14E-06	2.27E-06	8.38E-06
0.55	2.75	2.27E-06	1.00E-09	1.00E-09	1.14E-06
1.65	2.75	2.15E-04	3.51E-03	1.60E-04	1.54E-03
2.75	2.75	5.14E-02	1.25E-01	5.48E-02	5.10E-02
3.85	2.75	2.50E-01	2.69E-01	3.04E-01	1.41E-01
4.95	2.75	1.01E-01	9.91E-02	2.40E-01	1.49E-01
6.05	2.75	1.65E-03	4.98E-03	5.52E-03	4.31E-03
7.15	2.75	2.26E-06	5.42E-06	3.36E-06	2.55E-06
0.55	3.85	2.11E-06	1.35E-06	3.94E-06	5.85E-06
1.65	3.85	1.53E-03	1.25E-02	1.07E-03	1.33E-02
2.75	3.85	1.76E-01	1.63E-01	1.58E-01	3.00E-01
3.85	3.85	7.42E-01	3.92E-01	5.61E-01	4.52E-01
4.95	3.85	3.07E-01	2.46E-01	3.18E-01	2.28E-01
6.05	3.85	6.00E-03	2.48E-02	6.92E-03	5.90E-03
7.15	3.85	3.35E-06	7.81E-06	2.62E-06	4.10E-06
0.55	4.95	5.98E-07	2.68E-07	7.07E-07	1.80E-06
1.65	4.95	9.83E-04	3.87E-03	3.05E-04	2.44E-03
2.75	4.95	5.88E-02	1.33E-01	3.80E-02	1.10E-01
3.85	4.95	2.45E-01	2.78E-01	2.04E-01	2.52E-01
4.95	4.95	1.32E-01	1.45E-01	7.81E-02	1.36E-01
6.05	4.95	3.46E-03	8.96E-03	4.43E-04	3.70E-03
7.15	4.95	1.00E-09	3.43E-06	1.74E-06	1.82E-06
0.55	6.05	1.94E-06	2.34E-07	1.77E-07	2.34E-06
1.65	6.05	7.04E-06	1.93E-05	2.54E-05	4.80E-06
2.75	6.05	4.16E-04	4.57E-03	7.92E-05	3.45E-03
3.85	6.05	9.84E-04	2.47E-02	6.61E-04	2.20E-02
4.95	6.05	1.46E-03	4.70E-03	3.66E-04	3.37E-03
6.05	6.05	6.34E-05	2.57E-05	1.21E-05	3.65E-05
7.15	6.05	6.57E-07	1.71E-06	1.84E-06	2.12E-06
0.55	7.15	7.77E-07	1.00E-09	2.27E-07	7.06E-07
1.65	7.15	3.17E-06	1.10E-06	1.51E-07	1.00E-09
2.75	7.15	4.78E-07	9.87E-07	1.04E-05	6.51E-06
3.85	7.15	1.00E-09	4.68E-07	8.83E-06	3.60E-05
4.95	7.15	1.79E-06	1.67E-07	2.93E-06	7.03E-06

6.05	7.15	2.99E-07	1.00E-09	2.25E-06	1.16E-06
7.15	7.15	1.00E-09	5.85E-07	1.59E-06	4.10E-07

References

Annable, M. D., K. Hatfield, J. Cho, H. Klammer, B. L. Parker, J. A. Cherry, and P. S. C. Rao (2005), Field-scale evaluation of the passive flux-meter for simultaneous measurement of groundwater and contaminant fluxes, Environ. Sci. Technol., 39(18), 7194–7201, doi: 10.1021/es050074g.

Anneser, B., F. Einsiedl, R. U. Meckenstock, L. Richters, F. Wisotzky, and C. Griebler (2008), High-resolution monitoring of biogeochemical gradients in a tar oil-contaminated aquifer, Appl. Geochem., 23(6), 1715–1730, doi: 10.1016/j.apgeochem.2008.02.003.

Atkins, P. W. (1990), Physical Chemistry, Oxford Univ. Press, Oxford, U. K.

Bauer, R. D., M. Rolle, P. K€urzinger, P. Grathwohl, R. U. Meckenstock, and C. Griebler (2009), Two-dimensional flow-through microcosms—Versatile test systems to study biodegradation processes in porous aquifers, J. Hydrol., 369(3–4), 284–295, doi: 10.1016/j.jhydrol.2009.02.037.

Bear, J. (1972), Dynamics of Fluids in Porous Media, Dover, N. Y.

Bear, J., and Y. Bachmat (1967), A generalized theory on hydrodynamic dispersion in porous media, in IASH Symposium on Artificial Recharge and Management of Aquifers, IASH Publ. 72, pp. 7–16, Int. Union Geod. Geophys., Haifa, Israel.

Bijeljic, B., and M. J. Blunt (2007), Pore-scale modelling of transverse dispersion in porous media, Water Resour. Res., 43, W12S11, doi: 10.1029/2006WR005700.

Bijeljic, B., A. Raeini, P. Mostaghimi, and M. J. Blunt (2013), Predictions of non-Fickian solute transport in different classes of porous media using direct simulation on pore-scale images, Phys. Rev. E, 87, 013011, doi: 10.1103/PhysRevE.87.013011.

Bjerg, P. L., N. Tuxen, L. A. Reitzel, H. J. Albrechtsen, and P. Kjeldsen (2011), Natural attenuation processes in landfill leachate plumes at three Danish sites, Ground Water, 49(5), 688–705, doi: 10.1111/j.1745-6584.2009.00613.x.

Carsel, R. F., and R. S. Parrish (1988), Developing joint probability distributions of soil water retention characteristics, Water Resour. Res., 24(5), 755–769.

Castro-Alcala, E., D. Fernandez-Garcia, J. Carrera, and D. Bolster (2012), Visualization of mixing processes in a heterogeneous sand box aquifer, Environ. Sci. Technol., 46(6), 3228–3235, doi: 10.1021/es201779p.

Chen, Q., W. Kinzelbach, and S. Oswald (2002), Nuclear magnetic resonance imaging for studies of flow and transport in porous media, J. Environ. Qual., 31(2), 477–486.

Chiogna, G., and A. Bellin (2013), Analytical solution for reactive solute transport considering incomplete mixing within a reference elementary volume, Water Resour. Res., 49, 2589–2600, doi: 10.1002/wrcr.20200.

Chiogna, G., C. Eberhardt, P. Grathwohl, O. A. Cirpka, and M. Rolle (2010), Evidence of compound-dependent hydrodynamic and mechanical transverse dispersion by multitracer laboratory experiments, Environ. Sci. Technol., 44(2), 688–693, doi: 10.1021/es9023964.

Chiogna, G., O. A. Cirpka, P. Grathwohl, and M. Rolle (2011a), Transverse mixing of conservative and reactive tracers in porous media: Quantification through the concepts of flux-related and critical dilution indices, Water Resour. Res., 47, W02505, doi: 10.1029/2010WR009608.

Chiogna, G., O. A. Cirpka, P. Grathwohl, and M. Rolle (2011b), Relevance of local compound-specific transverse dispersion for conservative and reactive mixing in heterogeneous porous media, Water Resour. Res., 47, W07540, doi: 10.1029/2010WR010270.

Chiogna, G., D. L. Hochstetler, A. Bellin, P. K. Kitanidis, and M. Rolle (2012), Mixing, entropy and reactive solute transport, Geophys. Res. Lett., 39, L20405, doi: 10.1029/2012GL053295.

Chiogna, G., M. Rolle, A. Bellin, and O. A. Cirpka (2014), Helicity and flow topology in three-dimensional anisotropic porous media, Adv. Water Resour., 73, 134–143, doi: 10.1016/j.advwatres.2014.06.017.

Chiogna, G., O. A. Cirpka, M. Rolle, and A. Bellin (2015), Helical flow in three-dimensional non-stationary anisotropic heterogeneous porous media, Water Resour. Res., 51, 261–280, doi: 10.1002/2014WR015330.

Cirpka, O. A., and S. Attinger (2003), Effective dispersion in heterogeneous media under random transient flow conditions, Water Resour. Res., 39(9), 1257, doi: 10.1029/2002WR001931.

Cirpka, O. A., E. O. Frind, and R. Helmig (1999), Numerical simulation of biodegradation controlled by transverse mixing, J. Contam. Hydrol., 40(2), 159–182, doi: 10.1016/S0169-7722(99)00044-3.

Cirpka, O. A., A. Olsson, Q. Ju, M. A. Rahman, and P. Grathwohl (2006), Determination of transverse dispersion coefficients from reactive plume lengths, Ground Water, 44(2), 212–221, doi: 10.1111/j.1745-6584.2005.00124.x.

Cirpka, O. A., F. P. J. de Barros, G. Chiogna, M. Rolle, and W. Nowak (2011), Stochastic flux-related analysis of transverse mixing in two-dimensional heterogeneous porous media, Water Resour. Res., 47, W06515, doi: 10.1029/2010WR010279.

Cirpka, O. A., M. Rolle, G. Chiogna, F. P. de Barros, and W. Nowak (2012), Stochastic evaluation of mixing-controlled steady-state plume lengths in two-dimensional heterogeneous domains, J. Contam. Hydrol., 138–139, 22–39, doi: 10.1016/j.jconhyd.2012.05.007.

Cirpka, O. A., G. Chiogna, M. Rolle, and A. Bellin (2015), Transverse mixing in three-dimensional non-stationary anisotropic heterogeneous porous media, Water Resour. Res., 51, 241–260, doi: 10.1002/2014WR015331.

Danquigny, C., P. Ackerer, and J. P. Carlier (2004), Laboratory tracer tests on three-dimensional reconstructed heterogeneous porous media, J. Hydrol., 294(1–3), 196–212, doi: 10.1016/j.jhydrol.2004.02.008.

Davis, G. B., C. Barber, T. R. Power, J. Thierrin, B. M. Patterson, J. L. Rayner, and Q. Wu (1999), The variability and intrinsic remediation of a BTEX plume in anaerobic sulphate-rich groundwater, J. Contam. Hydrol., 36, 265–290, doi: 10.1016/S0169-7722(98)00148-X.

de Anna, P., J. Jimenez-Martinez, H. Tabuteau, R. Turuban, T. Le Borgne, M. Derrien, and Y. Meheust (2014), Mixing and reaction kinetics in porous media: An experimental pore scale quantification, Environ. Sci. Technol., 48(1), 508–516, doi: 10.1021/es403105b.

de Barros, F. P. J., M. Dentz, J. Koch, and W. Nowak (2012), Flow topology and scalar mixing in spatially heterogeneous flow fields, Geophys. Res. Lett., 39, L08404, doi: 10.1029/2012GL051302.

de Dreuzy, J. R., J. Carrera, M. Dentz, and T. Le Borgne (2012), Time evolution of mixing in heterogeneous porous media, Water Resour. Res., 48, W06511, doi: 10.1029/20110078011360.

Dentz, M., and J. Carrera (2003), Effective dispersion in temporally fluctuating flow through a heterogeneous medium, Phys. Rev. E, 68(3), 036310, doi: 10.1103/PhysRevE.68.036310.

Devlin, J. F., P. C. Schilling, I. Bowen, C. E. Critchley, D. L. Rudolph, N. R. Thomson, G. P. Tsoflias, and J. A. Roberts (2012), Applications and implications of direct groundwater measurement at the centimetre scale, J. Contam. Hydrol., 127(1–4), 3–14, doi: 10.1016/ j.jconhyd.2011.06.007.

Fetter, C. W. (2000), Applied Hydrogeology, Prentice Hall, Upper Saddle River, N. J.

Haberer, C. M., M. Rolle, S. Liu, O. A. Cirpka, and P. Grathwohl (2011), A high-resolution non-invasive approach to quantify oxygen transport across the capillary fringe and within the underlying groundwater, J. Contam. Hydrol., 122(1–4), 26–39, doi: 10.1016/ j.jconhyd.2010.10.006.

Haberer, C. M., M. Rolle, O. A. Cirpka, and P. Grathwohl (2012), Oxygen transfer in a fluctuating capillary fringe, Vadose Zone J., 11(3), doi: 10.2136/vzj2011.0056.

Haberer, C. M., O. A. Cirpka, M. Rolle, and P. Grathwohl (2014), Experimental sensitivity analysis of oxygen transfer in the capillary fringe, Ground Water, 52(1), 37–49, doi: 10.1111/gwat.12028.

Haberer, C. M., M. Rolle, O. A. Cirpka, and P. Grathwohl (2015), Impact of heterogeneity on oxygen transfer in a fluctuating capillary fringe, Ground Water, 53(1), 57–70, doi: 10.1111/gwat.12149.

Ham, P. A. S., R. J. Schotting, H. Prommer, and G. B. Davis (2004), Effects of hydrodynamic dispersion on plume lengths for instantaneous bimolecular reactions, Adv. Water Resour., 27(8), 803–813, doi: 10.1016/j.aadvwatres.2004.05.008.

Hazen, A. (1892), Some physical properties of sands and gravels with special reference to their use in filtration, in 24th Annual Report, Mass. State Board Health, pp. 541–556, Mass.

Heinz, J., and T. Aigner (2003), Three-dimensional GPR analysis of various Quaternary gravel-bed braided river deposits (southwestern Germany), in Ground Penetrating Radar in Sediments, vol. 211, edited by C. Bristow and H. Jol, pp. 99–110, Spec. Publ. Geol. Soc., London, U. K.

Herrera, P. A., and A. J. Valocchi (2006), Positive solution of two-dimensional solute transport in heterogeneous aquifers, Ground Water, 44(6), 803–813, doi: 10.1111/j.1745-6584.2006.00154.x.

Herrera, P. A., A. J. Valocchi, and R. D. Beckie (2010), A multidimensional streamline-based method to simulate reactive solute transport in heterogeneous porous media, Adv. Water Resour., 33(7), 711–727, doi: 10.1016/j.advwatres.2010.03.001.

Hochstetler, D. L., M. Rolle, G. Chiogna, C. M. Haberer, P. Grathwohl, and P. K. Kitanidis (2013), Effects of compound-specific transverse mixing on steady-state reactive

plumes: Insights from pore-scale simulations and Darcy-scaly experiments, Adv. Water Resour., 54, 1–10, doi: 10.1016/j.advwatres.2012.12.007.

Kitanidis, P. K. (1994), The concept of dilution index, Water Resour. Res., 30(7), 2011–2026, doi: 10.1029/94WR00762.

Klenk, I. D., and P. Grathwohl (2002), Transverse vertical dispersion in groundwater and the capillary fringe, J. Contam. Hydrol., 58(1–2), 111–128, doi: 10.1016/S0169-7722(02)00011-6.

Knutson, C., A. Valocchi, and C. Werth (2007), Comparison of continuum and pore-scale models of nutrient biodegradation under transverse mixing conditions, Adv. Water Resour., 30(6–7), 1421–1431, doi: 10.1016/j.advwatres.2006.05.012.

Le Borgne, T., M. Dentz, and E. Villermaux (2013), Stretching, coalescence, and mixing in porous media, Phys. Rev. Lett., 110(20), 204501, doi: 10.1103/PhysRevLett.110.204501.

Lerner, D. N., S. F. Thornton, M. J. Spence, S. A. Banwart, S. H. Bottrell, J. J. Higgo, H. E. H. Mallinson, R. W. Pickup, and G. M. Williams (2000), Ineffective natural attenuation of degradable organic compounds in a phenol-contaminated aquifer, Ground Water, 38(6), 922–928, doi: 10.1111/j.1745-6584.2000.tb00692.x.

Liedl, R., A. J. Valocchi, P. Dietrich, and P. Grathwohl (2005), Finiteness of steady state plumes, Water Resour. Res., 41, W12501, doi: 10.1029/2005WR004000.

Liedl, R., P. K. Yadav, and P. Dietrich (2011), Length of 3-D mixing-controlled plumes for a fully penetrating contaminant source with finite width, Water Resour. Res., 47, W08602, doi: 10.1029/2010WR009710.

Mace, R. E., R. S. Fisher, D. Welch, and S. Parra (1997), Extent, mass, and duration of hydrocarbon plumes from leaking petroleum storage tank sites in Texas, Geol. Circ. 97-1, Bur. of Econ. Geol., Univ. of Tex., Austin.

Maier, U., and P. Grathwohl (2006), Numerical experiments and field results on the size of steady state plumes, J. Contam. Hydrol., 85(1–2), 33–52, doi: 10.1016/j.jconhyd.2005.12.012.

Marica, F., S. A. Jofre, K. U. Mayer, B. J. Balcom, and T. A. Al (2011), Determination of spatially-resolved porosity, tracer distributions and diffusion coefficients in porous media using MRI measurements and numerical simulations, J. Contam. Hydrol., 125(1–4), 47–56, doi: 10.1016/j.jconhyd.2011.04.008.

Mayer, K. U., S. G. Benner, E. O. Frind, S. F. Thornton, and D. N. Lerner (2001), Reactive transport modeling of processes controlling the distribution and natural attenuation of phenolic compounds in a deep sandstone aquifer, J. Contam. Hydrol., 53(3–4), 341–368, doi: 10.1016/ S0169-7722(01)00173-5.

McCray, J. E., and R. W. Falta (1997), Numerical simulation of air sparging for remediation of NAPL contamination, Ground Water, 35(1), 99–110, doi: 10.1111/j.1745-6584.1997.tb00065.x.

Oswald, S., W. Kinzelbach, A. Greiner, and G. Brix (1997), Observation of flow and transport processes in artificial porous media via magnetic resonance imaging in three dimensions, Geoderma, 80(3–4), 417–429, doi: 10.1016/S0016-7061(97)00064-5.

Oswald, S. E., and W. Kinzelbach (2004), Three-dimensional physical benchmark experiments to test variable-density flow models, J. Hydrol., 290(1–2), 22–42, doi: 10.1016/j.jhydrol.2003.11.037.

Pedretti, D., D. Fernandez-Garcia, D. Bolster, and X. Sanchez-Vila (2013), On the formation of breakthrough curves tailing during convergent flow tracer tests in three-dimensional heterogeneous aquifers, Water Resour. Res., 49, 4157–4173, doi: 10.1002/wrcr.20330.

Pollock, D. W. (1988), Semi-analytical computation of path lines for finite-difference models, Ground Water, 26(6), 743–750, doi: 10.1111/j.1745-6584.1988.tb00425.x.

Porta, G. M., S. Chaynikov, J. Thovert, M. Riva, A. Guadagnini, and P. M. Adler (2013), Numerical investigation of pore and continuum scale formulations of bimolecular reactive transport in porous media, Adv. Water Resour., 62, 243–253, doi: 10.1016/j.advwatres.2013.09.007.

Prommer, H., N. Tuxen, and P. Bjerg (2006), Fringe-controlled natural attenuation of phenoxy acids in a landfill plume: Integration of field-scale processes by reactive transport modeling, Environ. Sci. Technol., 40, 4732–4738, doi: 10.1021/es0603002.

Prommer, H., B. Anneser, M. Rolle, F. Einsiedl, and C. Griebler (2009), Biogeochemical and isotopic gradients in a BTEX/PAH contaminant plume: Model-based interpretation of a high-resolution field data set, Environ. Sci. Technol., 43, 8206–8212, doi: 10.1021/es901142a.

Rahman, M. A., S. C. Jose, W. Nowak, and O. A. Cirpka (2005), Experiments on vertical transverse mixing in a large-scale heterogeneous model aquifer, J. Contam. Hydrol., 80(3–4), 130–148, doi: 10.1016/j.jconhyd.2005.06.010.

Rashidi, M., L. Peurrung, A. F. B. Tompson, and T. J. Kulp (1996), Experimental analysis of pore-scale flow and transport in porous media, Adv. Water Resour., 19(3), 163–180, doi: 10.1016/0309-1708(95)00048-8.

Renard, P., and D. Allard (2013), Connectivity metrics for subsurface flow and transport, Adv. Water Resour., 51, 168–196, doi: 10.1016/ j.advwatres.2011.12.001.

Rolle, M., and P. K. Kitanidis (2014), Effects of compound-specific dilution on transient transport and solute breakthrough: A pore-scale analysis, Adv. Water Resour., 71, 186–199, doi: 10.1016/j.advwatres.2014.06.012.

Rolle, M., C. Eberhardt, G. Chiogna, O. A. Cirpka, and P. Grathwohl (2009), Enhancement of dilution and transverse reactive mixing in porous media: Experiments and model-based interpretation, J. Contam. Hydrol., 110(3–4), 130–142, doi: 10.1016/j.jconhyd.2009.10.003.

Rolle, M., D. L. Hochstetler, G. Chiogna, P. K. Kitanidis, and P. Grathwohl (2012), Experimental investigation and pore-scale modeling interpretation of compound-specific transverse dispersion in porous media, Transp. Porous Media, 93(3), 347–362, doi: 10.1007/s11242-012-9953-8.

Rolle, M., M. Muniruzzaman, C. M. Haberer, and P. Grathwohl (2013a), Coulombic effects in advection-dominated transport of electrolytes in porous media: Multicomponent ionic dispersion, Geochim. Cosmochim. Acta, 120, 195–205, doi: 10.1016/j.gca.2013.06.031.

Rolle, M., G. Chiogna, D. L. Hochstetler, and P. K. Kitanidis (2013b), On the importance of diffusion and compound-specific mixing for groundwater transport: An investigation

from pore to field scale, J. Contam. Hydrol., 153, 51–68, doi: 10.1016/j.jconhyd.2013.07.006.

Scheven, U. M. (2013), Pore-scale mixing and transverse dispersivity of randomly packed monodisperse spheres, Phys. Rev. Lett., 110, 214504, doi: 10.1103/PhysRevLett.110.214504.

Scheven, U. M., S. Khirevich, A. Daneyko, and U. Tallarek (2014), Longitudinal and transverse dispersion in flow through random packings of spheres: A quantitative comparison of experiments, simulations, and models, Phys. Rev. E, 89, 053023, doi: 10.1103/PhysRevE.89.053023.

Silliman, S. E. (1996), The importance of the third dimension on transport through saturated porous media: Case study based on transport of particles, J. Hydrol., 179(1–4), 181–195, doi: 10.1016/0022-1694(95)02838-2.

Stauffer F. (2007), Impact of highly permeable sediment units with inclined bedding on solute transport in aquifers, Adv. Water Resour., 30, 2194–2201, doi: 10.1016/j.advwatres.2007.04.008.

Tartakovsky, A. M., G. D. Tartakovsky, and T. D. Scheibe (2009), Effects of incomplete mixing on multicomponent reactive transport, Adv. Water Resour., 32(11), 1674–1679, doi: 10.1016/j.advwatres.2009.08.012.

Thornton, S. F., S. Quigley, M. J. Spence, S. A. Banwart, S. Bottrell, and D. N. Lerner (2001), Process controlling the distribution and natural attenuation of dissolved phenolic compounds in a deep sandstone aquifer, J. Contam. Hydrol., 53, 233–267, doi: 10.1016/S0169- 7722(01)00168-1.

van der Kamp, G., L. D. Luba, J. A. Cherry, and H. Maathuis (1994), Field study of a long and very narrow contaminant plume, Ground Water, 32(6), 1008–1016, doi: 10.1111/j.1745-6584.1994.tb00940.x.

van Genuchten, M. T. (1980), A closed-form equation for predicting the hydraulic conductivity in unsaturated soils, Soil Sci. Soc. Am. J., 44(5), 892–898, doi: 10.2136/sssaj1980.03615995004400050002x.

Werth, C. J., O. A. Cirpka, and P. Grathwohl (2006), Enhanced mixing and reaction through flow focusing in heterogeneous porous media, Water Resour. Res., 42, W12414, doi: 10.1029/2005WR004511.

Wexler, E. J. (1992), Analytical solutions for one-, two-, and three-dimensional solute transport in ground-water flow systems with uniform flow, in Applications of Hydraulics, vol. 3, chap. B7, U.S. Geol. Surv., N. Y.

Wiedemeier, T. H., H. S. Rifai, C. J. Newell, and J. T. Wilson (1999), Natural Attenuation and Fuels and Chlorinated Solvents in the Subsurface, John Wiley, Hoboken, N. J.

Willingham, T. W., C. J. Werth, and A. J. Valocchi (2008), Evaluation of the effects of porous media structure on mixing-controlled reactions using pore-scale modeling and micromodel experiments, Environ. Sci. Technol., 42(9), 3185–3193, doi: 10.1021/es7022835.

Worch, E. (1993), A new equation for the calculation of diffusion coefficients for dissolved substances, Vom Wasser, 81, 289–297.

Ye, Y., G. Chiogna, O. A. Cirpka, P. Grathwohl, and M. Rolle (2015), Experimental investigation of compound-specific dilution of solute plumes in saturated porous

media: 2-D vs. 3-D flow-through systems, J. Contam. Hydrol., 172, 33–47, doi: 10.1016/j.jconhyd.2014.11.002.

Yoon, H., and S. A. McKenna (2012), Highly parameterized inverse estimation of hydraulic conductivity and porosity in a three-dimensional, heterogeneous transport experiment, Water Resour. Res., 48, W10536, doi: 10.1029/2012WR012149.

Zarlenga, A., and A. Fiori (2013), Steady plumes in heterogeneous porous formations: A stochastic Lagrangian approach, Water Resour. Res., 49, 864–873, doi: 10.1002/wrcr.20106.

Zarlenga, A., and A. Fiori (2014), Stochastic analytical modeling of the biodegradation of steady plumes, J. Contam. Hydrol., 157, 106–116, doi: 10.1016/j.jconhyd.2013.11.003.

4. Experimental Evidence of Helical Flow in Porous Media

Yu Ye, Gabriele Chiogna, Olaf Cirpka, Peter Grathwohl and Massimo Rolle

Physical Review Letters (2015), vol. 115, pp. 194502, doi: 10.1103/PhysRevLett.115.194502.

Abstract

Helical flow leads to deformation of solute plumes and enhances transverse mixing in porous media. We present experiments in which macroscopic helical flow is created by arranging different materials to obtain an anisotropic macroscopic permeability tensor with spatially variable orientation. The resulting helical flow entails twisting streamlines which cause a significant increase in lateral mass exchange and thus a large enhancement of plume dilution (up to 235%) compared to transport in homogenous media. The setup may be used to effectively mix solutes in parallel streams similarly to static mixers, but in porous media.

Mixing processes are widely studied in fluid mechanics due to their relevance for many industrial and environmental processes [1–4]. While in turbulent flows efficient mixing can be easily achieved [5], slow diffusive processes mixing in laminar and creeping flows encountered in engineering systems such as chemical separators, chromatography columns, micromixers and filters, as well as in natural geologic formations like aquifers and oil reservoirs [6–8]. Under these conditions, the topology of the flow field and its complex structure are fundamental to enhance and control mixing processes [1,6,9,10]. Flows in porous media have been mainly analyzed focusing on the shearing effects of heterogeneity on scalar mixing [11–14]. Most studies have considered heterogeneous isotropic porous media, in which the flow has a zero helicity density; i.e., the flow vector is always perpendicular to the vorticity vector [15]. However, a few theoretical and numerical studies [16–18] have shown that helical flows with nonzero helicity density can occur in three-dimensional anisotropic porous media. Yet, an experimental proof of the real occurrence of such flows in porous media is still missing.

In this Letter, we present laboratory flow-through experiments in a three-dimensional heterogeneous, anisotropic packed bed that prove the existence of helical flows in porous media, and we quantify the impact of such flows on steady-state transport and dilution of solute plumes.

Figure 1 shows a photograph of the experimental setup. The three-dimensional flow-through chamber has an inner dimension of 30 cm × 7.7 cm × 10 cm. It has 25 ports (5 × 5 array) at the inlet and 49 ports (7 × 7 array) at the outlet. The ports at the inlet are equally spaced with a distance of 1.54 cm, while at the outlet the distance between the ports is reduced to 1.1 cm in order to increase the spatial resolution of solute concentration and flow rate measurements. Rubber septa are plugged at all ports and stainless-steel syringe needles are inserted into the septa for liquid injection and extraction. High-precision multichannel peristaltic pumps (Ismatec, Glattbrugg, Switzerland) are used to establish steady-state flow in the flow-through setup. The pumping rates are individually calibrated for each channel of the inlet and outlet pumps before the experiments, and they are monitored during the experimental runs to ensure stable flow conditions. The porous medium in the three-dimensional flow-through chamber consists of three layers. It has spatially heterogeneous and anisotropic permeability at the relevant scale for the observation of helical flow [18], but isotropic porosity. Both layer 1 and layer 2 consist of two types of glass beads (Sigmund Lindner, Warmensteinach, Germany), one with a fine grain size of 0.4–0.6 mm and the other with a coarse grain size of 1.5–2.0 mm.

The porosity was determined gravimetrically, and a value of 0.4 found for both the fine and the coarse material. The architecture of the porous medium was obtained by alternating angled stripes of high and low hydraulic conductivity in layer 1 and layer 2 (Fig. 4.1), and it was designed to achieve a simplified representation of herringbone cross-stratification, a pattern observed in subsurface sedimentary depositional environments [19]. Therefore, the porosity is invariant through the medium, but the permeability, and thus the hydraulic conductivity, varies from one stripe to the next. The hydraulic conductivity within the stripes is locally isotropic; its value was calculated from the grain size following Hazen [20]. A metal frame was used to achieve this arrangement during the filling of each layer and then removed. The height of the two layers was identical (3.08 cm). A homogeneous layer of fine material (0.4–0.6 mm) saturated for a thickness of 1.54 cm was placed on top of layer 2. Such a layer was needed to maintain water-saturated conditions in the coarse glass beads in layer 1 and layer 2. The average seepage velocity in the porous medium was 3 m/day for all experimental runs, which leads to a maximum of grain-Péclet number (i.e., $Pe=vd/D_{aq}$, where v is the seepage velocity, d is the grain diameter and D_{aq} is the aqueous diffusion coefficient) of 2.25 $\times$ 10^3, and a maximum grain-Reynolds number (i.e., $Re=qd/v$, where q is the specific discharge and v is the kinematic viscosity) of 1.08 (data derived from the numerical simulations). After establishing steady-state flow conditions, a dilute sodium fluorescein solution with a concentration of 15 mg/l was injected from a selected inlet port. Three experiments were performed exchanging the tracer injection port. After flushing 8 pore volumes, steady-state transport conditions were achieved and samples were collected at the 49 outlet ports. Fluorescein concentrations at all ports were measured using a UV-spectrometer (Perkin Elmer LS-3B), and the flow rate at each port was determined gravimetrically by weighting the samples and measuring the sampling time.

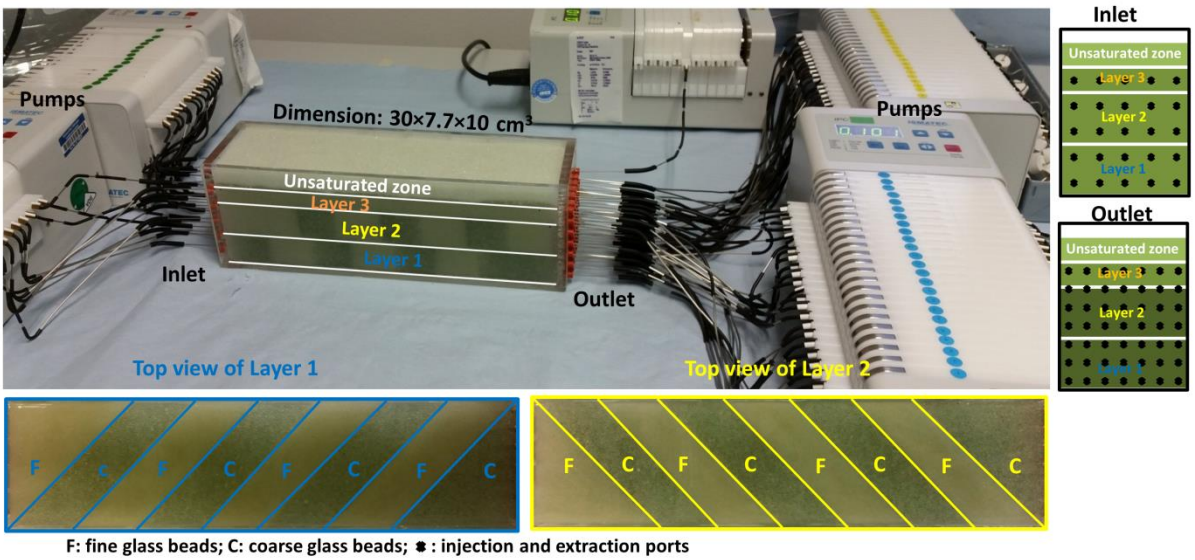

Fig. 4.1. Photograph of the experimental setup: Top view of the two layers with alternate stripes of fine and coarse material used to build the heterogeneous anisotropic porous medium, and side views of the inlet and the outlet with marked injection and extraction ports, respectively.

We performed flow and transport simulations using the numerical code described in Ref. [21] to quantitatively interpret the experimental observations. Flow was calculated according to the governing steady-state flow equation in saturated porous media obtained by combining Darcy's law and the continuity equation:

$$\nabla \cdot \left(\mathbf{q}(\mathbf{x})\right) = \nabla \cdot \left(-\mathbf{K}(\mathbf{x}) \nabla \phi(\mathbf{x})\right) = 0 \tag{4.1}$$

where $\mathbf{x}$ [L] denotes the vector of spatial coordinates, $\mathbf{K}$ [LT^{-1}] is the hydraulic conductivity tensor (here assumed isotropic as the stripes of different materials are spatially resolved), ϕ [L] is the hydraulic head, and $\mathbf{q}$ [LT^{-1}] is the specific discharge vector as defined by Bear [22]. In our experimental setup the permeabilities and their differences are low, thus the Brinkman correction term in Darcy's law can be neglected [23]. Equation (4.1) was solved considering fixed-flux boundary conditions for each injection and extraction port, while no-flow conditions were applied at the other boundaries of the flow-through chamber. Steady-state non-reactive transport was described by the advection-dispersion equation:

$$\mathbf{v} \cdot \nabla c - \nabla \cdot \left(D_t \nabla c\right) = 0 \tag{4.2}$$

where c [ML^{-3}] is the concentration, $\mathbf{v}=\mathbf{q}/\theta$ [LT^{-1}] is the seepage velocity vector (also denoted as linear average velocity of water), θ [-] is the porosity and D_t [L^2T^{-1}] is the transverse dispersion coefficient. For continuous injection under steady-state transport conditions the

longitudinal dispersion term in the advection-dispersion equation can be neglected [24]. The accurate description of the transverse dispersion coefficient should properly capture the coupled interaction between the aqueous diffusivity of the solute ($D_{aq,fluorescein}$ = 0.48×10^{-9} m^2/s) and mechanical dispersion [25,26]. In this study, we used the nonlinear compound-specific parameterization proposed by Chiogna et al. [27] with the parameters for the materials reported by Ye et al. [28]. A constant injection concentration was applied as boundary condition for the inlet ports. The fixed concentration was 15 mg/l for the tracer injection port and 0 mg/l for all surrounding ports through which pure water was pumped into the flow-through system.

Dilution of steady-state solute plumes along the main flow direction x is quantified using the flux-related dilution index $E_Q(x)$ [L^3T^{-1}] [29]:

$$E_Q(x) = \exp\left(-\int_\Omega \left[p_Q(x,y,z)\ln p_Q(x,y,z)\right] q_x(x,y,z)\,dA\right) \tag{4.3}$$

where Ω is the cross-section perpendicular to the main flow direction, $q_x(x,y,z)$ [LT^{-1}] is the specific-discharge component in the longitudinal direction x and $p_Q(x,y,z)$ [TL^{-3}] is the flux-weighted probability density function of the solute mass, defined as

$$p_Q(x,y,z) = \frac{c(x,y,z)}{\int_\Omega c(x,y,z)\,q_x(x,y,z)\,dA} \tag{4.4}$$

The metric E_Q was derived in analogy to the (volume-related) dilution index E [L^3] [30] and has been used in both Darcy and Stokes flows [31]. It represents the exponential of the Shannon or information entropy, which is a measure of disorder [32] of the solute mass flux and quantifies how a given solute mass flux is distributed over the water flux transporting the solute at a given longitudinal position x. While Eq. (4.3) contains the logarithm of a dimensional property (here p_Q), it is dimensionally correct and may be written as the limit of a discrete exponential of the entropy where all terms in exponents and logarithms are dimensionless [30]. E_Q was calculated at the inlet and at the outlet according to the experimental measurements of concentration and flow rate, while it was computed at all cross sections along the travel distance in the numerical simulations.

Figure 4.2 shows the tracer concentrations at the outlet of the flow-through setup for the three experiments performed injecting the tracer solution from three different inlet ports. The results are shown as normalized concentrations measured at the outlet ports (i.e., measured

values normalized the concentration of fluorescein in the tracer solution). The two-dimensional maps showing the experimental distribution of fluorescein at the outlet [Figs. 4.2(a)–4.2(c)] are obtained by interpolating the concentration measurements at the 49 outlet ports with the cubic interpolation algorithm implemented in Matlab. Figures 4.2(d)–4.2(f) show the concentration distribution computed in the numerical simulations of the different experiments. Notice that the results at the outlet show that the plume location, the peak concentration, as well as the shape of the plume changed considerably in the different experiments. Because of the flow field in the three-dimensional setup, the location of the plume at the outlet significantly deviates from the position of the inlet port used to inject the tracer solution and indicated by a white cross in Fig. 4.2. Also, the peak concentrations observed at the outlet differ depending on the port chosen to inject the tracer. Figure 4.2(b) shows the highest peak concentrations while Fig. 4.2(c) shows the lowest value. Furthermore, the shape of the plume at the outlet cross section is also different in the three cases. These effects indicate that the flow field exerts a significant control on tracer transport, on the deformation of the material surface of the plume, and on plume dilution. Figures 4.2(g)–4.2(i) show the comparison of the normalized concentrations measured at the outlet ports and the values obtained from the purely forward simulation of the different flow-through experiments. The experimental error ε [–] is estimated applying the reduced χ^2 test:

$$\chi^2 = \frac{1}{n_{ports}} \sum_{n=1}^{n_{ports}} \frac{(c_{meas} - c_{simu})^2}{\varepsilon^2} \tag{4.5}$$

such that χ^2 meets its expected value of unity. Here, n_{ports} [–] is the number of the outlet ports (49 in our setup), c_{meas} [–] is the measured normalized concentration at each port, and c_{simu} [–] is the simulated normalized concentration at each port. The experimental error estimated according to Eq. (4.5) is shown as dashed lines in Figs. 4.2(g)–4.2(i). The forward model captures the main flow and transport processes occurring in the experimental setup. In particular, a very good agreement was found between the measured and simulated results in the first two experiments, whereas the deviations were larger in the third flow-through experiment.

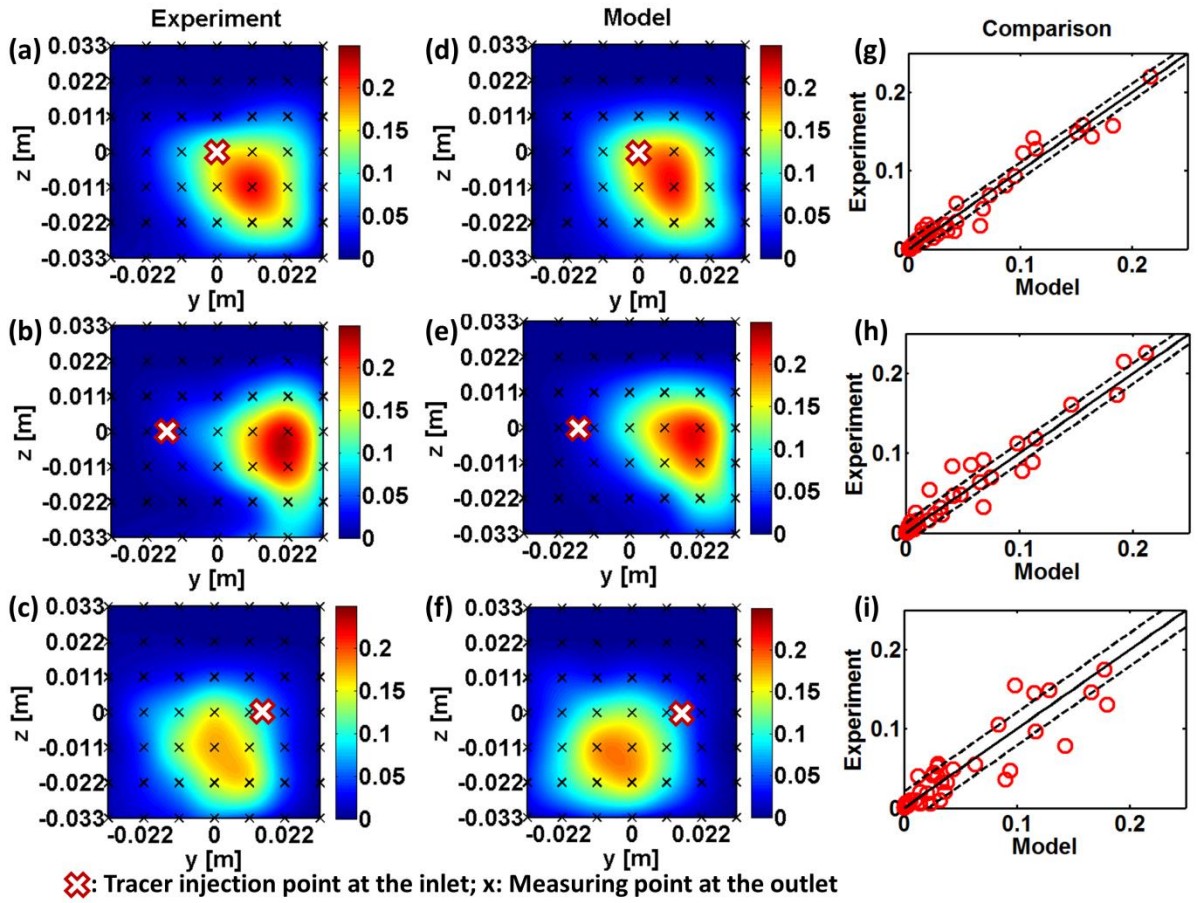

Fig. 4.2. Results of normalized concentration distributions at the outlet of the heterogeneous anisotropic flow-through system for the three experiments performed using different tracer injection ports. (a)–(c) The experimental results. (d)–(f) The model results. (g)–(i) The comparison between observed and simulated normalized concentrations.

The simulations are instrumental to visualize and explain the laboratory results and, in particular, the remarkable deviation of the peak concentration location at the outlet with respect to the inlet injection port. To further illustrate this point, numerical simulations of streamlines, determined by particle tracking [33] according to Eq. (4.1), are shown in Figs. 4.3(a)–4.3(c). The streamlines (black lines) provide a clear image of the complex velocity field in the three-dimensional setup. Streamlines starting at the source twist along the travel distance, assuming a helical shape, and terminate with remarkable shifts compared to the inlet location. Such behavior is caused by the interaction of macroscopically anisotropic hydraulic conductivity with changing orientation in the different layers and the no-flow boundary conditions [18]. Figure 3 also shows the occurrence of deformed isosurfaces [color surfaces in Figs. 4.3(a)–4.3(c)] with constant hydraulic head ϕ. These isosurfaces are not perpendicular to the streamlines, indicating therefore the occurrence of nontrivial Lamb surfaces and hence nonzero helicity density.

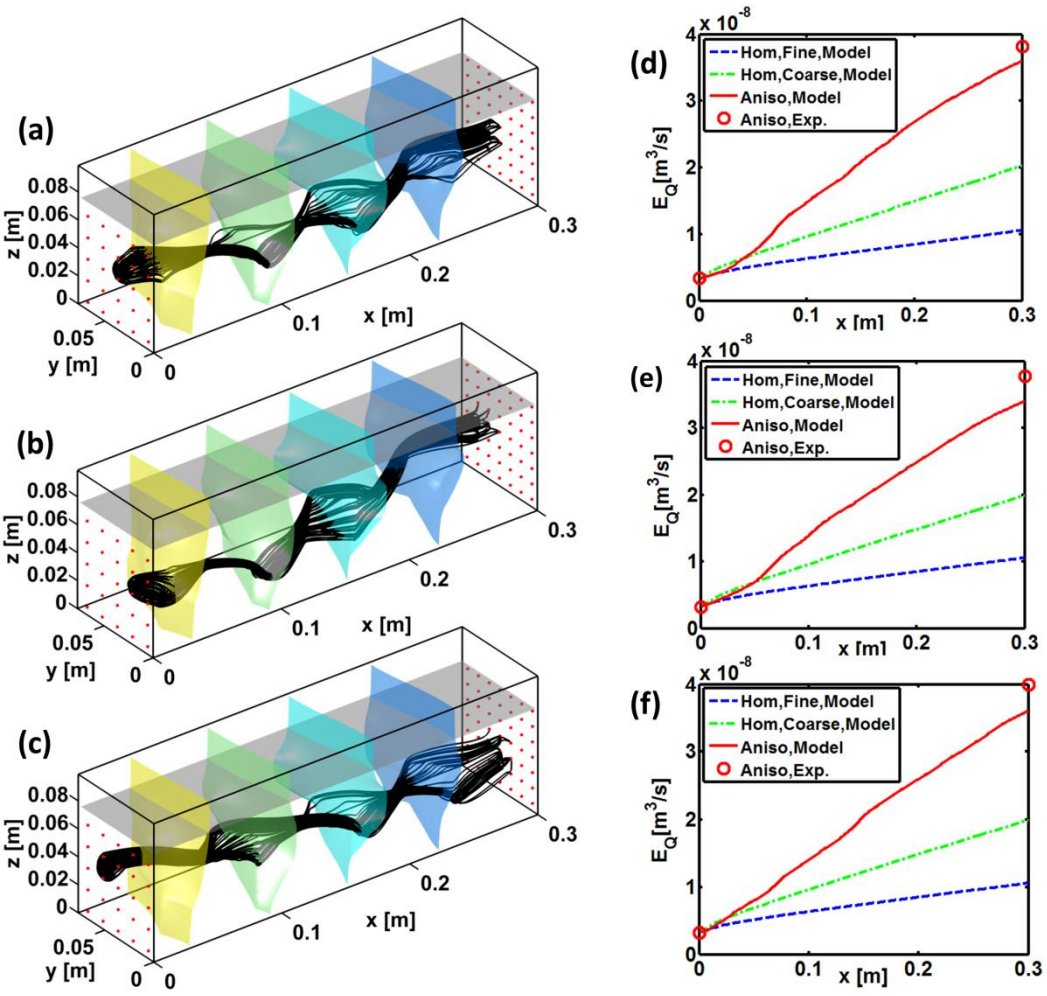

Fig. 4.3. (a)–(c) Streamlines traced from the inlet injection ports show a helical behavior; black lines: streamlines; colored surfaces: isosurfaces representing points with constant hydraulic head ϕ; grey surfaces: water level. (d)–(f) Flux-related dilution index observed (circles) and simulated (lines) at cross-sections along the travel distance in the three flow-through experiments.^

The helical flow occurring in our experimental setup affects mixing and dilution processes by deforming the material surface of the plume, causing an increase of diffusive and transverse dispersive fluxes, thus increasing the probability of mass exchange between two streamlines. As a result, plume dilution is considerably enhanced. The flux-related dilution index, quantifying plume dilution at different cross sections, is shown in Figs. 4.3(d)–4.3(f). The solid red lines show the simulated behavior of the flux-related dilution index along the main flow direction in the flow-through system, whereas the red circles represent the experimental values measured at the inlet and at the outlet of the setup. The monotonic increase of E_Q with the travel distance captures the spatial increase of the entropy of the plume due to the lateral diffusive and dispersive processes that distribute the solute mass flux over an increasing water flux. The increase of plume dilution between the inlet and the outlet of the setup is remarkable,

and the values of E_Q at the outlet of the setup in the three flow-through experiments are in the range 3.5×10^{-8} - 4.0×10^{-8} m^3/s and show more than a tenfold increase compared to the values at the inlet. To assess the contribution of helical flow to plume dilution, it is interesting to compare the outcomes obtained for the heterogeneous anisotropic domains with homogeneous porous media. To this end, the flux-related dilution index has been also computed using the numerical model for two homogeneous porous media, entirely packed with fine glass beads (dashed blue lines in Fig. 4.3) or with coarse glass beads (dash-dotted green lines in Fig. 4.3), respectively. Both the values of E_Q and its rate of increase show that plume dilution in the heterogeneous and anisotropic porous medium is considerably larger compared to the homogeneous domains. In particular, the values at the outlet show an average dilution enhancement in the anisotropic setups of 235% and 75% compared to the homogeneous fine and coarse grain size scenarios, respectively. This indicates the relevance of the occurrence of helical flow in porous media and its remarkable effect on solute transport and mixing processes.

In conclusion, we provide first experimental evidence of helical flows in porous media. Such flows with twisting streamlines have a large impact on the dilution enhancement of steady-state solute plumes. Since this is the rate limiting step for mixing-controlled reactions, helical flow will lead to strongly enhanced chemical reactions in plumes. The outcomes of this study extend the findings of complex flows and associated mixing processes carried out for Stokes flows in microchannels [6,34] to Darcy flows in porous media, occurring at larger scales. These results are relevant for an improved understanding of dilution and mixing processes occurring in engineered systems such as packed bed reactors as well as in natural systems such as geologic formations and aquifer systems.

This work was supported by the DFG (Deutsche Forschungsgemeinschaft, Grants No. RO 4169/3-1 and No. CI-26/11-1). The authors thank four anonymous reviewers for their constructive comments.

References

[1] V. Hessel, H. Löwe, and F. Schönfeld, Chem. Eng. Sci. **60**, 2479 (2005).
[2] G. Chiogna, D. L. Hochstetler, A. Bellin, P. K. Kitanidis, and M. Rolle, Geophys. Res. Lett. **39**, L20405 (2012).
[3] J. J. Hidalgo, J. Fe, L. Cueto-Felgueroso, and R. Juanes, Phy. Rev. Lett. **109**, 264503 (2012).
[4] M. Icardi, G. Boccardo, D. L. Marchisio, T. Tosco, and R. Sethi, Phy. Rev. E **90**, 013032 (2014).
[5] J. M. Ottino, The Kinematics of Mixing (Cambridge University, Cambridge, 1989).
[6] A. D. Stroock, S. K. W. Dertinger, A. Ajdari, I. Mezić, H. A. Stone, and G. M. Whitesides, Science **295**, 647 (2002).
[7] B. Bijeljic, P. Mostaghimi, and M. J. Blunt, Phy. Rev. Lett. **107**, 204502 (2011).
[8] J. C. Giddings, Dynamics of Chromatography (Dekker, New York, 1965).
[9] E. Villermaux, A. D. Stroock, and H. A. Stone, Phy. Rev. E **77**, 015301 (2008).
[10] H. K. Moffatt, Proc. Natl. Acad. Sci. U. S. A. **111**, 3663 (2014).
[11] P. de Anna, T. Le Borgne, M. Dentz, A. M. Tartakovsky, D. Bolster, and P. Davy, Phy. Rev. Lett. **110**, 184502 (2013).
[12] P. de Anna, J. Jimenez-Martinez, H. Tabuteau, R. Turuban, T. Le Borgne, M. Derrien, and Y. Méheust, Environ. Sci. Technol. **48**, 508 (2014).
[13] F. P. J. de Barros, M. Dentz, J. Koch, and W. Nowak, Geophys. Res. Lett. **39**, L08404 (2012).
[14] S. Torquato, Random Heterogeneous Materials (Springer-Verlag, New York, 2002).
[15] G. Sposito, Water Resour. Res. **30**, 2395 (1994).
[16] M. Bakker, and K. Hemker, Adv. Water Resour. **27**, 1075 (2004).
[17] G. Chiogna, M. Rolle, A. Bellin, and O. A. Cirpka, Adv. Water Resour. **73**, 134 (2014).
[18] G. Chiogna, O. A. Cirpka, M. Rolle, and A. Bellin, Water Resour. Res. **51**, 261 (2015).
[19] G. Nichols, Sedimentology and Stratigraphy (Wiley-Blackwell, Chichester, 2009).
[20] A. Hazen, Ann. Rep. State Board of Health Mass **24**, 541 (1892).
[21] O. A. Cirpka, G. Chiogna, M. Rolle, and A. Bellin, Water Resour. Res. **51**, 241 (2015).
[22] J. Bear, Dynamics of Fluids in Porous Media (Dover Publications, New York, 1972).
[23] H. C. Brinkman, Appl. Sci. Res. **A1**, 27-34 (1949).
[24] O. A. Cirpka, F. P. J. de Barros, G. Chiogna, M. Rolle, and W. Nowak, Water Resour. Res. **47**, W06515 (2011).
[25] U. M. Scheven, Phy. Rev. Lett. **110**, 214504 (2013).
[26] U. M. Scheven, S. Khirevich, A. Daneyko, and U. Tallarek, Phy. Rev. E **89**, 053023 (2014).
[27] G. Chiogna, C. Eberhardt, P. Grathwohl, O. A. Cirpka, and M. Rolle, Environ. Sci. Technol. **44**, 688 (2010).
[28] Y. Ye, G. Chiogna, O. A. Cirpka, P. Grathwohl, and M. Rolle, J. Contam. Hydrol. **172**, 33 (2015).
[29] M. Rolle, C. Eberhardt, G. Chiogna, O. A. Cirpka, and P. Grathwohl, J. Contam. Hydrol. **110**, 130 (2009).
[30] P. K. Kitanidis, Water Resour. Res. **30**, 2011 (1994).

[31] M. Rolle, G. Chiogna, D. L. Hochstetler, and P. K. Kitanidis, J. Contam. Hydrol. **153**, 51 (2013).
[32] E. T. Jaynes, Phys. Rev. **106**, 620 (1957).
[33] D. W. Pollock, Ground Water **26**, 743 (1988).
[34] C. Simonnet, and A. Groisman, Phy. Rev. Lett. **94**, 134501 (2005).

5. Experimental Investigation of Transverse Mixing under Helical Flow Conditions in Saturated Porous Media

Yu Ye, Gabriele Chiogna, Olaf Cirpka, Peter Grathwohl and Massimo Rolle

To be submitted to Phys. Rev. E…

Abstract

Transverse dilution and mixing can be enhanced by helical flow occurring in three-dimensional anisotropic heterogeneous porous media. In this study, we provide experimental observations of plume deformation and dilution under helical flow conditions at cross-sections perpendicular to the travel distance. Steady-state bench-scale transport experiments are performed in a three-dimensional saturated porous media at the flow velocity of 3 m/day. A set of experiments is conducted injecting a fluorescein solution at different inlet ports of the flow-through system. Concentrations are then measured at high spatial resolution at the outlet ports. We qualitatively observe the evolution of the plume location and its shape at selected cross sections in the flow-through system. Dilution of the conservative plume is quantified applying the flux-related dilution index. The relevance of transverse mixing enhancement for the case of reactive solute transport is computed numerically using the length of a reactive plume and its critical dilution index as metrics. These results are relevant to quantify mixing enhancement in packed bead reactors and in natural geological formations.

Keywords: dilution; transverse mixing; helical flow; laboratory experiment; heterogeneity; anisotropy; critical dilution index

5.1 Introduction

Mixing of reaction partners is fundamental for the occurrence of chemical and biological reactions, since they require the simultaneous occurrence of the reactants in the same place. In engineered systems like mixers the flow field is often turbulent, thus achieving sufficient mixing and reaction rates are controlled by their kinetic [Ottino, 1989]. However, in porous media such as aquifers, oil reservoirs and packed bead reactors, creeping flow dominates. Under such flow conditions, slow diffusive processes determine the rate of mixing [Bijeljic et al., 2011] and hence reactions may become mixing controlled [Chiogna et al., 2011; Cirpka and Valocchi, 2007; Lerner et al., 2000], particularly at the transverse directions at quasi steady-state. This is confirmed by the observations of very thin plume fringes in many laboratory studies and at the field scale [Bauer et al., 2009a; Prommer et al., 2009; Willingham et al., 2008]. Studies of transverse dispersion and mixing during transport are mostly based on the numerical simulations [Bolster et al., 2010; Le Borgne et al., 2011] and theoretical analyses [Le Borgne et al., 2013; Scheven 2013]. In particular, reactive transport modelling is frequently used for the determination of plume length and to evaluate the contribution of heterogeneity of the porous media to the plume degradation [Bauer et al., 2009b; Dentz et al., 2011; Engdahl et al., 2014].

In three-dimensional anisotropic heterogeneous porous media mixing can be enhanced by the occurrence of helical flows with non-zero helicity density [Bakker and Hemker, 2004, Chiogna et al., 2015; Cirpka et al., 2015; Chiogna et al., 2016; Dean et al., 2008]. In previous experimental study [Ye et al., 2015], we investigated the occurrence of helical flow interpreting the concentration pattern measured at the outlet of a flow-through system. Yet, experimental observations of plume development inside the porous medium are still missing.

In this study, we present the results of laboratory flow-through experiments with the aim of showing the effect of helical flow on plume deformation inside anisotropic heterogeneous porous media. We also show the influence of grain size and of the tracer injection position on plume dilution. Finally, we numerically compute the length of a reactive plume undergoing an instantaneous complete bimolecular reaction, the critical dilution index and the effective dispersion coefficient as a function of the critical mixing ratio.

5.2 Experimental Operation and Model Description

Laboratory flow-through experiments were carried out in a three-dimensional flow-through chamber with an inner dimensions of $30 \times 7.7 \times 10$ cm^3 [Figure 5.1(a)]. The chamber is made of acrylic glasses and it has 25 equally spaced injection ports at the inlet and 49 equally spaced extraction ports at the outlet. Peristaltic pumps (Ismatec, Glattbrugg, Switzerland) were used to obtain constant flow conditions during the experimental runs. A detailed description of the experimental setup is provided in Ye et al. [2015]. In this study, two sets of experiments were carried out using different types of glass bead (Sigmund Lindner, Warmensteinach, Germany) as porous media in the flow-through chamber. In the first series of the experiments, fine materials with the grain size of 0.4-0.6 mm (indicated as FF) and 1.5-2.0 mm (indicated as FC) were used for the construction of low and high conductivity stripes, respectively. In the second series of the experiments, coarser materials with the grain size of 0.6-0.9 mm (indicated as CF) and 2.4-2.9 mm (indicated as CC) were applied. The ratio of the average grain size between fine and coarse materials in the two setups is identical (i.e., 3.5). In each of the experimental series, the two types of the glass beads were packed alternating the angled stripes in layer 1 and layer 2 (Figure 5.1), such that a simplified herringbone cross-stratification were achieved. Similar structures are observed in subsurface sedimentary depositional environments [Nichols, 2009]. In layer 3, finer glass beads (FF or CF) were homogeneously packed, facilitating water-saturated conditions in layer 1 and layer 2. The thickness of layer 1 and layer 2 was 3.08 cm. Layer 3 had a thickness of 1.54 cm. Dry glass beads (relatively fine ones) were placed on top of layer 3, maintaining an unsaturated zone. The porosity of the porous media was gravimetrically determined and it was approximately 0.4 for all types of the glass beads. Hydraulic conductivity was calculated according to the grain size [Hazen, 1892], and it was manually calibrated for the CC glass beads by a factor of 1.1. Therefore, at the relevant scale for observation, the permeability of the porous media is spatially heterogeneous and anisotropic, while the porosity is isotropic.

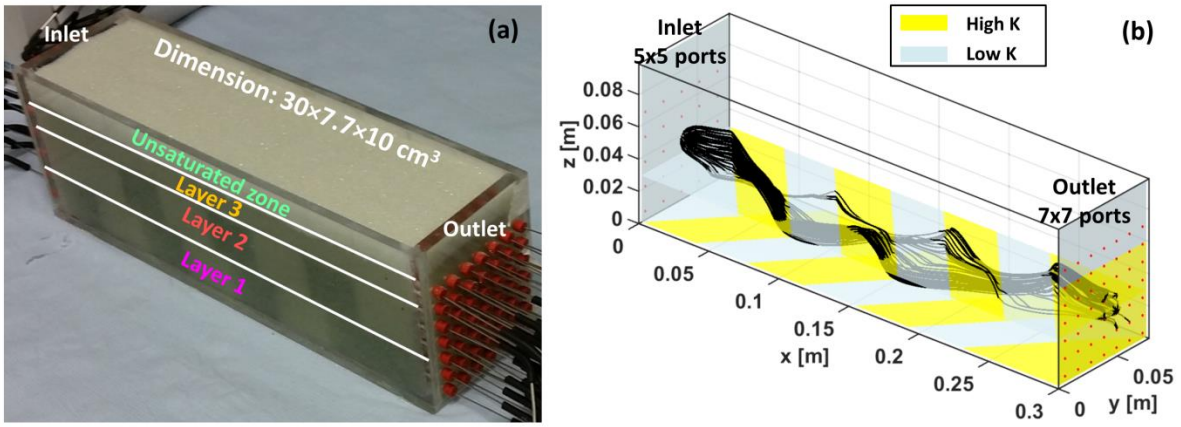

Fig. 5.1. (a) Photograph of the experimental setup with marked layers; (b) The inner herringbone structures of the high and low hydraulic conductivity porous media and the streamlines traced from the central injection port.

All the experiments were performed at the average flow velocity of 3 m/day. After steady-state flow condition was established, a tracer solution of sodium fluorescein with a concentration of 15 mg/l was injected through one injection port. After replacing eight pore volumes, steady-state transport conditions were achieved. Samples were collected at the high-resolution extraction ports at the outlet and the concentrations of the collected samples were measured using a UV-spectrometer (Perkin Elmer LS-3B). Flow rate at each extraction port was obtained by weighting the collected samples at specific time intervals.

New coccine was used as tracer in one experiment to show the plume distributions at different cross-sections inside the flow through system. This tracer was used since its color is easier to be distinguished from the color of glass beads compared to fluorescein. Notice that this experiment was performed in the porous media constructed with the FF and FC glass beads. The slices of the cross-sections were obtained with the help of very thin metal sheets. After reaching steady-state transport conditions, the pumps were switched off and the metal sheets were inserted vertically into the porous media. Then, the flow-through chamber was disconnected from the pumps and it was frozen in the freezer. After the ice block of the porous media was taken out from the chamber, the slices can be separated easily from the rest of the ice blocks. The color of the photographs taken for the slices was manually adjusted to further facilitate the appearance of the plume.

The experimental results were compared to the numerical simulations using the model proposed by Cirpka et al. [2015]. Steady-state flow was calculated according to the continuity equation:

$$\nabla \cdot \left(\mathbf{q}(\mathbf{x})\right) = \nabla \cdot \left(-\mathbf{K}(\mathbf{x}) \nabla \phi(\mathbf{x})\right) = 0 \tag{5.1}$$

while steady-state conservative transport was computed using the advection-dispersion equation:

$$\mathbf{v} \cdot \nabla c - \nabla \cdot \left(D_t \nabla c\right) = 0 \tag{5.2}$$

where $\mathbf{q}$ [LT^{-1}] denotes the specific discharge vector, $\mathbf{x}$ [L] is the vector of spatial coordinates, $\mathbf{K}$ [LT^{-1}] is the hydraulic conductivity tensor (here assumed isotropic as the stripes of different materials are spatially resolved), ϕ [L] is the hydraulic head, $\mathbf{v}=\mathbf{q}/\theta$ [LT^{-1}] is the seepage velocity vector, θ [-] is the porosity, c [ML^{-3}] is the concentration, and D_t [L^2T^{-1}] is the transverse dispersion coefficient. According to the experimental setup, Eq. (5.1) was solved considering constant-flux boundary conditions at the injection and extraction ports and no-flow boundary conditions at the other sides of the flow-through chamber. The complex flow field is shown by the streamlines traced from injection ports using particle tracking schemes. As shown in Figure 5.1(b), streamlines traced from the central port at the inlet twist along the travel distance, and preferentially flow in the high permeability zones, thus creating helical flow conditions in the porous medium. Constant-concentration boundary conditions (15 mg/l for tracer injection port and 0 mg/l for the other water injection ports) were used for the solution of Eq. (5.2). Under steady-state conditions, longitudinal dispersion can be neglected in case of continuous injection [Cirpka, 2011]. A non-linear compound-specific transverse dispersion coefficient [Chiogna et al., 2010], $D_t = D_p + D_{aq}\left(\frac{Pe^2}{Pe + 2 + 4\delta^2}\right)^{\beta}$, was used in Eq. (5.2), such that the dependence of mechanical dispersion on the aqueous diffusivity raised from incomplete mixing in pore channels can be accounted for. Here $D_p=D_{aq}\times\theta$ [L^2T^{-1}] denotes the pore diffusion coefficient, D_{aq} [L^2T^{-1}] is the aqueous diffusion coefficient, $Pe=vd/D_{aq}$ [-] is the grain Péclet number, v [LT^{-1}] is the absolute value of the seepage-velocity vector, d [L] is the average grain size, δ [-] is the ratio between the length of a pore channel and its hydraulic radius, and β [-] is an empirical exponent that accounts for the degree of incomplete mixing within the pore channels. The parameters reported by Ye et al. [2015] (i.e., β=0.5 and δ=5.37) were used in our study.

5.3 Quantification of Dilution and Spreading

Transverse mixing of the steady-state conservative plumes can be quantified by the flux-related dilution index E_Q [L^3T^{-1}], defined as [Rolle et al 2009]:

$$E_Q(x) = \exp\left(-\int_\Omega \left[p_Q(x,y,z)\ln p_Q(x,y,z)\right] q_x(x,y,z)dA\right) \tag{5.3}$$

where Ω is the cross-section perpendicular to the longitudinal direction x, $p_Q = \frac{c}{\int_\Omega c q_x dA}$ [TL^{-3}] is the flux-weighted probability density function of the solute mass, and q_x [LT^{-1}] is the specific-discharge at the longitudinal direction x. The flux-related dilution index was derived following the dilution index E [L^3] [Kitanidis, 1994], which is volume-related and used for the case of transient solute transport. E_Q measures the exponential of the Shannon entropy and it quantifies the distribution of the solute mass flux over the water flux along the travel distance. In our experiments, we computed the flux-related dilution index in a discrete form using the measured concentrations and the flow rates at the inlet and the outlet ports.

To characterize the plume distribution we also consider the second central moment of the plume computed at the outlet of the flow-through system. In contrast to the dilution index, this is a measure of the spreading of the conservative plume in both transverse horizontal and vertical directions:

$$M_{2C,h} = \frac{\int_0^{w_{tot}} \left(y - M_{1,h}\right)^2 c_h dy}{\int_0^{w_{tot}} c_h dy} \tag{5.4}$$

$$M_{2C,v} = \frac{\int_0^{h_{tot}} \left(z - M_{1,v}\right)^2 c_v dz}{\int_0^{h_{tot}} c_v dz} \tag{5.5}$$

where w_{tot} [L] and h_{tot} [L] are the total width and the total height of the three-dimensional domain, $M_{1,h}$ [L] and $M_{1,v}$ [L] are the first spatial moment in horizontal and vertical directions, defined as:

$$M_{1,h} = \frac{\int_0^{w_{tot}} y c_h dy}{\int_0^{w_{tot}} c_h dy} \tag{5.6}$$

$$M_{1,v} = \frac{\int_0^{h_{tot}} z c_v dz}{\int_0^{h_{tot}} c_v dz} \tag{5.7}$$

and $c_h = \frac{\int_0^{h_{tot}} c dz}{h_{tot}}$ and $c_v = \frac{\int_0^{w_{tot}} c dy}{w_{tot}}$ represent the average concentration along vertical and horizontal directions, respectively.

5.4 Theory about Reactive Transport

To investigate the relevance of mixing enhancement for reactive solute transport, we model a very simple instantaneous bimolecular reaction of the form A+B→C. The reaction rate is entirely controlled by mixing processes between the reactants. Species A is considered as the injected reaction partner, while species B is present in the ambient water. Assuming the aqueous diffusion coefficient to be identical between A and B, a virtual conservative compound *X* [-] (denoted as mixing ratio) can be considered to model the reactive problem [Cirpka and Valocchi, 2007]. Here the concentration of *X* is unit at the injection port of A and it is 0 in the ambient water. We define the critical mixing ratio as $X_{crit} = \frac{c_B^{amb}}{c_B^{amb} + c_A^{in}}$, where c_B^{amb} is the concentration of species B at the inlet ambient water and c_A^{in} is the concentration of species A at the injection port of A. Where *X* equals X_{crit}, the concentrations of both reactants are zero.

In the three-dimensional homogeneous porous media, the mixing ratio satisfies the analytical solution for the non-reactive transport of the solute plumes continuously injected by a square source [Domenico and Palciauskas, 1982]:

$$X(x,y,z) == \frac{1}{4}\left\{\mathrm{erf}\left[\frac{y+Y/2}{2\sqrt{D_t\, x/v}}\right] - \mathrm{erf}\left[\frac{y-Y/2}{2\sqrt{D_t\, x/v}}\right]\right\}\left\{\mathrm{erf}\left[\frac{z+Z/2}{2\sqrt{D_t\, x/v}}\right] - \mathrm{erf}\left[\frac{z-Z/2}{2\sqrt{D_t\, x/v}}\right]\right\} \tag{5.8}$$

provided the conditions pointed out by Srinivasan et al. [2007] is met. Here *Y* [L] and *Z* [L] denote the source width and the source thickness, which are identical (i.e., 1.54 cm) in our study. The end of the plume is defined as the point where species A is completely consumed by the reaction, i.e., where the mixing ratio equals X_{crit}. Thus, the plume length, *L* [L], is defined as the minimal distance from the source at which $X = X_{crit}$ at the entire cross-section

along the travel distance [Cirpka et al., 2006]. For a three-dimensional homogeneous case, the plume length can be derived from Eq. (5.8) and reads as:

$$L = \frac{vY^2}{16D_t\left[inverf\left(\sqrt{X_{crit}}\right)\right]^2} \tag{5.9}$$

No analytical solution exists for the concentration distribution in case of helical flow in heterogeneous porous media. We define therefore an effective dispersion coefficient, considering a homogeneous system with the same solute mass flux and plume length observed in the heterogeneous case. Therefore, $D_{t,eff}$ [L^2T^{-1}], can be obtained from Eq. (5.9) as:

$$D_{t,eff} = \frac{vY^2}{16L\left[inverf\left(\sqrt{X_{crit}}\right)\right]^2} \tag{5.10}$$

Considering the effect of heterogeneity and anisotropy of the porous media on mixing, $D_{t,eff}$ is larger than the local transverse dispersion coefficient.

Chiogna et al. [2011] introduced the critical dilution index for the analysis of reactive transport in two-dimensional porous media. This metric quantifies the amount of mixing required for the complete degradation of a reactive plume undergoing an instantaneous complete bimolecular reaction. The value of the critical dilution index can be computed from the flux-related dilution index of a conservative tracer plume at the distance L, where L is the length of the reactive plume considering the same flow field and for the same mass flux as in the conservative transport. The critical dilution index, as well as the first order approximation (see Appendix), for the three-dimensional porous media is defined as:

$$CDI = E_Q(L) = \frac{E_Q(0)}{X_{crit}}\exp(1) \tag{5.11}$$

Chiogna et al. [2011] observed that the critical dilution index is independent on the heterogeneity of the porous medium.

5.5 Results and Discussion

5.5.1 Conservative Transport

Figure 5.2 shows the experimental plume distributions at the cross-sections at the travel distance of 11, 15, 24 and 29 cm from the source. Since the color of the photographs was

adjusted, the degree of the color does not represent the concentration of the plume. Numerical results of the plume distributions are also shown as contour lines of the normalized concentration (i.e., absolute concentration divided by the concentration at the source) in Figures 5.2(a)-5.2(d) and as color plots in Figures 5.2(e)-5.2(h) for the qualitative comparison with the experimental results. The experimental results match very well to the numerical simulations, confirming the capability of the model prediction. In Figure 5.2, the plume position at different cross-sections deviate from the tracer injection points (red crosses). Furthermore, the shape of the plume changes significantly along the travel distance. Both the position and the shape of the plume indicate a complex flow field in the three-dimensional anisotropic heterogeneous porous media. Notice that the no-flow boundary at the sides of the flow-through system also exerts a non-negligible role to the spreading of the plume.

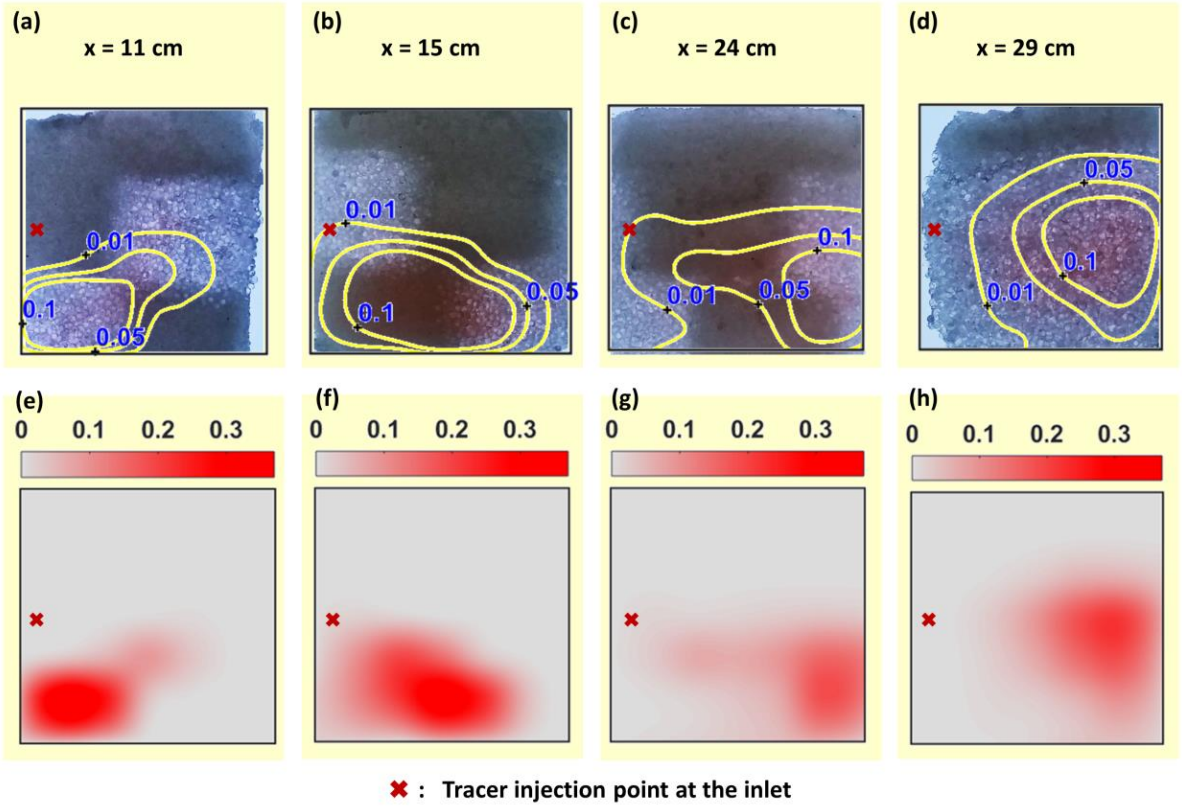

Fig. 5.2. Plume distributions at the cross-sections at the travel distance of 11, 15, 24 and 29 cm from the source. (a)-(d): Photograph of the experimental tracer plume. Contour lines of the normalized concentration from numerical simulation are added to the photographs for direct comparison. (e)-(h): Numerical results of the plume development at the same cross-sections.

Normalized concentration distributions of fluorescein at the outlet of the flow-through system were measured and interpolated using cubic interpolation algorithm implemented in Matlab. Figure 5.3 shows the experimental and numerical results of two experiments performed in

fine (FF and FC) and coarse (CF and CC) materials. Here the central inlet port was selected as the tracer injection port (red crosses in Figure 5.3). Comparison of concentrations at the outlet ports between experimental and numerical results are shown in Figure 5.3(c) and 5.3(f). The experimental error ε [-] was estimated using the reduced χ^2 test, i.e., $\chi^2 = \frac{1}{n_{ports}} \sum_{n=1}^{n_{ports}} \frac{(c_{meas} - c_{simu})^2}{\varepsilon^2}$, such that χ^2 equals to unity. Here n_{ports} [-] denotes the number of the outlet ports (49 in our setup), c_{meas} [-] is the measured normalized concentration at each port and c_{simu} [-] is the simulated normalized concentration at each port. The normalized error is plotted as dashed lines in Figure 5.3(c) and 5.3(f). The error is smaller for the experiments packed with fine materials (grain size of 0.4-0.6 mm and 1.5-2.0 mm) than with the coarse materials (grain size of 0.6-0.9 mm and 2.4-2.9 mm). This phenomenon can be explained by the mixing of two glass bead between the stripes and the layers. Indeed, CF may intrude into CC more than FF can intrude into FC, thus creating larger and irregular mixing zones for the coarse materials. In Figure 5.3, the peak concentration of the plume at the outlet is higher for the setup packed with fine materials, indicating a smaller transverse mixing in comparison to the case packed with coarse materials. Yet the position and the shape of the plume are similar between the two cases. Therefore, the dimension of the grain size influences the degree of plume dilution (as expected from parameterization of the transverse dispersion coefficient and the flux-related dilution index), but it does not affect the structure of the flow field and hence the shape of the plume.

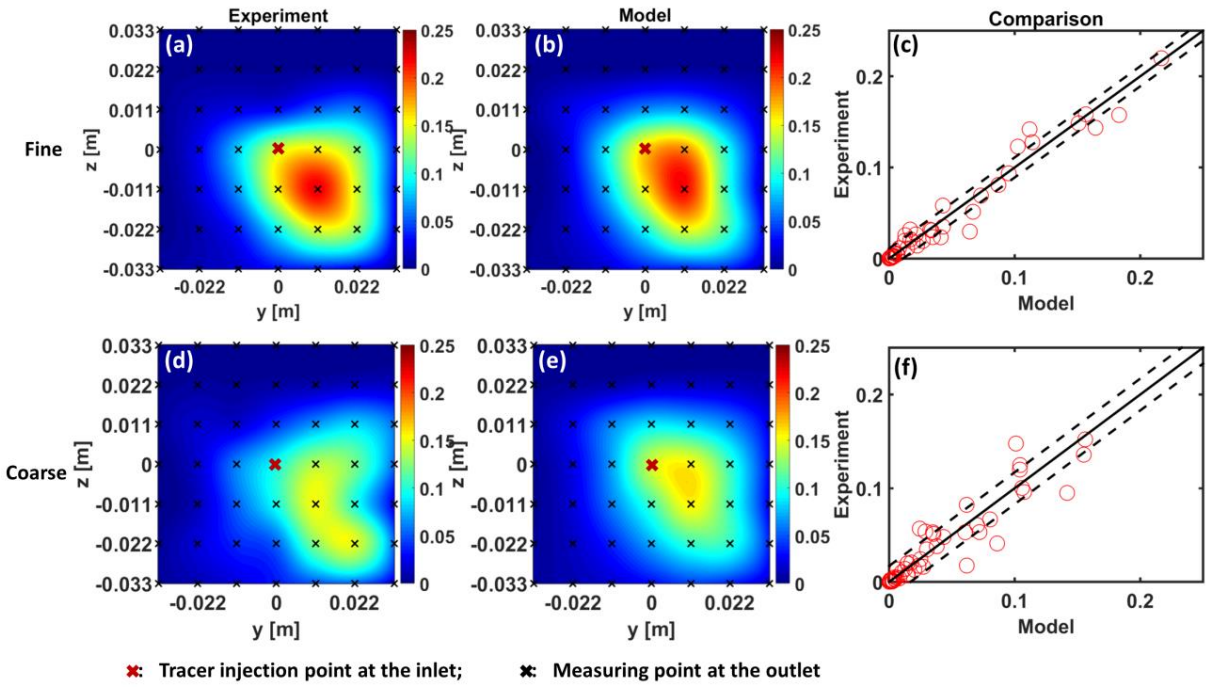

Fig. 5.3. Experimental and model results of the normalized concentration distributions at the outlet of the anisotropic heterogeneous flow-through system packed with the fine (grain size of 0.4-0.6 mm and 1.5-2.0 mm) and coarse (grain size of 0.6-0.9 mm and 2.4-2.9 mm) porous medium.

The second central moment as well as the flux-related dilution index are calculated for the two cases (noted as F3-3 and C3-3) shown in Figure 5.3. Furthermore, another neighboring injection port was also tested and the experiments were performed in both fine and coarse materials (noted as F3-2 and C3-2). Table 5.1 lists the second central moment while Figure 5.4 shows the flux-related dilution index for all the scenarios. Not only the spreading but also the dilution of the plume is stronger in the coarse materials than in the fine materials, being consistent to the observations of peak concentrations in Figure 5.3. The low normalized error of the second central moment (absolute difference divided by the experimental value) shows a good prediction of the numerical model. The difference of the flux-related dilution index between the experimental and the model results in Figure 5.4 also proves that the numerical model can capture the transport mechanisms controlling the plume development.

Table 5.1. Experimental and model results of the second central moment of the plume at the transvers vertical and transverse horizontal directions at the outlet of the flow-through system packed with fine (F) and coarse (C) porous medium and using the central inlet port (3-3) and the neighboring one (3-2) as the tracer injection ports.

Case	Moment	Experiment	Model	Normalized error
F3-3	$M_{2C,v}$ [m^2]	1.50×10^{-4}	1.62×10^{-4}	8.0%
	$M_{2C,h}$ [m^2]	1.89×10^{-4}	1.77×10^{-4}	6.3%
F3-2	$M_{2C,v}$ [m^2]	1.90×10^{-4}	1.69×10^{-4}	11.1%
	$M_{2C,h}$ [m^2]	1.75×10^{-4}	1.70×10^{-4}	2.9%
C3-3	$M_{2C,v}$ [m^2]	2.11×10^{-4}	2.04×10^{-4}	3.3%
	$M_{2C,h}$ [m^2]	2.20×10^{-4}	2.17×10^{-4}	1.4%
C3-2	$M_{2C,v}$ [m^2]	2.14×10^{-4}	1.98×10^{-4}	7.5%
	$M_{2C,h}$ [m^2]	2.34×10^{-4}	1.96×10^{-4}	16.2%

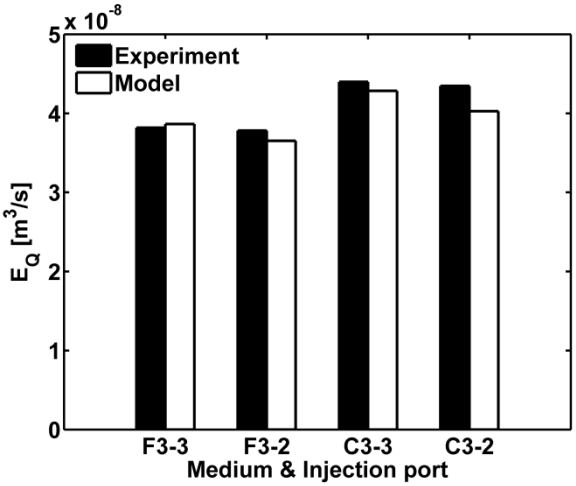

Fig. 5.4. Experimental and model results of the flux-related dilution index at the outlet of the flow-through system packed with fine (F) and coarse (C) porous medium and using the central inlet port (3-3) and the neighboring one (3-2) as the tracer injection ports.

5.5.2 Reactive Transport

Three different critical mixing ratios, i.e., 0.8, 0.5 and 0.25 were selected for the study of the reactive transport in the same setups. As an example, Figure 5.5 shows the development of the reactive plume (see red plume) with the critical mixing ratio of 0.5 in the heterogeneous anisotropic porous media packed with fine materials. Here the central inlet port was used to inject the tracer solution. The plume bends and meanders along the travel distance, and it disappears before the half-way of the flow-through system. As a comparison, the plume (see

blue plume in Figure 5.5) computed in the homogeneous porous media (grain size of 1 mm) goes straight and it is longer than the length of the flow-through chamber.

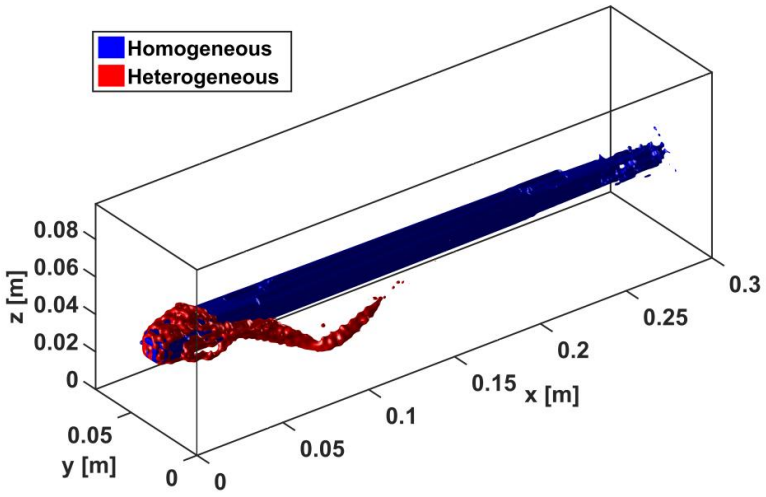

Fig. 5.5. Boundaries of the reactive plumes (X_{crit}=0.5) in heterogeneous (paced with FF and FC glass beads) and homogenous (grain size of 1 mm) porous media.

The plume length is calculated numerically for all the critical mixing ratios and all the scenarios considered in our study (Table 5.2). It is longer for the smaller critical mixing ratio, due to the larger concentration in the source. For any critical mixing ratio, the plume length is shorter in the coarse porous media, consistently to the dilution shown in Figure 5.4. Here the injection port also exerts a role in determining the plume length. As a comparison, the plume length (L_{hom}) in the homogeneous porous media (grain size of 1 mm) was analytically computed according to Eq. (5.9). The plume length in the homogeneous porous media is more than two times longer when compared to the heterogeneous case, indicating a strong mixing enhancement by the helical flow created in the anisotropic heterogeneous porous media. The effective dispersion coefficient was computed according to Eq. (5.10) and listed in Table 5.2 as well. Again, the value of $D_{t,eff}$ is larger in coarse materials. However there is no particular relationship between the critical mixing ratio and the effective dispersion coefficient. This can be explained using Eq. (5.10): the plume length is shorter when the critical mixing ratio is larger, and both parameters are present in the denominator. The local D_t values are 0.16×10^{-8} m^2/s, 0.41×10^{-8} m^2/s, 0.22×10^{-8} m^2/s, and 0.54×10^{-8} m^2/s for the glass beads of the FF, FC, CF and CC, respectively, with the critical mixing ratio of 0.5 and at the average flow velocity of 3 m/day. As also shown by Chiogna et al. [2011] for the two-dimensional case, $D_{t,eff}$ is always larger than the local D_t values in the three-dimensional homogenous porous media, since the effect of the heterogeneity is entailed in the parameterization of the $D_{t,eff}$ values. The critical

dilution index (*CDI*), as well as its first order approximation (CDI_{theo}) are computed according to Eq. (5.11) and the values are shown in Table 5.2. For each of the scenarios, the critical dilution index increases with decreasing mixing ratio, showing the same trend of the plume length. However, the *CDI* values are close to each other for the four cases, provided the mixing ratio is the same. This phenomenon illustrates that the mixing required for the complete degradation of a specific plume by reacting with the ambient water is unique, independent of the anisotropy and the heterogeneity of the porous media. The CDI_{theo} computed according to Eq. (5.11) shows a good approximation of the critical dilution index computed using the numerical model (mean normalized difference of 12%, 5% and 7% at the critical mixing ratio of 0.8, 0.5 and 0.25.).

Table 5.2 Influence of X_{crit} on the effective dispersion coefficient, plume length, critical dilution index in different scenarios. As a comparison, plume length is also computed analytically for the homogeneous case (grain size of 1 mm) and theoretical critical dilution index is also computed analytically.

Case	**F3-3**			**F3-2**			**C3-3**			**C3-2**		
X_{crit} [-]	0.8	0.5	0.25	0.8	0.5	0.25	0.8	0.5	0.25	0.8	0.5	0.25
$D_{t,eff} \times 10^8$ [m^2s^{-1}]	0.54	0.73	0.87	0.61	0.78	0.78	0.62	0.91	1.13	0.64	0.93	0.89
L [cm]	7.3	12.9	26.5	6.5	12.1	29.7	6.1	9.9	19.3	5.9	9.7	24.5
L_{hom} [cm]	14.5	34.4	83.7	14.5	34.4	83.7	14.4	34.0	82.7	14.4	34.0	82.7
$CDI \times 10^7$ [m^3s^{-1}]	0.11	0.18	0.33	0.09	0.17	0.34	0.10	0.17	0.31	0.09	0.15	0.34
$CDI_{theo} \times 10^7$ [m^3s^{-1}]	0.11	0.18	0.36	0.11	0.18	0.36	0.11	0.17	0.35	0.11	0.17	0.35

5.6 Conclusions

In this study, we provided experimental observations of plume development in three-dimensional anisotropic heterogeneous porous media under helical flow conditions. The laboratory experiments were reproduced with numerical simulations which are qualitatively and quantitatively consistent with the experimental results. Spreading and dilution were calculated applying the second central moment and the flux-related dilution index, respectively. While the influence of the injection ports to the plume distribution is quite small, plume dilution is much larger in coarse porous media than in fine porous media. Plume length, effective transverse dispersion coefficient, and critical dilution index were computed for the reactive plume using the numerical model. The length of the plume is more than two times shorter in the heterogeneous porous media compared to the homogeneous setup, which further proves the enhancement of transverse mixing by helical flows created in the anisotropic

heterogeneous porous media. The effective dispersion coefficient is larger than the local transverse dispersion coefficient, indicating the effect of heterogeneity and helical flow to transverse mixing during transport. The critical dilution index does not depend on heterogeneity and anisotropy and the dilution required for the complete degradation of the plume, provided the concentration and the flux of the plume at the source is unique. These results offer a more in depth experimental investigation of mixing enhancement in helical flows in porous media and its effect on mixing controlled reactive solute transport. In engineering systems herringbone configurations are used in micromixers for mixing enhancement [Villermaux et al., 2008]. Our structure can be designed and applied in natural porous formations for stronger mixing and for efficient remediation.

Acknowledgments

This work was supported by the DFG (Deutsche Forschungsgemeinschaft, grants RO 4169/3-1 and CI-26/11-1).

Appendix C. Analytical expression of the critical dilution index for the plumes in the three-dimensional homogeneous systems

For the square source (Y=Z) in the three-dimensional system, inverse dynamic Péclet numbers in the transverse vertical and transverse horizontal directions were defined in Ye et al. [2015], read as:

$$\varepsilon_y = \varepsilon_z = \frac{nxD_t}{q_x Y^2} \tag{C1}$$

If we insert Eq. (C1) into Eq. (5.9), we obtain:

$$\varepsilon_y = \varepsilon_z = \frac{1}{16\left[inverf\left(\sqrt{X_{crit}}\right)\right]^2} \tag{C2}$$

If we take the first-order approximation for the Taylor expression of the inverse function, i.e., $inverf\left(\sqrt{X_{crit}}\right) = \frac{1}{2}\sqrt{\pi X_{crit}}$, Eq. (C2) turns to be:

$$\varepsilon_y = \varepsilon_z = \frac{1}{4\pi X_{crit}} \tag{C3}$$

The semi-analytical expression of the flux-related dilution index reads as [Ye et al., 2015]:

$$E_Q\left(\varepsilon_y, \varepsilon_z\right) = YZq_x\left(1 - \sqrt{\frac{4\pi\varepsilon_y}{4\pi\varepsilon_y + 1 + f\left(\varepsilon_y\right)}} + \sqrt{4\pi\exp(1)\varepsilon_y}\right)$$
$$\left(1 - \sqrt{\frac{4\pi\varepsilon_z}{4\pi\varepsilon_z + 1 + f\left(\varepsilon_z\right)}} + \sqrt{4\pi\exp(1)\varepsilon_z}\right) \tag{C4}$$

Assuming the plume is long, the second term in both brackets in Eq. (C4) tends to be 1. By inserting Eq. (C3), Eq. (C4) turns to be:

$$E_Q(L) = YZq_x\frac{\exp(1)}{X_{crit}} = \frac{E_Q(0)}{X_{crit}}\exp(1) \tag{C5}$$

References

[1] J. M. Ottino, The Kinematics of Mixing (Cambridge University, Cambridge, 1989).
[2] B. Bijeljic, P. Mostaghimi, and M. J. Blunt, Phy. Rev. Lett. 107, 204502 (2011).
[3] G. Chiogna, O. A. Cirpka, P. Grathwohl, and M. Rolle, J. Contam. Hydrol. 172, 33 (2011).
[4] O. A. Cirpka, and A. J. Valocchi, Adv. Water Resour. 30, 1668 (2007).
[5] D. N. Lerner, S. F. Thornton, M. J. Spence, S. A. Banwart, S. H. Bottrell, J. J. Higgo, H. E. H.
[6] R. D. Bauer, M.Rolle, P. Kürzinger, P. Grathwohl, R. U. Meckenstock, and C. Griebler, J. Hydrol. 369, 284 (2009a).
[7] H. Prommer, B. Anneser, M. Rolle, F. Einsiedl, and C. Griebler, Environ. Sci. Technol. 43, 8206 (2009).
[8] T. W. Willingham, J. C. Werth, and A. J. Valocchi, Environ. Sci. Technol. 42, 3185 (2008).
Mallinson, R. W. Pickup, and G. M. Williams, Ground Water 38, 922 (2000).
[9] D. Bolster, D. A. Benson, T. Le Borgne, and M. Dentz, Phy. Rev. E 82, 021119 (2010).
[10] T. Le Borgne, M. Dentz, P. Davy, D. Bolster, J. Carrera, J. de Dreuzy, and O. Bour, Phy. Rev. E 84, 015301 (2011).
[11]T. Le Borgne, M. Dentz, and E. Villermaux, Phy. Rev. Lett. 110, 204501 (2013).
[12] U. M. Scheven, Phy. Rev. Lett. 110, 214504 (2013).
[13] R. D. Bauer, M.Rolle, S. Bauer, C. Eberhardt, P. Grathwohl, O. Kolditz, R. U. Meckenstock, and C. Griebler, J. Contam. Hydrol. 105, 56 (2009b).
[14] M. Dentz, J. Carrera, and J. R. de Dreuzy, Phy. Rev. E 84, 019904 (2011).
[15] N. B. Engdahl, D. A. Benson, and D. Bolster, Phy. Rev. E 90, 051001 (2014).
[16] M. Bakker, and K. Hemker, Adv. Water Resour. 27, 1075 (2004).
[17] G. Chiogna, O. A. Cirpka, M. Rolle, and A. Bellin, Water Resour. Res. 51, 261 (2015).
[18] O. A. Cirpka, G. Chiogna, M. Rolle, and A. Bellin, Water Resour. Res. 51, 241 (2015).
[19] G. Chiogna, B. Majone, K. C. Paoli, E. Diamantini, E. Stella, S. Mallucci, V. Lencioni, F. Zandonai, and A. Bellin, Sci. Total Environ. 540, 429 (2016).
[20] D. S. Dean, I. T. Drummond, and R. R. Horgan, Phy. Rev. E 63, 061205 (2001).
[21] Y. Ye, G. Chiogna, O. A. Cirpka, P. Grathwohl, and M. Rolle, Phy. Rev. Lett. 115, 194502 (2015).
[22] G. Nichols, Sedimentology and Stratigraphy (Wiley-Blackwell, Chichester, 2009).
[23] A. Hazen, Ann. Rep. State Board of Health Mass 24, 541 (1892).
[24] O. A. Cirpka, F. P. J. de Barros, G. Chiogna, M. Rolle, and W. Nowak, Water Resour. Res. 47, W06515 (2011).
[25] G. Chiogna, C. Eberhardt, P. Grathwohl, O. A. Cirpka, and M. Rolle, Environ. Sci. Technol. 44, 688 (2010).
[26] Y. Ye, G. Chiogna, O. A. Cirpka, P. Grathwohl, and M. Rolle, J. Contam. Hydrol. 172, 33 (2015).
[27] M. Rolle, C. Eberhardt, G. Chiogna, O. A. Cirpka, and P. Grathwohl, J. Contam. Hydrol. 110, 130 (2009).
[28] P. K. Kitanidis, Water Resour. Res. 30, 2011 (1994).
[29] P. A. Domenico, and V. V. Palciauskas, Ground Water 20, 303 (1982).

[30] V. Srinivasan, T. P. Clement, and K. K. Lee, Ground Water 45, 136 (2007).
[31] O. A. Cirpka, A. Olsson, Q. Ju, M. A. Rahman, and P. Grathwohl, Ground Water 44, 212(2006).
[32] M. Rolle, C. Eberhardt, G. Chiogna, O. A. Cirpka, and P. Grathwohl, Water Resour. Res. 47, W02505 (2011).
[33] E. Villermaux, A. Stroock, and H. Stone, Phy. Rev. E 77, 015301(2008).

6. Conclusions and Outlook

6.1 Conclusions

In this study, we experimentally investigated transverse dispersion and plume dilution during solute transport in three-dimensional porous media. We constructed a fully three-dimensional setup with high-resolution measurement points and performed experiments with progressively increasing complexity of the filled porous media. As a first step, we performed steady-state flow-through experiments in homogeneous porous media, considering fluorescein and oxygen as tracer solutes. Transverse dispersion coefficients were determined for each solute by fitting the measured concentrations to the analytical solution at different flow velocities ranging between 0.5-8 m/day. Subsequently, we inserted high-permeability inclusions in the homogeneous matrix to investigate the effect of flow-focusing in the inclusions. In the end, macroscopic anisotropy was constructed by arranging high and low conductivity materials alternating spatial orientation in different layers. In each of the experiment performed in homogenous and heterogeneous porous media, dilution was calculated using the measured concentrations and flow rates at the inlet and at the outlet ports. Numerical models were used to quantitatively interpret the experimental observations. Theoretical analyses were also conducted and (semi-)analytical solutions were developed for the parameters quantifying mixing in homogeneous porous media and mixing enhancement in heterogeneous porous media.

The main outcomes of this study can be summarized in the following points:

- *Influence of dimensionality on transverse dilution.* Plume dilution by transverse dispersion is more pronounced in three-dimensional than in two-dimensional flow-through systems. However, dilution enhancement by heterogeneity was found to be larger for two-dimensional domains compared to the three-dimensional ones. Thus, using results obtained from two-dimensional studies will underestimate the transverse dilution and overestimate the dilution enhancement in predicting three-dimensional plume transport.
- *Compound-specific effects.* Transverse dispersion of multi-tracer experiments shows significant compound-specific effects during solute transport at different flow conditions. This study showed that such effects are more pronounced in three-dimensional flow-through systems compared to two-dimensional domains.

Furthermore, the heterogeneity of the porous media does not decrease the compound-specific effects on transverse mixing. Therefore, the parameterization of transverse dispersion coefficient is critical to properly describe plume transport, in particular in fully three-dimensional systems. A non-linear compound-specific parameterization of transverse dispersion previously proposed for 2-D transport (e.g., Chiogna et al., 2010; Rolle et al., 2012) was applied in our 3-D study and validated with the experimental measurements.

- *Dilution enhancement by flow-focusing.* In high-permeability inclusions, the distance between the streamlines, as well as the travel time of the solute particles, are reduced. In two-dimensional systems since the decrease of transverse dispersion distance prevails over the decrease of mixing time, transverse mixing and dilution are always enhanced in the inclusions. However, in three-dimensional systems the two effects cancel out if the flow-focusing in both transversal directions is isotropic. In particular, no enhancement of transverse mixing would occur if the local transverse dispersion coefficient is uniform. Yet, the transverse dispersion coefficient depends on the flow velocity and on the grain size. The higher flow velocity, as well as the larger grain size, in the inclusions compared to the matrix leads to a higher dispersion coefficient, thus resulting in an enhancement of the transverse mixing. If flow-focusing is not identical in the two transversal directions, mixing is more enhanced in the direction in which the plume fringe is more strongly focused and mixing is less enhanced or even decreases in the direction in which the plume is less focused. The total dilution also depends on whether the plume fringe is focused in the high-permeability inclusions. If the plume fringe is not focused in the inclusions, the plume meanders in regions with lower flow velocity and this can lead to a decrease of mixing. Therefore, mixing enhancement by flow-focusing effects in heterogeneous porous media depends not only on the contrast of permeability between fine and coarse materials and the volumetric ratio of the two materials, but also on the spatial arrangement of the inclusions with respect to the location of the plume fringe.
- *Dilution enhancement by helical flow.* Helical flow can occur in three-dimensional heterogeneous anisotropic porous media. In this work, helical flow was created in a laboratory setup by alternating angled stripes of high and low hydraulic conductivity materials in different layers. Such complex flow field facilitates streamlines twisting and the deformation of the material surfaces of the plume, thus leading to a significant increase of lateral mass exchange. Therefore, transverse mixing and plume dilution are

strongly enhanced (i.e., enhancement of dilution can reach up to 235% compared to the transport in homogeneous porous media) with important consequences for conservative and mixing-controlled reactive transport.

This study, based on high-resolution flow-through experiments has shown the relevance of dimensionality, heterogeneity, macroscopic anisotropy and compound-specific effects on solute transport and plume dilution. Although the conditions tested are considerably simplified compared to actual field conditions in groundwater contamination problems, specific insights and improved understanding of mixing and mixing enhancement are important also at larger scale and may help improving the description of solute transport and the interpretation of experimental datasets. The results presented may also have an impact beyond the field of subsurface contaminant hydrology; for instance, they may be relevant in engineering applications dealing with mixing processes in packed bed reactors.

6.2 Outlook

Further investigation can be carried out along the research directions explored in this thesis. Interesting points that could be investigated in future work include:

- *Flow-through reactive experiments.* Mixing-controlled biodegradations were experimentally studied in two-dimensional porous media (e.g., Bauer et al., 2008; Cirpka et al., 1999). Yet, high-resolution experimental investigations of reactive processes in fully 3-D porous media are less common. Since the transverse mixing and the mixing enhancement in three-dimensional porous media show a significant different performance on plume dilution and transport compared to the two-dimensional systems, mixing-controlled reactions should also be studied independently in full three-dimensional systems. As a further step, one could also include more reactants to analyze conditions closer to those occurring in contaminated groundwater.
- *Experiments with natural porous media.* In our experiments, glass beads with regular shapes were used. Also, heterogeneity and anisotropy were built using very simple architectures. Since the natural porous media are more complex, more realistic geological structures could be designed and constructed in future experiments. Furthermore, reactive minerals can be included in the porous media. For instance, an

inclusion made by reactive minerals can be inserted in the otherwise homogenous glass beads matrix.

- *Implementation at larger scale.* The numerical model used in our study was validated with the high-resolution experimental data. Therefore, the model represents a useful tool to explore the effect of transverse mixing on plume transport at larger scale. Future modeling studies at the field scale could solve flow and transport problems in realistic sedimentary structures incorporating detailed insights from geologic interpretation. Modeling investigation of transport in complex fully three-dimensional porous media should also be extended to include reactive processes affecting the fate of contaminant plumes in aquifer systems.
- *Implement in engineering systems.* The herringbone cross-stratification of the porous media created in some of the experiments presented in this thesis can be further applied in engineering systems for the purpose of enhancing mixing between reactants in packed beds. Packed bed mixers and reactors could be constructed and the efficiency could be tested by including various herringbone structures.
- *Development of non-invasive measuring techniques.* In this study high-resolution measurements of concentration and flow rate at the outlet were used to quantify plume dilution and a technique based on freezing and slicing of the porous medium was adopted to qualitatively locate color tracer plumes at different cross sections. A current limitation for three-dimensional experiments is still the difficulty in quantitative imaging 3-D plumes inside porous media. Therefore, the development of non-invasive techniques would be highly beneficial. Index-matching techniques (e.g., Dijksman et al., 2012; Kong et al., 2011) and nuclear magnetic resonance imaging techniques (e.g., Oswald and Kinzelbach, 2004) might be advantageous and could be tested in future experiments to determine plume shapes and concentration distributions directly inside porous media.

References

Bauer, R. D., P. Maloszewski, Y. Zhang, R. U. Meckenstock, and C. Griebler (2008), Mixing-controlled biodegradation in a toluene plume – Results from two-dimensional laboratory experiments, J. Contam. Hydrol., 96(1-4), 150-168, doi: 10.1016/j.jconhyd.2007.10.008.

Chiogna, G., C. Eberhardt, P. Grathwohl, O. A. Cirpka, and M. Rolle (2010), Evidence of compound-dependent hydrodynamic and mechanical transverse dispersion by multitracer laboratory experiments, Environ. Sci. Technol., 44(2), 688-693, doi: 10.1021/Es9023964.

Cirpka, O. A., E. O. Frind, and R. Helmig (1999), Numerical simulation of biodegradation controlled by transverse mixing, J. Contam. Hydrol., 40(2), 159-182, doi: 10.1016/S0169-7722(99)00044-3.

Dijksman, J. A., F. Rietz, K. A. Lorincz, M. van Hecke, and W. Losert (2012), Invited article: Refractive index matched scanning of dense granular materials, Rev. Sci. Instrum., 83(1), 011301, doi: 10.1063/1.3674173.

Kong, X. Z., M. Holzner, F. Stauffer, and W. Kinzelbach (2011), Time-resolved 3D visualization of air injection in a liquid-saturated refractive-index-matched porous medium, Exp. Fluids, 50(6), 1659-1670, doi: 10.1007/s00348-010-1018-6.

Oswald, S. E., and W. Kinzelbach (2004), Three-dimensional physical benchmark experiments to test variable-density flow models, J. Hydrol., 290(1-2), 22-42, doi: 10.1016/j.jhydrol.2003.11.037.

Rolle, M., D. L. Hochstetler, G. Chiogna, P. K. Kitanidis, and P. Grathwohl (2012), Experimental investigation and pore-scale modeling interpretation of compound-specific transverse dispersion in porous media, Transp. Porous Media, 93(3), 347-362, doi: 10.1007/s11242-012-9953-8.